“The brick walls are there for a reason.

The brick walls are not there to keep us out.

The brick walls are there to give us a chance to show how badly we want something.

Because the brick walls are there to stop the people who don’t want it badly enough.

They’re there to stop the other people.”

– Randolph Frederick “Randy” Pausch,

The Last Lecture

MYOSIN REGULATORY LIGHT CHAIN PHOSPHORYLATION AND ITS EFFECT ON THE CONTRACTILE ECONOMY OF MOUSE FAST MUSCLE

Jordan Alexander Bunda, BSc(Kin)

Submitted in partial fulfillment of the requirements for the degree of
Master of Science in Applied Health Sciences
(Kinesiology)

Faculty of Applied Health Sciences
Brock University
500 Glenridge Ave.
St. Catharines, ON
L2S 3A1

Abstract

Activated by elevations in myoplasmic calcium concentration, myosin light chain kinase (skMLCK) phosphorylates the regulatory light chains (RLCs) of fast muscle myosin. This covalent modification potentiates force production, but requires an investment of ATP. Our objective was to investigate the effect of RLC phosphorylation on the contractile economy (mechanical output:metabolic input) of fast twitch skeletal muscle. Extensor digitorum longus muscles isolated from Wildtype and skMLCK$^{-/-}$ mice mounted *in vitro* (25°C) were subjected to repetitive low-frequency stimulation (10Hz,15s) known to cause activation of skMLCK, and staircase potentiation of force. With a 3-fold increase in RLC phosphate content, Wildtype generated 44% more force than skMLCK$^{-/-}$ muscles over the stimulation period (P = .002), without an accompanied increase in energy cost (P = .449). Overall, the contractile economy of Wildtype muscles, with an intact RLC phosphorylation mechanism, was 73% greater than skMLCK$^{-/-}$ muscles (P = .043), demonstrating an important physiological function of skMLCK during repetitive contractile activity.

Acknowledgments

Dr. Vandenboom

Thank you for believing in me and providing me with this incredible opportunity.
You placed your trust in me and granted me the freedom to work independently,
and I have grown immensely as a result.

My Supervisory Committee

Thank you to my committee members, Dr. Peters and Dr. Gabriel; my external examiner,
Dr. Grange; and my defence chair, Dr. Adkin, for taking part in this journey with me.

Dr. Peters

Thank you for investing time and effort into providing me with one-on-one lab training.
Your compassion and expertise allowed me to complete the project I had my heart set on.

The Boom Squad

I will not soon forget all of the time we spent bouncing ideas off one another, turning the
lab music up to 11, celebrating every milestone humanly possible, and having Friday
Frijoles feasts – not to mention the hours of Briscola and all of the consequences.
I could not have asked for a better group of labmates to spend the past two years with.

William

Thank you for being a great friend, a mentor, and our lab MacGyver.
Without your guidance, none of this work would have been possible.
I am forever indebted to you for taking me under your wing.

Josh

We have been roommates throughout two degrees, and you have always had my back.
You are like a brother to me. Thank you for keeping me (somewhat) sane with your
support at home and at the lab; without it, I would not be where I am today.

Stephen

From our days of undergraduate coursework to guitar serenades
and acoustic rap battles, you have been here with me every step of the way.
Thanks for being a true friend for all of these years.

The Brock Community

Brock University has been my home for six years, and has shaped who I have become. To all of the friends, colleagues, and professors that have impacted my time here, thank you for the incredible memories, and making my time here an amazing experience.

My MacBook

The amount of time we have spent together over the past two years is truly scary:
Researching, reading, writing, editing, organizing, analyzing, Netflixing…
Thanks for not dying during the endless hours of use and abuse you endured.

My Family

Everything I have achieved was built upon the extraordinary support structure that I have. Thank you to each and every member of my family for continually encouraging me to pursue every goal that I have. You are amazing individuals and I love you all.

Edsel

It is impossible to calculate the mileage you have racked up during my time at Brock. Late nights on the patio, and impromptu pool at The Beach have been my therapy sessions for as far back as I can remember. Thanks for being there at the drop of a hat.

Mom

You have been my best friend for twenty-five years.
Your unconditional love and support mean the world to me,
and have kept me afloat any time I fear I will sink.
Thank you so much for everything that you do.

Table of Contents

Abstract iii

Acknowledgments iv

Table of Contents vi

List of Figures ix

List of Tables x

List of Equations xi

List of Abbreviations xii

1. Introduction 1

2. Review of Literature 3

2.1. Skeletal Muscle Structure and Function 4

2.1.1. Myosin 5

2.1.2. S1 Fragment 7

2.1.3. The Thin Filament 7

2.2. Brief Overview of Excitation-Contraction Coupling 9

2.2.1. The Intracellular Calcium Transient 11

2.2.2. Cooperativity 12

2.3. Crossbridge Cycling 13

2.3.1. Lymn-Taylor Four State Cycle 13

2.3.2. Kinetic Cycle 15

2.4. Myosin Regulatory Light Chain Phosphorylation 17

2.4.1. Myosin Light Chain Kinase 17

2.4.2. Myosin Light Chain Phosphatase 19

2.4.3. RLC Phosphorylation-Mediated Force Potentiation 19

2.4.4. Physiological Function of RLC Phosphorylation 20

2.4.5. Brenner Two-State Model 22

2.4.6. Why Phosphorylate the RLC? 25

2.5. Metabolic Considerations of Mammalian Skeletal Muscles 27

2.5.1. Energetics of Skeletal Muscle Contraction 27

2.5.2. Activation Energy Turnover 28

2.5.3. Efficiency of Muscle Contraction 30

2.5.4. Possible Factors Impacting Efficiency and Economy 33

2.5.5. Energy Producing Processes in Skeletal Muscle 35

2.5.6. Quantifying Anaerobic ATP Provision 41

2.6. Metabolic Consequences of Potentiation 42

2.6.1. Evidence of No Consequence 42

2.6.2. Evidence of Increased Economy 43

2.6.3. Evidence of Decreased Economy 43

3. Statement of Problem 45

3.1. Purpose 45

3.2. Hypotheses 46

3.3. Rationale 47

4. Methods 48
4.1. Animals 48
4.2. Materials 48
4.3. Muscle Model and Experimental Apparatus 49
4.4. Surgical Procedures and Preparation of Muscle Tissue 51
4.5. Contractile Experiment Protocol 52
4.5.1. Equilibration and Determination of Optimal Length 52
4.5.2. Contractile Experiment 53
4.5.3. Quantifying Force Potentiation 53
4.5.4. Kinetic Analysis 54
4.5.5. Quantifying Force-Time Integral (FTI) 54
4.6. Biochemical Analysis of Skeletal Muscle Tissue 54
4.6.1. Quantifying Myosin RLC Phosphate Content 54
4.6.2. Quantifying High Energy Phosphate Consumption 55
4.6.3. Quantifying Contractile Economy 56
4.7. Experimental Timeline 56
4.8. Data Presentation and Statistical Analyses 58

5. Results 60
5.1. Animal Characteristics 60
5.2. Contractile Data 61
5.2.1. Absolute Twitch Force 61
5.2.2. Relative Force Potentiation 62
5.2.3. Twitch Kinetics 62
5.2.4. Force-Time Integral 64
5.2.5. Effects of BTS Incubation on Force Production 65
5.3. Myosin RLC Phosphorylation 65
5.4. Metabolite Concentrations 68
5.4.1. Resting Levels 68
5.4.2. Stimulated Metabolite Levels 68
5.4.3. Energy Consumption 69
5.5. Contractile Economy 72

6. Discussion 73
6.1. General Summary 73
6.2. Myosin RLC Phosphorylation 73
6.2.1. Comment on BTS Specificity 74
6.3. Contractile Performance of Wildtype and skMLCK$^{-/-}$ Muscles 75
6.3.1. Staircase Potentiation of Force 75
6.3.2. Inhibition of Force Production 77
6.3.3. Potentiation of the Force-Time Integral 78
6.4. Skeletal Muscle Energetics 78
6.4.1. Total Energy Consumption (E_{Total}) 79
6.4.2. Crossbridge Component of Energy Consumption (E_{XB}) 79
6.4.3. Activation Energy Turnover (E_A) 84
6.5. Contractile Economy 88

7. Conclusions & Significance 90
7.1. Major Findings 90
7.2. Significance 90
7.3. Future Considerations 91

7.4. Assumptions 91
7.5. Limitations 92

References 94

Appendix I: Preliminary Procedures for Contractile Experiments 105

Setting Up the In Vitro Apparatus 105
Surgical Procedures 105
Mounting Isolated Muscles 105
Equilibration and Determining L_o 106

Appendix II: Measurement of Myosin Regulatory Light Chain Phosphorylation by Urea/Glycerol-PAGE with Immunoblotting 107

Sample Preparation 107
Prepare Stock Solutions 107
Prepare Buffers 108
Sample Denaturation 108
Sample Homogenization 108
Resuspension 109
Hand Casting of Polyacrylamide Gels 109
Electrophoretic Separation of Proteins 110
Pre-Electrophoresis 110
Electrophoretic Separation of Proteins 110
Transferring Protein From Polyacrylamide Gel to the Nitrocellulose Membrane 111
Immunobloting 112
Blocking of Non-Specific Sites 112
Primary Antibody Incubation 112
Secondary Antibody Incubation 112
Detection of Target Proteins 112

Appendix III: Lyophilization of Muscle Tissue 113

Appendix IV: Metabolite Extraction 114

Required Solutions 114
Perchloric Acid Metabolite Extraction Procedure 115

Appendix V: Fluorometric Assays 116

Muscle Adenosine Triphosphate (ATP) and Phosphocreatine (PCr) Assay 117
Muscle Creatine (Cr) Assay 120
Muscle Lactate Assay 122

List of Figures

Figure I. Schematic representation of sarcomeric structure and organization. 5
Figure II. Myosin subfragments created by enzymatic digestion. 7
Figure III. Key proteins involved in excitation-contraction coupling. 11
Figure IV. The Lymn-Taylor four state crossbridge cycle. 15
Figure V. Mechanochemical reaction cycle between actin and myosin. 16
Figure VI. Sequential activation of skMLCK and covalent modification of the myosin RLC. 18
Figure VII. Mass movement of myosin heads upon RLC phosphorylation. 21
Figure VIII. Major energy consuming processes during skeletal muscle contraction. 28
Figure IX. Allocation of isolated EDL muscles to experimental groups. 48
Figure X. The EDL of the mouse hind limb (A) is composed of predominately fast fibres (B). 49
Figure XI. Schematic diagram of the in vitro muscle testing system used for contractile experiments. 50
Figure XII. Overview of the timeline of experimental procedures. 56
Figure XIII. Contractile experiment timeline for Control (A) and BTS (B) conditions 57
Figure XIV. Representative force traces of (A) skMLCK$^{-/-}$ and (B) Wildtype muscles 61
Figure XV. Precense of skMLCK potentiates twitch force during repetitive low-frequency stimulation. 62
Figure XVI. Traces of isometric twitches of evoked from skMLCK$^{-/-}$ (A) and Wildtype (B) muscles. 63
Figure XVII. Effects of skMLCK expression and BTS incubation on isometric work performed 64
Figure XVIII. An 80 min incubation in 25 μM BTS abolishes ~94% of twitch force production 65
Figure XIX. Concomitant myosin RLC phosphorylation and isometric twitch force potentiation 67
Figure XX. Change in metabolite concentration between contralateral pairings 69
Figure XXI. Precense of skMLCK does not augment energy turnover 70
Figure XXII. Total high-energy phosphate consumption partitioned 71
Figure XXIII. RLC phosphorylation increases contractile economy of isolated mouse EDL 72

List of Tables

Table I. Anthropometric characterization of experimental mice. 60
Table II. The effect of a potentiating stimulus on isometric force production. 61
Table III. Kinetic characteristics of twitches sampled throughout the potentiating stimulus. 63
Table IV. RLC phosphate content of EDL muscles from Wildtype and skMLCK$^{-/-}$ mice 66
Table V. Effect of BTS and skMLCK on metabolites in mouse EDL muscle in basal state. 68
Table VI. Effect of BTS and skMLCK on metabolites in mouse EDL muscle after stimulation. 68
Table VII. Total energy consumption partitioned into Crossbridge and Activation components. 70
Table VIII. Previously reported activation energy turnover of mouse EDL. 86

List of Equations

Equation I. Fraction of crossbridges in the force-generating state. 23
Equation II. Isometric force equation. 23
Equation III. Rate of force redevelopment equation. 24
Equation IV. Isometric myosin ATPase rates. 25
Equation V. Hydrolysis of adenosine triphosphate. 27
Equation VI. ATP consumed during a single instantaneous phosphorylation of 50% of RLCs. 30
Equation VII. General efficiency equation. 30
Equation VIII. Work defined as the product of force and displacement. 31
Equation IX. Enthalpy change is useful work and its thermal accompaniment. 31
Equation X. Mechanical efficiency is the ratio of work to enthalpy. 31
Equation XI. Thermodynamic efficiency. 32
Equation XII. Free energy released during ATP hydrolysis. 32
Equation XIII. Economy calculated using consumption of high-energy phosphates. 33
Equation XIV. Adenylate energy charge. 36
Equation XV. Regeneration of ATP through the creatine kinase reaction. 38
Equation XVI. Adenylate kinase reaction. 39
Equation XVII. AMP deaminase reaction. 40
Equation XVIII. Summary of the glycolysis pathway starting with glycogen. 40
Equation XIX. Lactate dehydrogenase reaction. 40
Equation XX. Calculating total ATP provision from substrate level phosphorylation. 41
Equation XXI. Calculating the area under the force-time curve. 54
Equation XXII. Calculating high-energy phosphate consumption. 56
Equation XXIII. Calculating contractile economy of skeletal muscle. 56
Equation XXIV. Correcting for residual force production during myosin inhibition. 70

List of Abbreviations

ADP	Adenosine diphosphate
AK	Adenylate kinase
AMP	Adenosine monophosphate
APS	Ammonium persulfate
ATP	Adenosine triphosphate
ATPase	Adenosine triphosphatase
BDM	2,3-butanedione monoxime
BTS	*N*-benzyl-*p*-toluene sulfonamide
Ca^{2+}	Calcium ion
$CaCl_2$	Calcium chloride
CaM	Calmodulin
CK	Creatine kinase
Cr	Creatine
DHPR	Dihydropyridine receptor
DMSO	Dimethyl sulfoxide
DTT	Dithiothreitol
E_A	Activation energy turnover
E_{Total}	Total energy turnover
E_{XB}	Crossbridge energy turnover
ECC	Excitation-contraction coupling
EDL	Extensor digitorum longus
EDTA	Ethylenediaminetetraacetic acid
ELC	Essential light chain of myosin
FTI	Force-time integral
G-6-P-DH	Glucose-6-phosphate dehydrogenase
HEPC	High-energy phosphate consumption
HK	Hexokinase
HMM	Heavy meromyosin
IC	Intracardiac
ICT	Intracellular calcium transient

IP	Intraperitoneal
IMP	Inosine monophosphate
KCl	Potassium chloride
kDa	Kilodalton
$KHCO_3$	Potassium bicarbonate
LDH	Lactate dehydrogenase
LMM	Light meromyosin
L_o	Optimal length
$MgCl_2$	Magnesium chloride
MHC	Myosin heavy chain
MLC	Myosin light chain
NaCl	Sodium chloride
NaCN	Sodium cyanide
NAD	Nicotinamide adenine dinucleotide, oxidized
NADH	Nicotinamide adenine dinucleotide, reduced
NADP	Nicotinamide adenine dinucleotide phosphate, oxidized
NADPH	Nicotinamide adenine dinucleotide phosphate, reduced
$NaHCO_3$	Sodium bicarbonate
$NaHPO_4$	Sodium phosphate
Na^+-K^+ ATPase	Sodium-potassium ATPase
NH_3	Ammonia
NMR	Nuclear magnetic resonance
PEP	Phosphoenolpyruvate
PCA	Perchloric acid
PCr	Phosphocreatine
P_i	Inorganic phosphate
P_o	Peak tetanic force
P_t	Peak twitch force
PTP	Post-tetanic potentiation
RLC	Regulatory light chain
$RT_{1/2}$	Half-relaxation time

RyR	Ryanodine receptor
S1	Myosin subfragment 1
S2	Myosin subfragment 2
SEM	Standard error of the mean
SERCA	Sarco-endoplasmic reticulum calcium-ATPase
skMLCK	Myosin light chain kinase (skeletal muscle isoform)
skMLCK$^{-/-}$	Mice or muscles devoid of skMLCK ("knockouts")
skMLCP	Myosin light chain phosphatase (skeletal muscle isoform)
SR	Sarcoplasmic reticulum
TA	Tibialis anterior
TBST	Tris-buffered saline with Tween 20
TCA	Trichloroacetic acid
TEMED	Tetramethylethylenediamine
Tm	Tropomyosin
Tn	Troponin
TnC	Troponin - calcium binding subunit
TnI	Troponin - inhibiting subunit
TnT	Troponin - tropomyosin binding subunit
Tm	Tropomyosin
TPT	Time to peak tension
+ dP/dt	Rate of force development
- dP/dt	Rate of relaxation
ΔG_{ATP}	Free energy of ATP hydrolysis

1. Introduction

Skeletal muscle is a biological motor that functions to convert chemical energy into mechanical energy. The main contractile components of muscle are actin and myosin, which polymerize to form the thin and thick filaments, respectively (Huxley, 1957). Myosin also plays an important enzymatic role in muscle, as it is an ATPase capable of producing motility by moving actin (Rayment & Holden, 1994). Chemical energy is converted into mechanical energy via myosin crossbridges during their cyclical interactions with actin, referred to as crossbridge cycling, which results in filament sliding and the production of force (Lymn & Taylor, 1971).

The myosin molecule is a hexamer composed of two heavy chains, and two pairs of light chains (Rayment, Rypniewski, et al., 1993b). The regulatory light chain (RLC) of myosin exists non-covalently bound to the myosin heavy chain, and is responsible for performing both a stabilizing and regulatory role (Alamo et al., 2008). A rise in intracellular calcium concentration, the same signal that initiates muscle contraction, leads to activation of the enzyme skeletal myosin light chain kinase (skMLCK) which catalyzes the phosphorylation of the myosin RLC (Stull, Kamm, & Vandenboom, 2011). This phosphotransferase activity introduces a negative charge to the RLC, and through myosin head-rod interactions causes a mass movement of myosin heads off the thick filament backbone, projecting them towards the actin filament, increasing the likelihood of actin-myosin interaction (Duggal et al., 2014). This phosphorylation-induced loss of helical ordering increases the number of crossbridges in the force producing state, modulating the calcium sensitivity of the contractile apparatus; thus, potentiating force production and the hastening the rate of force development (Stull et al., 2011).

This phenomenon is known as RLC phosphorylation-mediated force potentiation, and can greatly increase force, work, and power (Vandenboom, Gittings, Smith, Grange, & Stull, 2013). Although RLC phosphorylation requires a continual investment of ATP, it results in a dramatic increase in submaximal force output across a range of intracellular calcium concentrations, i.e. with no increased energy cost of calcium handling. Therefore, if RLC phosphorylation is able to augment the relationship between the total energy consumed during contraction, and the force produced, it may play an important

role in determining the contractile economy (i.e. mechanical output:metabolic input) of fast twitch skeletal muscle.

To date, no one has attempted to quantify the "energetic overhead" associated with skMLCK-mediated RLC phosphorylation in mammalian skeletal muscle, although Homsher (1987) predicted that the ATP consumed for this process is upwards of 5% of the energy used during a 5 second tetanus. Early research did attempt to investigate the relationship between RLC phosphorylation and energy consumption during contraction; however, no consensus has been reached. One of the earliest studies attempting to answer this research question reported a correlation between RLC phosphorylation and a reduced energy cost for isometric tetani (Crow & Kushmerick, 1982b). Subsequently, Barsotti and Butler (1984) found that RLC phosphorylation had no consistent relationship with the energy consumed during stimulation. Most recently, Abbate, Velden, Stienen, and De Haan (2001) stated that potentiation increased the energetic cost of contraction to a larger extent than work. Thus, previous results were equivocal and contradictory, and this question remains one of the most interesting in our field. One could argue that the vast differences between the findings of previous studies are attributable to the differing stimulation paradigms; however, the most glaring limitation of all previous work is the lack of a *proper negative control* for RLC phosphorylation. Any skeletal muscle contraction, no matter how brief, will result in fractional activation of skMLCK, and lead to the phosphorylation of myosin RLCs. Fortunately, a group of researchers developed a unique skMLCK *knockout* model by ablating the gene coding for skMLCK from C57BL/6 mice (Zhi et al., 2005). Our lab at Brock University is currently the only institution with a colony of skMLCK devoid ($skMLCK^{-/-}$) mice, affording us the unique opportunity of using a robust negative control to explore this unresolved conflict.

2. Review of Literature

This literature review was completed in preparation for an experiment exploring the potential relationship that exists between myosin RLC phosphorylation and the metabolic cost of muscle contraction. The first section of the review, entitled *Skeletal Muscle Structure and Function*, explores the key structural and functional aspects of mammalian skeletal muscle, touching on microanatomy and organization of the sarcomere, with a description of the main structural and functional proteins that form the macromolecular machine. An overview of both *Excitation-Contraction Coupling* and the *Crossbridge Cycle* follow, in an attempt to quickly familiarize the reader with the processes that initiate, regulate, and actuate contraction of skeletal muscle. A basic understanding of skeletal muscle anatomy, and the mechanisms that govern its ability to produce force and/or work will benefit the discussions of the interaction of RLC phosphorylation, force potentiation, and metabolism that follow.

The next major section of the review explores modulation of the contractile apparatus by the phenomenon of *Myosin Regulatory Light Chain Phosphorylation*. Here, focus is given to the enzymes that regulate myosin RLC phosphorylation, and the remarkable physiological utility of this covalent modification. Significant discoveries within in the field of RLC phosphorylation-mediated force potentiation of fast-twitch skeletal muscle are examined. The way in which this phosphate-incorporation modulates the interaction between the proteins responsible for contraction is explored using the framework of the Brenner Two-State Model.

Metabolic Considerations of Mammalian Skeletal Muscle considers the principle reactions that harness the energy released during ATP hydrolysis to perform biological work during skeletal muscle contraction, the potential sources of ATP resynthesis during muscular activity, and the pathways responsible for maintaining the energy balance within the cell. Special focus is given to anaerobic ATP production via substrate-level phosphorylation, exploring the mechanisms and importance of the creatine kinase reaction, the adenylate kinase and AMP deaminase reactions, the glycolytic pathway, and the lactate dehydrogenase reaction. The metabolism section concludes with a look into the mechanical efficiency of skeletal muscle, and the economy of contraction.

Properties of RLC phosphorylation-mediated force potentiation and energetic aspects of muscle contraction are amalgamated in the final major chapter of the review, entitled *The Metabolic Consequences of Potentiation*. All relevant publications dedicated to exploring the relationship between potentiation and metabolism, albeit small in number, are discussed. Previous research has been unable to reach an agreeable conclusion, leaving the question largely unanswered; thus, all major possible relationships and theoretical explanations are considered.

2.1. Skeletal Muscle Structure and Function

Vertebrate skeletal muscle is a truly fascinating piece of biological machinery. The function of skeletal muscle is to generate force and/or produce movement, and is mechanically designed with tightly packed, remarkably organized contractile elements to achieve these goals with extraordinary efficiency. The fundamental contractile unit of skeletal muscle is the *sarcomere*, a highly ordered multi-protein complex containing partially interdigitating arrays of thick and thin filaments (Craig & Padrón, 2004; Craig & Woodhead, 2006). Sarcomeres are intricate structures containing an assortment of contractile, regulatory, and structural proteins that govern its structural regularity. This collection of proteins allows skeletal muscle to activate in milliseconds, shorten rapidly, and transduce chemical energy to mechanical energy (Craig & Padrón, 2004).

Each sarcomere (Figure I) is demarcated at each end by what appears in electron micrographs as a dark, narrow line referred to as the Z-line - or more appropriately, the Z-disc. These Z-discs fall at the centre of a relatively lighter I-band (*isotropic*), which is a section shared between adjacent sarcomeres. At the heart of each sarcomere is the M-line that bisects the H-zone, a less dense region inside of a darker band known as the A-band (*anisotropic*). The characteristic appearance of each band is due to areas of partial of overlap between thin and thick filaments (Huxley & Hanson, 1954).

The thick filaments, 110 Å in diameter, are anchored at the M-line and protrude outwards, while the thin filaments, 40 Å in diameter, are connected to the Z-discs and project inwards toward the centre of the sarcomere (Huxley & Hanson, 1954). The thin filaments run longitudinally from their attachment sites at the Z-disc, through the I-band into the A-band where they partially overlap with the thick filaments. The A-band is the densest region of the sarcomere due to the overlap between thick and thin filaments. The

lighter H-zone at its centre contains only thick, while the I-band contains only thin filaments. The H-zone is less dense than the rest of the A-band owing to the absence of overlapping thin filaments

The process of converting chemical energy into mechanical energy is accomplished via myosin crossbridges during their cyclic interactions with actin filaments (Barclay, 1996). The sliding filament model of contraction, states that the thick and thin filaments themselves remain constant in length, while the shortening of muscle is explained by sliding of the overlapping filaments past each other (Huxley & Hanson, 1954). Therefore, with filament length held constant, shortening of the sarcomere is associated with decrease in the length of the I-band (Huxley & Hanson, 1954). Actin and myosin are the main contractile proteins that polymerize into the thin and thick filaments respectively, accounting for more than 70% of myofibrillar protein (Craig & Padrón, 2004).

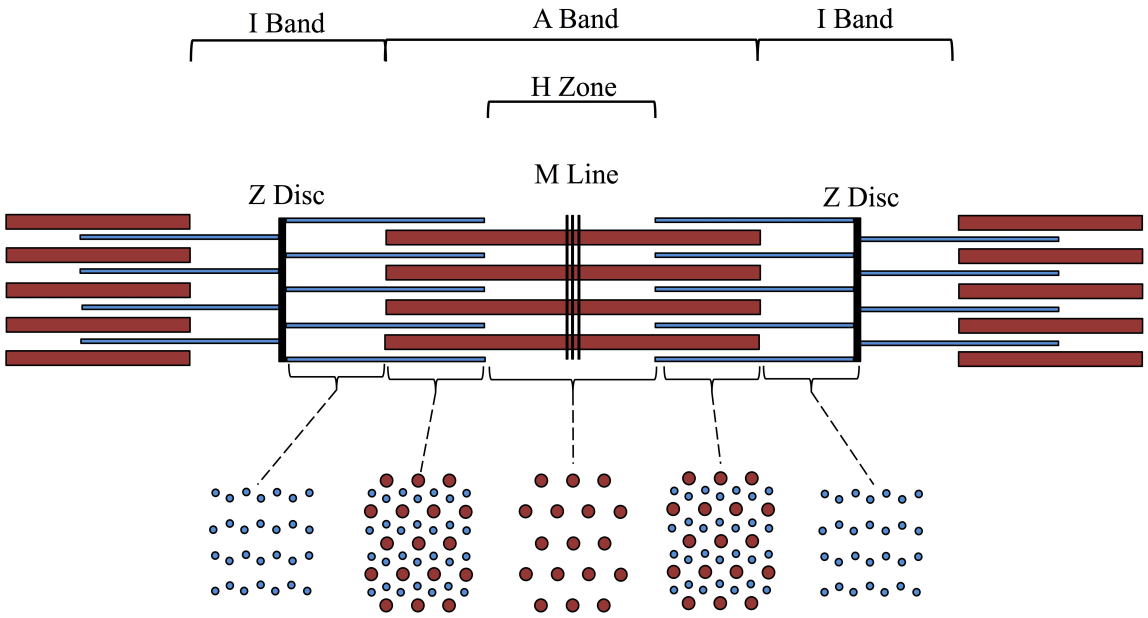

Figure I. Schematic representation of sarcomeric structure and organization.

2.1.1. Myosin

Myosin II plays an important structural and enzymatic role in muscle contraction and is the major constituent of the thick filament. It is a member of the myosin protein superfamily capable of producing motility by moving actin, and is an adenosine triphosphatase (ATPase). Myosin is a highly asymmetrical molecule, composed of two

globular heads attached to an elongated tail (Rayment & Holden, 1994). The native myosin II molecule of skeletal muscle has a molecular weight of 520 kDa, existing as a hexamer composed of two 220 kDa myosin heavy chains (MHCs) and two pairs of myosin light chains (MLCs) between 15 and 22 kDa (Rayment et al., 1993b). The carboxy (C)-terminals of the MHCs form an α-helical tail that twist around each other forming a *coiled-coil*, while the amino (N)-terminal of each MHC associates with one of each chemically distinct MLCs to form an elongated globular head region (Craig & Woodhead, 2006; Winkelmann, Baker, & Rayment, 1991). The head of the myosin molecule is the motor domain responsible for both actin-binding and ATP hydrolysis, while the C-terminal tail is mainly responsible for dimerization of heavy chains and thus the formation of the thick filament backbone (Krendel & Mooseker, 2005).

Controlled enzymatic digestion produces distinctive fragments of the myosin molecule (Figure II), and aids our understanding of the roles of the various domains. The first fragment to be considered, cleaved by trypsin, is light meromyosin (LMM): The α-helical tail that accounts for the distal two-thirds of the myosin molecule. The remaining one-third of the myosin molecule, heavy meromyosin (HMM), is composed of the two globular heads and a shorter section of tail. Alternatively, limited papain digestion isolates the two myosin heads, or subfragment 1 (S1), from the myosin rod. The myosin rod is the isolated myosin tail, and is composed of LMM and subfragment 2 (S2) of HMM (Sweeney & Houdusse, 2010).

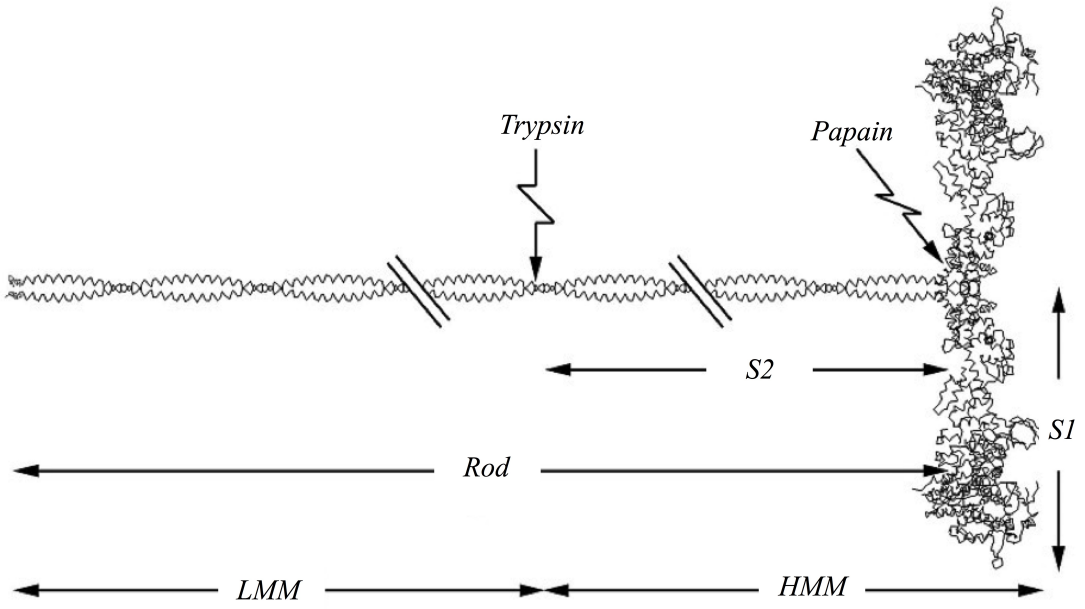

Figure II. Myosin subfragments created by enzymatic digestion.

2.1.2. S1 Fragment

The proteolytic fragment S1 is comprised the first 843 residues of the MHC, in addition to the two light chains; it is the morphological *crossbridge* and contains all of the enzymatic activity of myosin (Preller & Holmes, 2013). The heavy chain portion of the S1 comprises three domains: A 50 kDa domain at the N-terminal, a centrally located 25 kDa domain, and a 20 kDa domain at the C-terminal that associates with two light chains and creates a junction with the tail. The motor domain is composed of the 50 kDa and 25 kDa domains, and is responsible for both binding to actin and hydrolyzing ATP. The rest of the head, referred to as the light chain domain or the neck region, containing the 20 kDa heavy chain enveloped by the RLC and ELC, functions as a lever arm (Sweeney & Houdusse, 2010) that translates local conformational changes to large scale movements (Preller & Holmes, 2013).

2.1.3. The Thin Filament

To form the thin filament, actin monomers, known as globular (G)-actin (~42 kDa), self-associate into fibrillar (F)-actin. Two strands of F-actin then twist around each other, forming an elongated helical chain (Koubassova & Tsaturyan, 2011). The

contractile apparatus is regulated by the thin-filament protein complex Troponin (Tn) and Tropomyosin (Tm), which are attached at regular intervals along the F-actin backbone. These two molecules respond to changes in the intracellular concentration of calcium (Ca^{2+}), and together govern the actin-myosin interaction. Thus, Tm and Tn are the proteins responsible for regulation of both muscular contraction and relaxation (Koubassova & Tsaturyan, 2011).

Tm is a coiled-coil protein, formed by two helices of 65 kDa that join end-to-end or head-to-tail to form long helical rods strands along the helices of F-actin (Dominguez, 2011; Koubassova & Tsaturyan, 2011). Tm functions to stabilize the thin filament, and provides molecular scaffolding for the positioning of the Ca^{2+}-sensitive Tn molecule. Tm is associated with seven actin monomers, and during thin filament activation, Tm displays remarkable conformational plasticity by translocating across the surface of F-actin, exposing the myosin binding sites. This molecule functions as a *gatekeeper* by controlling myosin's access to the thin filament (Dominguez, 2011). Tn is an 80 kDa molecular complex that attaches at regular intervals to specific sites on Tm, and consists of three non-covalently linked subunits: The tropomyosin-binding (TnT), inhibiting (TnI) and Ca^{2+}-sensor (TnC) subunits (Craig & Padrón, 2004).

2.2. Brief Overview of Excitation-Contraction Coupling

The term *Excitation-Contraction Coupling* (ECC), depicted in Figure III, was originally coined by Alexander Sandow and refers to a series of events linking depolarization of the sarcolemma to the release of Ca^{2+} from the sarcoplasmic reticulum (SR), resulting in muscular contraction (Sandow, 1952). When force is to be produced, an action potential is initiated and propagated down a motor neuron, and crosses the neuromuscular junction. The action potential then propagates along the plasma membrane, followed by a radial spread of the potential across the sarcolemma. This *wave of depolarization* is taken into the muscle cell via membrane invaginations called transverse (t)-tubules (Franzini-Armstrong & Porter, 1964). The tight connection that exists between the t-tubule system and the flanking terminal cisternae of the SR on either side was dubbed a *triad* (Porter & Palade, 1957). This functional grouping acts as a junction between external and internal membrane systems, ensuring that every section of the muscle fibre is within 1 μm of a membrane that is continuous with the sarcolemma (Dulhunty, 2006).

Communication between the t-tubules and SR occurs at specific structures called *calcium release units* (Franzini-Armstrong & Protasi, 1997), involving dihydropyridine receptors within the t-tubule, and ryanodine receptors embedded within the SR membrane (Block, Imagawa, Campbell, & Franzini-Armstrong, 1988). Dihydropyridine receptors (DHPRs) are calcium channels that consist of 5 subunits: the transmembrane α_1 subunit, the γ and δ subunits found associated with the membrane, the α_2 subunit which is disulphide linked to the δ subunit, and the intracellular β subunit (as reviewed by Rebbeck, Karunasekara, & Board, 2014). The α_1 subunit is the principle functional subunit of the DHPR and functions as a voltage-gated ion channel (Leong & MacLennan, 1998).

The ryanodine receptors (RyRs) (Pessah, Waterhouse, & Casida, 1985) are the channels through which Ca^{2+} is released from the SR (Imagawa, Smith, Coronado, & Campbell, 1987). They exist as a homotetramer, with 4 equal subunits of 565 kDa, whose hydrophobic sections form a base that spans the SR membrane, and hydrophilic segments form a cytoplasmic domain bridging the gap between t-tubular membrane and SR membrane (Tupling, 2009).

DHPR-mediated detection of changes in plasma membrane potential lead to allosteric interactions between DHPRs and RyRs, facilitating an efflux of Ca^{2+} from the SR, and a transient elevation of the intracellular calcium concentration ($[Ca^{2+}]_i$) in the myoplasm (Leong & MacLennan, 1998; MacIntosh, Holash, & Renaud, 2012). Ca^{2+} ions diffuse, activating both myoplasmic Ca^{2+} buffering systems and the contractile apparatus. Several of the buffers that complex with Ca^{2+} include myosin ATPase, parvalbumin, sarco-endoplasmic reticulum calcium-ATPase (SERCA), and most importantly for excitation-contraction coupling, TnC (Baylor & Hollingworth, 2011).

Essentially, the electrical signal brings about a rise in $[Ca^{2+}]_i$, allowing Ca^{2+} to modulate the position of Tm on F-actin through its interaction with the Tn complex. At low $[Ca^{2+}]$, TnI locks Tm in a position on F-actin where it obstructs the myosin-binding site, thus preventing contraction. When Ca^{2+} binds to TnC, Tm moves on the actin filament, exposing the myosin-binding site (Behrmann et al., 2012). Within milliseconds the Ca^{2+}-Tn interaction eliminates the stearic inhibition imposed by TnI and Tm on the actin-myosin interaction, allowing the myosin head to bind to the now exposed myosin-binding site on actin. Binding forms a functional structure known as a crossbridge that can perform a power stroke, ultimately shortening the sarcomere and/or developing tension (Ebashi, 1991). During relaxation, the disappearance of Ca^{2+} from the myoplasm is mediated by its movement to the mitochondria, its transport by Na^+/Ca^{2+} exchanger (NCX) and its final reuptake into the SR through SERCA (Calderón, Bolaños, & Caputo, 2014).

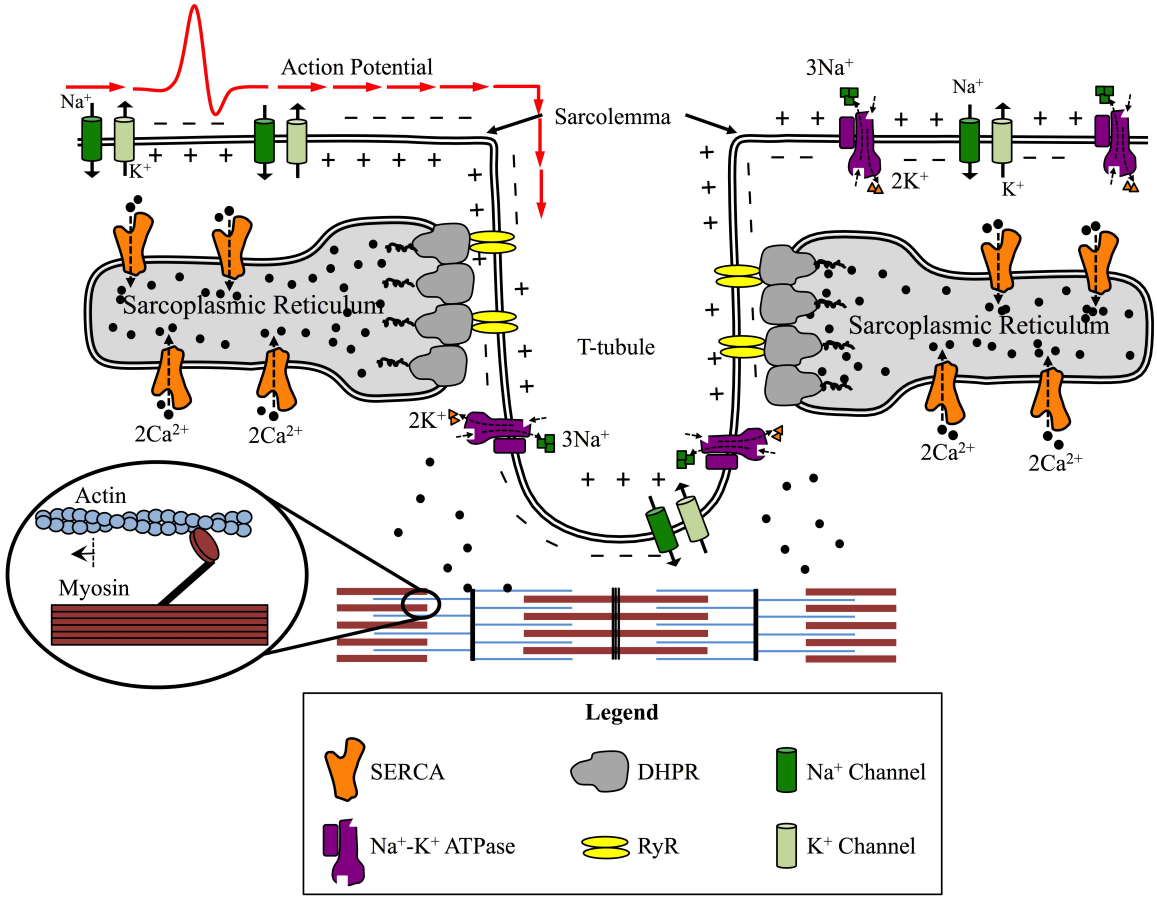

Figure III. Key proteins involved in excitation-contraction coupling.

2.2.1. The Intracellular Calcium Transient

The quanta of Ca^{2+} released from the SR during ECC leads to a temporary increase in myoplasmic [Ca^{2+}], referred to as an *intracellular calcium transient* (ICT). The amplitude and duration of the ICT is of fundamental importance to understanding muscle contraction because it directly determines the level of force generated and the amount of energy consumed by the muscle fibre, while also communicating with various downstream targets including enzymes and messenger proteins (Barclay, 2012; Chin, 2010). The rate of Ca^{2+} release from SR may be over 200 μmol/ms in fast twitch mammalian fibres, causing myoplasmic free calcium concentration ($[Ca^{2+}]_{free}$) to reach as high as 20 μM from a resting value of 100 nM (Baylor & Hollingworth, 2003) - a 200-fold increase. Incredibly, the maximum $[Ca^{2+}]_{free}$ is only a *small* fraction of the total Ca^{2+}

that is released, as a great deal of Ca^{2+} is buffered by binding to a variety of intracellular molecules.

2.2.2. Cooperativity

The ratio of the number of crossbridge cycles completed, to the number of TnC molecules complexed with Ca^{2+} provides information about cooperativity between Ca^{2+} binding and crossbridge attachment along the thin filament (Gordon, Homsher, & Regnier, 2000) and gives insight into the basis of the difference in energy expended on activation processes in fast and slow twitch muscle. Barclay (2012) suggests that rather than a single crossbridge cycle being performed for each molecule of TnC occupied by Ca^{2+}, binding of Ca^{2+} may actually facilitate the attachment of 1.7 crossbridges, on average. This is evidence of the phenomenon of *cooperativity*, in which binding of Ca^{2+} by TnC, inhibits stearic blocking of myosin-binding sites and allows attachment of a crossbridge, which itself facilitates the binding of *another* crossbridge without further Ca^{2+} binding. Ultimately, cooperativity increases thin filament activation without an increased cost of Ca^{2+} pumping (Gordon et al., 2000). Cooperativity is a likely a reason that inactivation of Ca^{2+} release occurs when a muscle fibre is stimulated twice within a short interval. During inter-pulse intervals under 100 ms, less Ca^{2+} is released in response to the second stimulus than in response to the first (Barclay, 2012). For example, according to *in situ* experiments, the motor unit firing rate that produces near-maximum force in fast twitch muscles from mouse hind-limbs is ~66 Hz (Manuel & Heckman, 2011). A stimulation frequency of 66 Hz corresponds to inter-pulse intervals of ~15 ms; an interval which displayed a 30% reduction in Ca^{2+} release between first and second twitches at 30°C (Barclay, 2012). It would seem that as stimulus rate increases, Ca^{2+} is released more often; however, less Ca^{2+} is released in response to each pulse. This relationship reduces the amount of energy needed to cycle Ca^{2+}, while cooperativity maintains a high level of thin filament activation.

In fast twitch fibres, two Ca^{2+} ions are required to fully occupy TnC, whereas only one Ca^{2+} ion per TnC is required in slow twitch fibres. Additionally, within the fast twitch EDL, Ca^{2+} binding to TnC at its maximum was 75%, compared to 84% in the slow twitch soleus. The difference in TnC occupancy reflects the competition for Ca^{2+} between Tn and parvalbumin (PV) in fast muscle, which is absent in slow muscle (Barclay, 2012).

Ultimately, we see higher cooperativity in slow twitch muscles such as the soleus, because half as much Ca^{2+} is required to occupy all available binding sites on the slow TnC isoform, and there is no competition between Tn and PV. The more complex TnC regulatory mechanism in fast muscle, combined with the presence of PV, gives the advantage of accelerated relaxation (Gillis, 1985); however, this comes at the expense of the additional energetic overhead associated with removing the extra Ca^{2+} from the myoplasm. Further energetic considerations of muscle activation, contraction, and relaxation will be discussed in sections to follow.

2.3. Crossbridge Cycling

The primary role of the intricately regulated interaction of actin and myosin is the generation of force and/or mechanical work (Winkelmann et al., 1991); this chief objective is accomplished as a consequence of the molecular dance known as *crossbridge cycling* (Krans, 2010). The term *crossbridge* stems from electron micrograph studies of skeletal muscle in rigor that revealed connections between the overlapping filaments, formed by the attachment of the globular head of myosin molecules to filamentous actin; these crossbridges are each *independent* force-generators (Rayment, Rypniewski, et al., 1993b). Cyclical interaction of the motor domain of myosin with the actin filaments is driven by the concomitant hydrolysis of ATP by myosin ATPases (Rayment, Holden, et al., 1993a): The binding and subsequent hydrolysis of ATP triggers a sequence of conformational changes in the myosin S1 that are associated with an approximately 10,000-fold change in its affinity for actin. The successive release of the hydrolysis products, P_i and ADP, causes large conformational changes that move myosin along actin filament (Behrmann et al., 2012).

In the early 1970's, the Lymn-Taylor Four State Cycle (Lymn & Taylor, 1971) was developed: A simplified framework used to comprehend the complex mechanochemical reaction cycle apparent during the cyclic interaction between actin and myosin.

2.3.1. Lymn-Taylor Four State Cycle

The four states of the cycle are Rigor, Post-Rigor, Pre-Power-Stroke, and Start-of-Power-Stroke (Figure IV). In the absence of ATP the myosin head remains bound to F-

actin in the Rigor complex. In Rigor, the cleft in the myosin head is closed, while the lever arm of myosin is in the *down* position. Upon binding of ATP, the large actin-binding cleft in the myosin head opens by rotational movements of the upper (U50K) and lower 50K (L50K) domains, disrupting the actin-binding site, causing the myosin head to rapidly dissociate from F-actin. With the crossbridge now detached and in the Post-Rigor State, there is an isomerization causing a recovery stroke, bringing the myosin head to a catalytically competent Pre-Power-Stroke state through a movement of the lever arm from the down position to the *up* position, accompanied by a half closing of the actin-binding cleft (Preller & Holmes, 2013). There is a rapid hydrolysis of ATP to form ADP and P_i on the free myosin head. The myosin-product complex is a meta-stable state with a long half-life which can await the arrival of an actin unit in the proper orientation to allow interaction (Lymn & Taylor, 1971). Now carrying the products of hydrolysis, the myosin head rebinds to the actin filament, followed by closing of the actin-binding cleft, and the crossbridge populates the Start-of-Power-Stroke State. Binding induces a conformational change, allowing the lever arm to swing from the up to the down position (Lymn & Taylor, 1971). After formation of the actin-myosin-product complex, dissociation of the products leaves the crossbridge in a configuration similar to that of a stretched spring, so tension is exerted or movement is produced in returning to the original conformation. This movement is called the Power Stroke, and facilitates sliding of actin past myosin. During the Power Stroke, P_i is released from the myosin head.

Small conformational changes in the myosin head domains or crossbridges are amplified to large-scale motions and translocation of the bound actin filaments. The large cleft separating the myosin head between the U50K and L50K domains, along with the neck region, acts as a lever arm and conveys together with the adjacent converter domain local conformational changes to large scale movements (Preller & Holmes, 2013). These conformational changes bring the steps full circle, and the crossbridge is now in once again in the Rigor state. Rapid rebinding of ATP leads to myosin dissociation from the filament and initiates a new cycle (Behrmann et al., 2012). These microscopic movements are amplified by the sarcomere arrangement, and result in macroscopic force production and muscle shortening (Barclay, Woledge, & Curtin, 2010a).

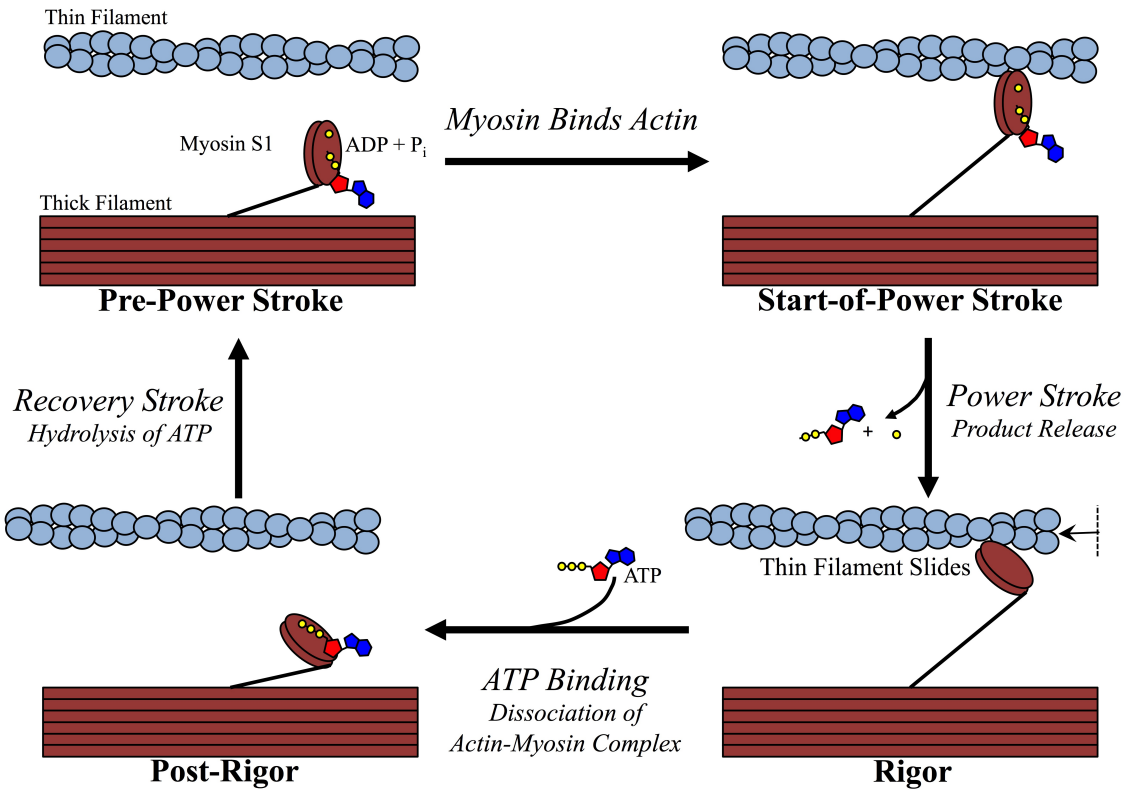

Figure IV. The Lymn-Taylor four state crossbridge cycle.

2.3.2. Kinetic Cycle

The Lymn-Taylor 4 Stage Cycle is a grossly oversimplified explanation of the crossbridge cycle, but is helpful to understand actin-myosin interaction in a general sense. In reality, the 4 major stages, and their associated transitions, can be broken down further to explore the sequence of events involved in the myosin ATPase reaction sequence. The following is a brief synopsis of the kinetic cycle, expanded to include weakly bound and strongly bound states (Figure V):

While sitting in rigor, the next kinetic cycle begins ATP rapidly binds to the myosin head which is currently associated with the actin filament, forming an actin-myosin-ATP complex ($AM \cdot ATP$), followed by the prompt dissociation of A from $M \cdot ATP$. Next, a fast and reversible cleavage of ATP on the myosin head forms $M \cdot ADP \cdot P_i$. The earlier rate of dissociation of the $AM \cdot ATP$ complex to A and $M \cdot ATP$ is so rapid and complete that virtually all cleavage of the nucleotide is completed on the

dissociated myosin head. Rapid reassociation of A and $M \cdot ADP \cdot P_i$ forms a weakly bound $A - M \cdot ADP \cdot P_i$ state that isomerizes to a more strongly bound $AM.ADP.P_i$ state - this transition is presumed to be regulated by Ca^{2+}. Strongly bound $AM \cdot ADP \cdot P_i$ isomerizes to produce force and lever arm motion, i.e. the Power Stroke ($AM** ADP \cdot P_i$), and may be stabilized in the strong binding force-exerting form by the release of P_i. The transition from weakly bound $A - M \cdot ADP \cdot P_i$ to $AM** ADP$ involves a large change in free energy and is the transition during which force is generated. Isomerization is followed by rapid release of ADP (Gordon et al., 2000).

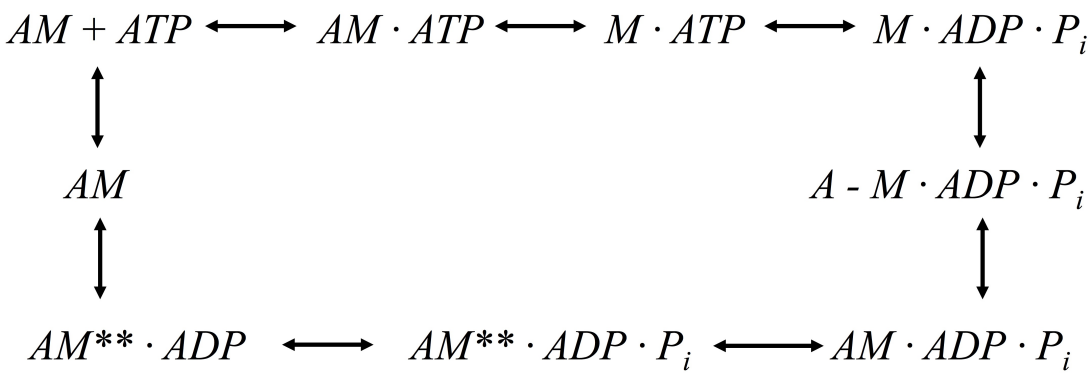

Figure V. Mechanochemical reaction cycle between actin and myosin.

2.4. Myosin Regulatory Light Chain Phosphorylation

The myosin II molecule contains two light chains, the regulatory light chain (RLC) and essential light chain (ELC), non-covalently bound to the α-helix of the MHC lever arm, functioning to both stabilize it and form a regulatory domain (Alamo et al., 2008). The myosin RLC has been known by several other names including light chain 2 (LC2), and perhaps most relevant to the current discussion, the *phosphorylatable* light chain (P-light chain). Phosphorylation of skeletal muscle myosin RLC was first noted in the early 1970s during electrophoretic analyses of rabbit skeletal muscle myosin (Perrie, Smillie, & Perry, 1973). In smooth muscle, RLC phosphorylation is recognized as the primary mechanism for initiating contraction (Ding et al., 2009); however, determining its role in skeletal muscle has required more rigorous examination.

2.4.1. Myosin Light Chain Kinase

Skeletal myosin light chain kinase (skMLCK) first emerged in the literature when Pires and colleagues (Pires, Perry, & Thomas, 1974) discovered that the enzyme responsible for phosphorylating the myosin RLC differed in several properties from the enzymes assumed to play this role, such as phosphorylase kinase. They noted that skMLCK was similar to the Tn-Tm regulatory system in its Ca^{2+}-sensitivity, and must therefore be fully active during the contractile cycle when myosin ATPase activity is high (Pires et al., 1974). In fact, the $[Ca^{2+}]_i$ required to regulate myosin ATPase activity through thin filament activation is sufficient to activate skMLCK; thus, it seemed that this new enzyme, and RLC phosphorylation, may play a role in the regulation of skeletal muscle contraction (Klug, Botterman, & Stull, 1982).

Only ~10% of RLCs are typically phosphorylated in resting skeletal muscle, as the activity of skMLCK is minimal in quiescent muscle. RLC phosphate content can be increased up to 7-fold when muscle is subjected to short duration (1-2 s) tetanic electrical stimulation or longer duration (5-20 s) low frequency (5-15 Hz) electrical stimulation (Manning & Stull, 1982). SkMLCK catalyzes phosphorylation of the phosphorylatable serine-15 residue within the N-terminus of myosin RLC, and as alluded to, is dependent upon Ca^{2+} and calmodulin (CaM) (Blumenthal & Stull, 1980). Activation of skMLCK is a two-step process (Figure VI) in which four Ca^{2+} ions bind to CaM forming a $Ca^{2+}{}_4$-

CaM complex that subsequently binds to the inactive form of skMLCK, creating a catalytically active holoenzyme capable of phosphotransferase activity (Blumenthal & Stull, 1980). In the absence of Ca^{2+}, as during rest, the kinase activity is auto-inhibited and CaM is not bound (Stull et al., 2011). The rate of CaM dissociation from skMLCK is slow, facilitating a longer period of skMLCK activity, even after $[Ca^{2+}]_i$ has diminished to levels allowing relaxation to occur; thus, RLC phosphorylation is able to continue for a brief period of time after relaxation. This slow rate of skMLCK inactivation has been referred to as a *biochemical memory* that enhances RLC phosphorylation after skeletal muscles fibers have relaxed (Stull et al., 2011).

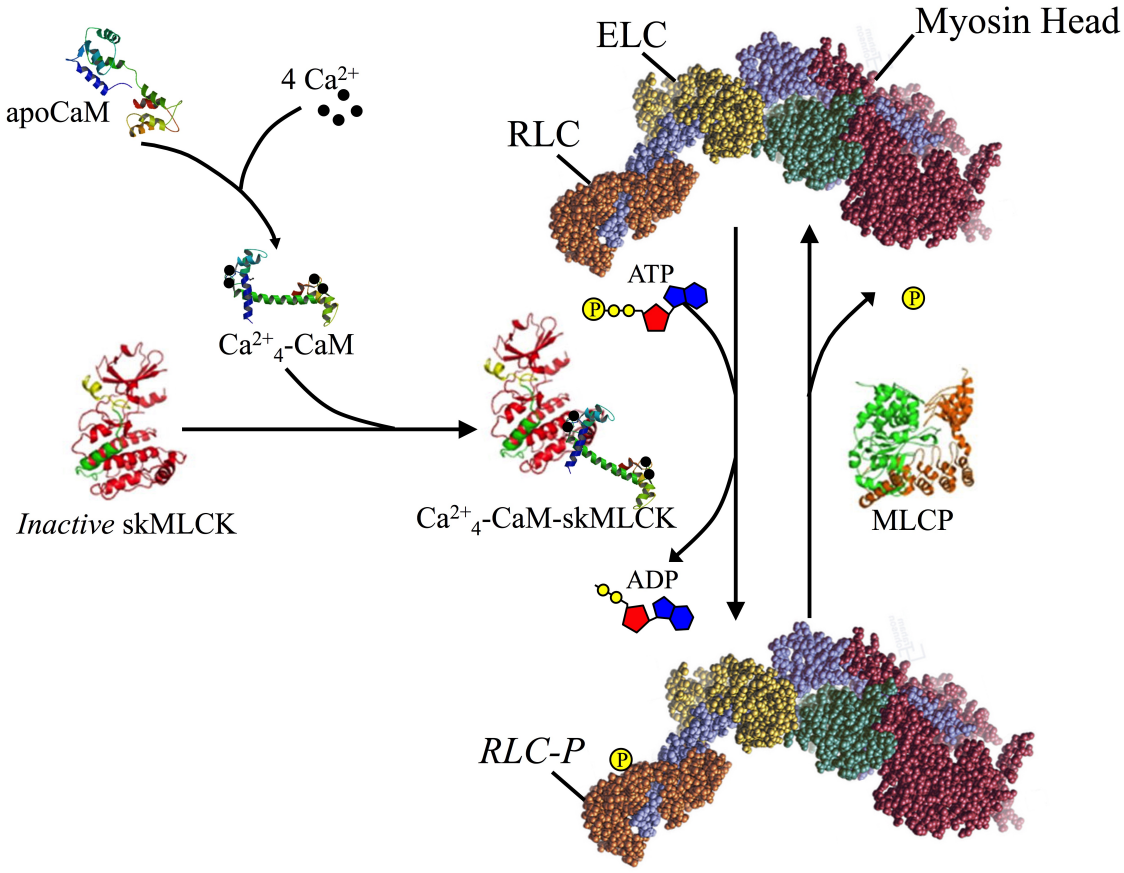

Figure VI. Sequential activation of skMLCK and covalent modification of the myosin RLC.

2.4.2. Myosin Light Chain Phosphatase

Since RLC phosphorylation is a form of covalent modulation catalyzed by skMLCK, there must exist another enzyme responsible for the reverse reaction, allowing the effect to remain transient. Indeed, it was soon discovered that the myosin RLC is dephosphorylated by a unique enzyme, highly specific for the RLC of myosin: Myosin light chain phosphatase (MLCP) (Morgan, Perry, & Ottaway, 1976). MLCP is composed of three distinct subunits including an isoform of protein phosphatase 1 (PP1cδ), a myosin-binding regulatory subunit isoform specific to striated skeletal muscle (MYPT2), and a small subunit whose function remains unknown (Matsumura & Hartshorne, 2008). In fast-twitch skeletal muscle, the maximal rate of RLC phosphorylation by skMLCK is ~50-times faster than the rate of dephosphorylation by MLCP (Stull et al., 2011). The existence of highly specific enzymes for phosphorylation and dephosphorylation of a single serine residue on the RLC of all vertebrate muscle myosin naturally raises the question of purpose. Researchers have taken to mechanistic studies in an attempt to discover the physiological function of RLC phosphorylation.

2.4.3. RLC Phosphorylation-Mediated Force Potentiation

Phosphorylation of the myosin RLC has a direct and predictable influence on the contractile performance of fast twitch skeletal muscle. A large body of research, spanning nearly a century, has demonstrated an irrefutable temporal correlation between RLC phosphorylation and potentiation of isometric twitch force (for a review, see Vandenboom et al., 2013). Potentiation is readily induced in fast twitch skeletal muscles, and this phenomenon is now considered a fundamental property of fast twitch skeletal muscle; some researchers even believe it may even be a normal operating feature of these muscles (Brown & Loeb, 1998).

Force potentiation is generally defined as an increase in isometric twitch force (P_t), independent of change to peak tetanic force (P_o), increasing the twitch to tetanus ratio (P_t:P_o) by heightening the Ca^{2+}-sensitivity of the contractile apparatus (Vandenboom et al., 2013). Since RLC phosphorylation is a biochemical memory of previous contractile activity, and depends on the activation of skMLCK by Ca^{2+} and CaM, the precise manifestation of potentiation is variable and depends greatly upon the stimulation

paradigm. Potentiation displayed after a fused tetanus is referred to as post-tetanic potentiation (PTP), while potentiation seen after low frequency, repetitive stimulation is referred to as staircase potentiation (Grange, Vandenboom, & Houston, 1993; Manning & Stull, 1982). In stark contrast to fast twitch muscle, slow twitch muscle demonstrates a post-tetanic *depression* of isometric twitch force (Buller, Kean, Ranatunga, & Smith, 1981).

Some of the most persuasive work, shifting the correlative nature of RLC-phosphorylation and force potentiation to a causal relationship, has come from studies using mice devoid of skMLCK (skMLCK$^{-/-}$). This unique model was created from the ablation of the MYLK2 gene, rendering the skMLCK$^{-/-}$ mice unable to express skMLCK (Zhi et al., 2005). Mice devoid of skMLCK do not display *isometric* PTP like their Wildtype counterparts; although, an attenuated staircase effect remains in response to low-frequency repetitive stimulation (Zhi et al., 2005). This discovery was somewhat unexpected, and had resounding implications for the field of study, as it is now believed that a secondary potentiation mechanism may exist.

2.4.4. Physiological Function of RLC Phosphorylation

Initial investigations attempting to discover a functional role of RLC phosphorylation in skeletal muscle relied on measurements of ATPase activity; however, RLC phosphorylation has no effect on maximal myosin ATPase rate (Sweeney, Bowman, & Stull, 1993). The effect of RLC phosphorylation is related to head-rod interactions, by which force is potentiated by moving the myosin head closer to the thin filament. In the relaxed state, i.e. in the presence of ATP and absence of Ca^{2+}, myosin heads exist in an ordered, helical array. Contrariwise, potentiation is associated with a disordering of active crossbridges (Duggal et al., 2014). The addition of a negatively charged phosphate moiety to the RLC results in charge repulsion between RLC and the thick filament backbone, disordering myosin heads positioned on the thick filament. This phosphorylation-induced loss of helical ordering is accompanied by a mass movement of myosin heads of about 6 nm away from the backbone surface (Figure VII), causing axial displacement of the heads out of the off-state towards the thin filament, resulting in modulation of Ca^{2+}-Tn-dependent force generation (Stull et al., 2011). Moving heads closer to actin increases the likelihood of interaction, which in turn increases the force

produced and rate of force development. This was supported through the observations made by Yang et al. (1998), that decreasing the distance between thick and thin filaments, effectively decreasing the lattice spacing and thus increasing the proximity of myosin and actin, potentiated force similar to the potentiation from RLC phosphorylation at greater spacing. RLC phosphorylation does not seem obligatory for contraction, and does not regulate, but rather *modulates* interaction with actin, by potentiating force at submaximal Ca^{2+} levels (Sweeney et al., 1993).

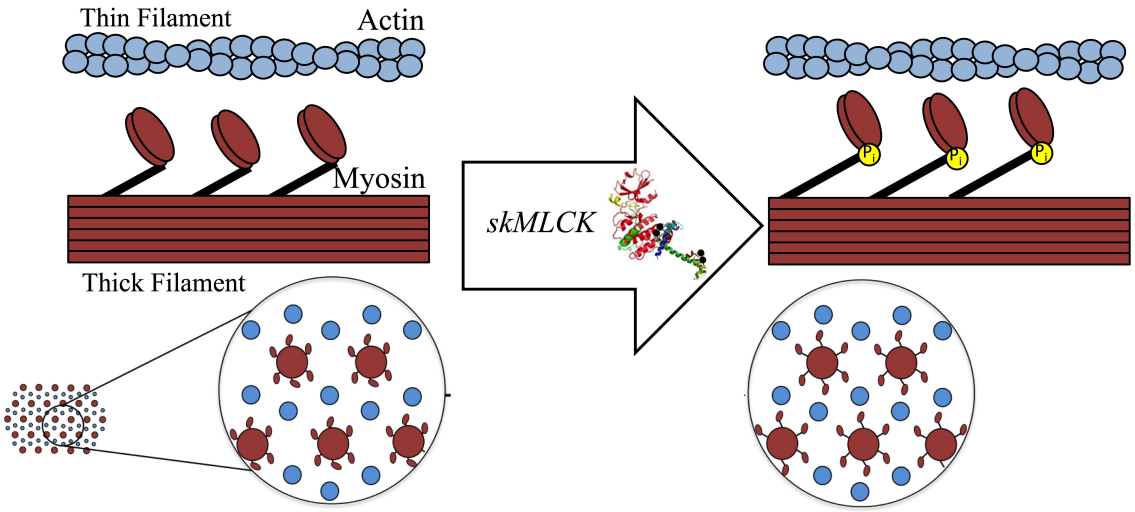

Figure VII. Mass movement of myosin heads away from thick filament backbone upon RLC phosphorylation.

RLC phosphorylation is also suspected to stiffen, and increase stability of the lever arm of myosin (Rayment, Holden, et al., 1993a). The neck region has been cited as a major source of crossbridge compliance; hence, a phosphorylation-induced stiffening of the lever arm would more efficiently transmit conformational changes into force, and could possibly increase unitary step size (Greenberg et al., 2009). The neck region also serves as a molecular strain sensor; thus, changing the stiffness of the lever arm would also change the strain sensitivity of the myosin biochemistry. The increased sensitivity to load would theoretically slow the rate of strain-dependent ADP release from the nucleotide pocket, increasing the myosin duty cycle (i.e. the fraction of time myosin spends bound to actin). Indeed, through use of an *in vitro* motility assay of endogenously

phosphorylated myosin, Greenberg et al. (2009) demonstrated a 44% increase in myosin duty cycle, accompanied by a 20% reduction in unloaded shortening velocity due to phosphorylation-based changes in myosin motor function. Overall, the *in vitro* motility assay demonstrated a reduced sliding velocity and an increased myosin duty cycle, resulting from phosphorylation-induced stiffening of the myosin lever arm.

2.4.5. Brenner Two-State Model

The simplified framework used to explain the physiological utility of myosin RLC phosphorylation was originally introduced by Brenner (1988), and extended the original crossbridge model of contraction (Huxley, 1957). This useful tool reduces the multiple states of the aforementioned crossbridge kinetic cycle to a simplistic two-state model. This model employs the apparent rate constants f_{app} and g_{app}, describing the transition from non-force generating to force generating states, and the transition from force-generating to non-force generating states, respectively (Sweeney & Stull, 1990).

RLC phosphorylation is believed to affect f_{app}, with no effect on g_{app}, or the number of cycling crossbridges. Therefore, the increase in force production seen at low levels of Ca^{2+} activation is not due to recruitment of *more* crossbridges into cycling *per se*, but rather due to an increase in the already cycling crossbridges that are strongly bound to actin and contributing to force production (i.e. f_{app}). This framework can also explain why increased force production is observed at submaximal $[Ca^{2+}]_i$, while increased rate of force development is observed at maximal $[Ca^{2+}]_i$, concomitant with RLC phosphorylation.

2.4.5.1. Force Production

Equation I describes the steady-state fraction of cycling crossbridges in the force-generating state (α_{Fs}) as a function of the rate constants f_{app} and g_{app}. In theory, the number of cycling crossbridges (n) and unitary force per crossbridge ($\bar{F}$) remain constant during RLC phosphorylation, while the fraction of crossbridges transitioning to the force-generating state (f_{app}) increases. During submaximal stimulation, $[Ca^{2+}]_i$ is low, the contractile apparatus is not yet fully activated, and g_{app} is theoretically greater than f_{app}. According to Equation I, during this time, a small increase in f_{app} will result in a large

change in the fraction of cycling crossbridges in the force-generating state, causing a large change in isometric force (as a function of number of crossbridges, unitary force, and the fraction of crossbridges contributing to force development, shown in Equation II).

$$\alpha_{Fs} = f_{app}/(f_{app} + g_{app})$$

Equation I. Fraction of crossbridges in the force-generating state.

$$F = n\bar{F}\alpha_{Fs}$$

Equation II. Isometric force equation.

Consequently, as f_{app} becomes increasingly larger relative to g_{app}, as expected during high levels of Ca^{2+} activation, any further increases in f_{app} resulting from RLC phosphorylation will have proportionally less effect on force.

When $[Ca^{2+}]_i$ is low $g_{app} \gg f_{app}$

$$\uparrow \alpha_{Fs} = \uparrow f_{app}/(\uparrow f_{app} + g_{app})$$

When $[Ca^{2+}]_i$ is high $g_{app} \ll f_{app}$

$$\leftrightarrow \alpha_{Fs} = \uparrow f_{app}/(\uparrow f_{app} + g_{app})$$

The myosin duty cycle, i.e. the time myosin is spent bound to actin, increases in the phosphorylated state because an increase in f_{app} with no change in g_{app} will lead to crossbridges that tends to populate the strongly bound state. While this will increase the force production, a higher duty ratio leads to decreased shortening velocity, as some crossbridges inevitably exert a *braking effect* on the sliding filament.

2.4.5.2. Rate of Force Redevelopment

The rate of isometric force redevelopment, represented in Equation III by the term K_{redev}, is equivalent to the sum of f_{app} and g_{app}. Therefore, in situations of low Ca^{2+} activation when f_{app} is smaller than g_{app}, a large fractional increase in f_{app} has little effect on K_{redev}, which theoretically approaches g_{app} at low [Ca^{2+}]. However, at higher Ca^{2+} activation, when f_{app} is larger than g_{app}, even a small fractional increase in f_{app} results in significant increase in K_{redev}; thus, the greatest effect of RLC phosphorylation on K_{redev} is observed at [Ca^{2+}] greater than where effects on force are observed.

$$K_{redev} = f_{app} + g_{app}$$

Equation III. Rate of force redevelopment equation.

$$\text{if } f_{app} \ll \boldsymbol{g_{app}} \text{ then } K_{redev} \approx g_{app}$$

$$\leftrightarrow K_{redev} = \uparrow f_{app} + \boldsymbol{g_{app}}$$

$$\text{if } \boldsymbol{f_{app}} \gg g_{app} \text{ then}$$

$$\uparrow K_{redev} = \uparrow \boldsymbol{f_{app}} + g_{app}$$

2.4.5.3. Myosin ATPase Rates

The steady-state isometric myosin ATPase rates (r_A) can be expressed as the product of the number of cycling crossbridges (n), the number of half sarcomeres in the fibre (b), g_{app}, and the fraction of crossbridges in the force-producing state (α_{Fs}) (Equation IV). Myosin ATPase activity has been shown to be proportional to force (Potma, Stienen, & Barends, 1994), and the relationship between isometric force (F) and r_A were determined experimentally to be linear (Brenner, 1988), validating the variable

terms in Equation II and Equation IV. Accordingly, RLC phosphorylation-mediated increases in f_{app} increase α_{Fs}, resulting in a proportional increase in both F and r_A.

$$r_A = nbg_{app}\alpha_{Fs}$$

Equation IV. Isometric myosin ATPase rates.

2.4.6. Why Phosphorylate the RLC?

Although a plethora of mechanistic research has proven that RLC phosphorylation benefits the contractile performance fast twitch skeletal muscles *in vitro*, Vandenboom et al. (2013) point out that a conclusive teleological role *in vivo* has not yet been identified. While some researchers believe that the potentiated state is the normal working state of fast twitch muscle (Brown & Loeb, 1998), others have suggested that phosphorylation of skeletal muscle RLC is only a residual trace of the evolution of cardiac myosin (Duggal et al., 2014). It may be that the mechanical changes observed during *in vitro* studies are nothing but an inevitable consequence incorporating a negative charge to the lever arm of myosin. In an evolutionary perspective, the eradication of an enzyme is only conceivable if its function can be dispensed with (Atkinson, 1977); thus, it stands to reason that the existence of highly specific enzymes responsible for the phosphorylation-dephosphorylation cycle of a single serine residue on the RLC of all skeletal muscle myosin signifies that RLC phosphorylation remains important to the performance of skeletal muscle.

Actin and myosin interact in skeletal muscle regardless of whether or not myosin is phosphorylated. Perhaps skMLCK plays yet another role that has yet to be elucidated, validating its very existence. An *in vitro* motility assay revealed that inactive skMLCK binds to actin, and inhibits actin-myosin interaction (Fujita et al., 1999). Interestingly, this inhibitory effect is overcome in a Ca^{2+}-dependent manner, such that the presence of $Ca^{2+}{}_4$-CaM, and the sequential activation of skMLCK, affects its actin-binding activity (Fujita et al., 1999). It seems possible that the actin-binding activity of skMLCK may be another level of regulation of thin-filament activation controlling actin-myosin interaction. If these findings are substantiated, it would have resounding implications on

the regulatory mechanism of contraction. The prospective story of the regulation of contraction may be the following:

During the initiation of contraction, Ca^{2+}-occupancy of TnC removes steric blocking of actin-myosin interaction by Tm. Simultaneously, $Ca^{2+}{}_4$-CaM complexes with skMLCK removing it from the actin filament, further disinhibiting the actin-myosin interaction. $Ca^{2+}{}_4$-CaM-skMLCK then phosphorylates the RLC, disorganizing the array of myosin heads, projecting them off the thick filament backbone, and increasing the likelihood of actin-myosin interaction and cooperativity, augmenting the Ca^{2+}-sensitivity of the contractile apparatus. All while RLC phosphorylation stabilizes the lever arm, improving the transmission of conformational changes into force.

2.5. Metabolic Considerations of Mammalian Skeletal Muscles

Adenosine triphosphate (ATP) is the best-known, and most widespread example of a common intermediate whose role is to carry chemical energy. ATP is colloquially referred to as the *energy currency* of the cell, and as such, is the immediate energy source for biological processes in skeletal muscle. Enzymes harness the energy released from the hydrolysis of ATP to perform useful work (Equation V).

$$ATP + H_2O \rightarrow ADP + P_i + Energy$$

Equation V. Hydrolysis of adenosine triphosphate.

During contractile activity, three principle enzymatic reactions hydrolyze ATP, constituting the majority of the ATP consumption within active skeletal muscle.

2.5.1. Energetics of Skeletal Muscle Contraction

The major ATP-consumers of skeletal muscle contraction include the following: The Sodium-Potassium ATPase (Na^+-K^+ ATPase), responsible for maintaining the electrochemical gradient, and thus the excitability of the sarcolemma; the myosin ATPase, responsible for powering the crossbridge cycle; and the Sarco-Endoplasmic Reticulum Calcium ATPase (SERCA), responsible for clearing Ca^{2+} from the myoplasm by sequestering it within the SR lumen (MacIntosh, Gardiner, & McComas, 2006; Rolfe & Brown, 1997; Tiidus, Tupling, & Houston, 2012). These 3 reactions (Figure VIII) dictate that force generation and trans-membrane ion pumping account for the vast majority of energy expended by contracting skeletal muscles, and that skeletal muscles require energy to both generate force and terminate contraction, via myosin ATPase and SERCA respectively (MacIntosh et al., 2012). During rest it is accepted that the Na^+-K^+ ATPases accounts for 19-28% of ATP consumption, while SERCA and myosin ATPases account for 4-8% and 2-8%, respectively (Rolfe & Brown, 1997) - the remainder being utilized for anabolic processes and cellular regeneration. However, during muscular contraction the relative contribution to ATP consumption shifts *drastically*.

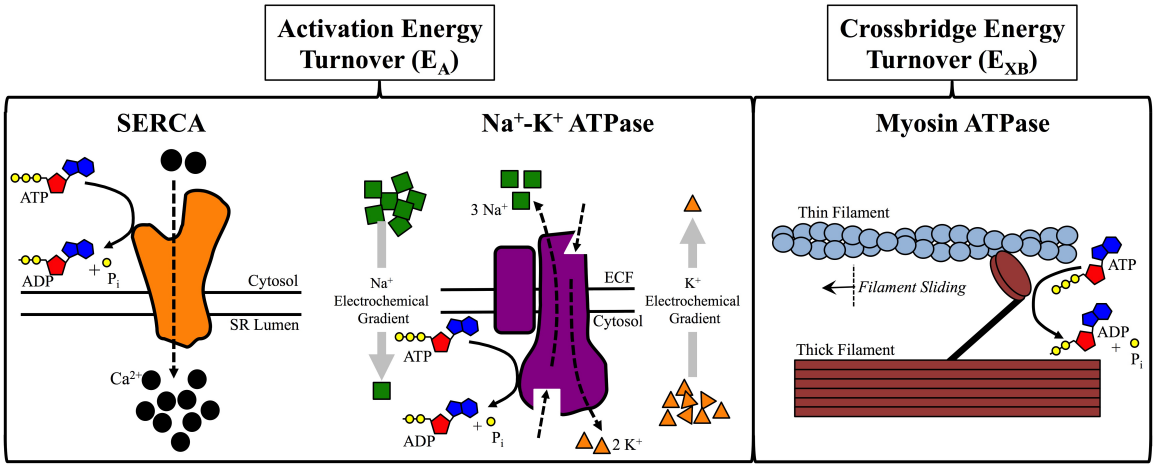

Figure VIII. Major energy consuming processes during skeletal muscle contraction.

2.5.2. Activation Energy Turnover

Since the majority of energy consumed by muscle contraction can be accounted for by two sets of ATP-dependent, cyclical processes (crossbridge cycling and Ca^{2+} cycling), it is commonplace for research investigating energy use by skeletal muscle to partition energy consumption into contractile and non-contractile ATP consumption. Energy turnover for ion pumping (i.e. Na^+-K^+ ATPase and SERCA), is referred to as the *activation energy turnover* (E_A) – and simply put, is all energy *unrelated* to crossbridge cycling (Barclay, Lichtwark, & Curtin, 2008; Barclay, Woledge, & Curtin, 2007). Energy partitioning is accomplished during *in vitro* studies through either pre-stretching the muscle to long sarcomere lengths to inhibit crossbridge cycling (Homsher, Mommaerts, Ricchiuti, & Wallner, 1972) or selective inhibition of crossbridge cycling through pharmacological agents such as 2,3-butanedione monoxime (BDM) or *N*-benzyl-*p*-toluene sulphonamide (BTS) (Barclay et al., 2008). BTS is currently the preferred pharmacological agent used to reversibly suppress force production of fast skeletal muscle due to its high specificity, and minimal interaction with Ca^{2+} metabolism (Cheung et al., 2001). The energy turnover in intact fibres is measured through either enthalpy production (e.g. Barclay, Constable, & Gibbs, 1993), biochemical analysis of metabolites (e.g. Homsher et al., 1972), or nuclear magnetic resonance (e. g. Baker, Brandes, & Schendel, 1994).

Historically, researchers believed that 50-80% of the total ATP consumed during skeletal muscle contraction was attributed to the myosin ATPase, with the remainder

accounted for by ion pumping (Zhang, Andersson, Sandstrom, Westerblad, & Katz, 2006). Yet, during continuous isometric tetanic contractions in which myosin ATPases had been inhibited via BTS, ATP turnover was reduced by only 20% (Zhang et al., 2006). This evidence suggested that ion pumping, and not crossbridge cycling, is the major user of energy during contraction in fast twitch skeletal muscle under near-physiological conditions. While these findings seemed groundbreaking at first glace, a letter to the editor by Barclay & Loiselle (2007) criticized Zhang's interpretation of data. Several of Barclay's subsequent papers called into question the methods used by Zhang et al. (2006), including their unacceptably slow freezing technique that may have allowed ATP hydrolysis to continue for several seconds (Barclay et al., 2007; 2008). In a response to the findings from Zhang et al. (2006), Barclay et al. (2008) determined that E_A accounts for just over 1/3 of energy turnover during isometric contractions in mouse EDL. These E_A values were the same regardless of the energy partitioning methods (i.e. reduced filament overlap or BTS).

E_A has been measured among muscles from different species (e.g. mouse, rat, fish, frog, human), all with different contractile and energetic properties. Regardless of these inherent differences, the experimental E_A value is often near 30% (Barclay et al., 2007; 2008). Lou, Curtin, and Woledge (1997) suggested that this 30% E_A is not simply an arbitrary value, and put forth the *Energy Minimization Hypothesis*. On one hand, slower SR Ca^{2+} reuptake would reduce E_A, but at the expense of slower relaxation leading to an extended crossbridge cycling cost. On the other hand, faster Ca^{2+} reuptake would hasten relaxation, halting energy consumption by crossbridge cycling, but at the expense of increased SERCA ATP consumption. It would seem that skeletal muscle, across many species, has evolved with a common goal of efficiency in mind.

An overlooked process that consumes ATP, and a potential contributor to E_A of fast twitch skeletal muscle, is phosphorylation of the myosin RLC. Although very little research has been done to investigate the energy turnover required to phosphorylate the RLC, it is likely that it is *not* a trivial amount. Following a fused tetanus, over 50% of the RLCs are phosphorylated (Vandenboom et al., 2013). It follows that if there are 125,822 crossbridges per μm^3, equating to a whole muscle concentration of 0.21 mM (Barclay, Woledge, & Curtin, 2010a), each with an RLC, then 1 cubic centimeter of muscle would

contain 0.21 μmol of RLCs. Phosphorylating 50% of the RLCs a single time would require the hydrolysis of 0.105 μmol of ATP (Equation VI); however, this is simply an instantaneous value, and the phosphorylation-dephosphorylation cycle that occurs *in vivo* during contraction would inevitably consume more ATP. Homsher (1987) predicted that the quantity of ATP consumed for this process may be equivalent to 5% of the energy used during a 5 s tetanus, but no research was conducted in attempt to reach a definitive answer.

$$0.21\ \frac{mmol\ XBs}{L} \cdot \left(\frac{1\ L}{1000\ cm^3}\right) \cdot \left(\frac{1000\ \mu mol}{1\ mmol}\right) = 0.21\ \mu mol\ XBs$$

$$0.21\ \mu mol\ XBs\ \cdot (50\%\ of\ RLCs) \cdot \left(\frac{1\ ATP}{1\ RLC}\right) = 0.105\ \mu mol\ ATP$$

Equation VI. ATP consumed during a single instantaneous phosphorylation of 50% of RLCs.

2.5.3. Efficiency of Muscle Contraction

Skeletal muscle is a thermodynamic machine, capable of directly transducing chemical energy into mechanical energy, and naturally, the transaction process occurs with some inherent degree of efficiency (Smith, Barclay, & Loiselle, 2005). Efficiency (Equation VII) is a quantification of the degree of conversion of chemical energy into work (Barclay, Woledge, & Curtin, 2010a), and can be defined in general terms as the ratio of mechanical power output (i.e. work completed) to metabolic power input (i.e. energy consumed) (Barclay, 1996).

$$Efficiency = \frac{Work\ completed}{Energy\ consumed}$$

Equation VII. General efficiency equation.

The precise definition of efficiency used depends on the method employed, the variables investigated, and the metabolic processes encompassed by the term metabolic power input. Several common definitions will be explored.

First, when a muscle contracts and shortens against a load it performs work (Equation VIII), fuelled by the expenditure of metabolic energy. Enthalpy is a term that describes thermodynamic potential, or the internal energy of system, and change in enthalpy (ΔH) reflects the difference in energy that occurs during the performance of work. Enthalpy (Equation IX), denoted with a negative sign signifying a decrement of internal energy, includes the thermal accompaniment of work, and is equated to work (w) plus heat (h). Thus, the ratio of work performed to enthalpy produced provides a measure of mechanical efficiency (ε), as shown in Equation X.

$$W = F \cdot d$$

Equation VIII. Work defined as the product of force and displacement.

$$-\Delta H = W + h$$

Equation IX. Enthalpy change is useful work and its thermal accompaniment.

$$\varepsilon = \frac{W}{\Delta H} = \frac{W}{W + h}$$

Equation X. Mechanical efficiency is the ratio of work to enthalpy.

As discussed, the energy turnover for Ca^{2+} cycling constitutes a substantial faction of the cost of contraction in skeletal muscle. Although this energy is essential for contraction, it cannot be converted into mechanical work; thus, the efficiency of intact muscle will inevitably be less than that of the work generated by crossbridges alone (Barclay et al., 2007). If the primary interest is in the efficiency of the actin-myosin crossbridges, the metabolic overheads associated with basal metabolism and ECC (i.e. E_A), together with those of subsequent metabolic recovery processes must be subtracted from the total heat and work observed (Smith et al., 2005).

Based on first law of thermodynamics, the *Law of Conservation of Energy*, the enthalpy change from chemical breakdown in a muscle is converted into either heat or work. The heat liberated from a muscle during contraction stems from the same biochemical reactions that power the work it performs when lifting a load; thus,

measurements of the rates of heat and work output from a muscle (i.e. enthalpy) can provide an indirect measure of the rate of ATP breakdown. While the metabolic power source for contraction is ATP hydrolysis, this reaction is rapidly reversed at the expense of phosphocreatine (PCr) through the creatine kinase (CK) reaction, which will be discussed in depth in the upcoming sections. Under normal working conditions, there is no net breakdown of ATP as is it rapidly resynthesized by the CK reaction. For that reason, the net chemical change during contraction is the breakdown of PCr, and the enthalpy liberated from a contracting muscle proportional to the rate of PCr hydrolysis which is reflected in the heat and work production (Barclay et al., 1993).

Although Equation X seems appealing for determining efficiency, it can be somewhat misleading as not all of the enthalpy change is actually *available* to perform useful work, and only a fraction of the heat produced during contraction can be explained by chemical changes (de Haan et al., 1986). Since the fraction available to perform work is termed the Gibbs free energy (ΔG), a more useful measurement in this area of study is *thermodynamic efficiency* (Equation XI):

$$\eta = \frac{W}{\Delta G_{ATP}}$$

Equation XI. Thermodynamic efficiency.

Where:

$$\Delta G_{ATP} = \Delta G^{\circ}_{ATP} + RT \ln \frac{[ADP][P_i]}{[ATP]}$$

Equation XII. Free energy released during ATP hydrolysis.

ΔG_{ATP} can be determined experimentally using Equation XII. Several terms remain constant, including ΔG°_{ATP}, the standard Gibbs free energy associated with ATP hydrolysis and R, the gas constant. Thus, by measuring T, temperature of the active muscle, and the intracellular ADP:ATP ratio, one can calculate ΔG_{ATP} and subsequently, thermodynamic efficiency.

Enthalpy and free energy change are common indices of the energy consumed; however, it is also possible to measure changes in intracellular concentrations of ATP

and/or PCr, without the equipment necessary to measure heat production. The extent of chemical breakdown, referred to as *high-energy phosphate consumption* or HEPC (e.g. Abbate et al., 2001), can be measured by stopping the chemical reactions at a set time by rapid freezing and analyzing the chemical composition of the extracts. This technique uses intact fibres, giving an advantage over skinned fiber studies in that the crossbridges are functioning in their normal intracellular environment (Barclay, Woledge, & Curtin, 2010a). The ratio of force or work produced to high-energy phosphate consumption is referred to as *economy* (Goldspink, 1978) to differentiate it from the classical thermodynamic definitions of efficiency. Economy (Equation XIII) can be expressed as Ns/μmol energy-rich phosphate (~P) (De Haan et al., 1986) or J/μmol ~P (Abbate et al., 2001).

$$Economy = \frac{F \text{ or } W}{HEPC}$$

Equation XIII. Economy calculated using consumption of high-energy phosphates.

2.5.4. Possible Factors Impacting Efficiency and Economy

2.5.4.1. Fibre Type

It is well established that the mechanical and energetic properties of muscle fibres are determined to a large extent my myosin isoforms. MHC isoforms determine isometric ATP consumption, tension cost and rate of tension redevelopment after unloaded shortening. The efficiency of fast twitch mouse EDL is 0.29 – 0.33, while slow twitch mouse soleus is 0.33 to 0.43 (Barclay, 1996; Barclay et al., 1993).

2.5.4.2. Temperature

It would seem plausible that since temperature has a drastic effect on enzymatic activity and metabolism, that temperature would also be a major factor in the mechanical efficiency of a working muscle. Interestingly enough, it appears that the maximum mechanical efficiency of isolated mouse muscle is little affected by temperature between the range of 20 to 30°C (Barclay, Woledge, & Curtin, 2010b).

2.5.4.3. Contraction Type

During isometric contractions, no shortening is performed; thus, no work is performed, making the previous efficiency calculations impossible. This hurdle is overcome by utilizing the area under the force-time curve, referred to as the *force-time integral* (FTI), which is commonly used to approximate *isometric work* (e.g. Chasiotis, Bergstrom, & Hultman, 1987; Crow & Kushmerick, 1982a; Hogan, Ingham, & Kurdak, 1998; Russ, Elliott, Vandenborne, Walter, & Binder-Macleod, 2002). Interestingly, brief intermittent contractions produce greater ATP turnover compared to longer sustained contractions when either the total contraction time (Bergstrom & Hultman, 1988) or total number of contractions (Hogan et al., 1998) remains constant. This led to the hypothesis that force generation is more costly than force maintenance. To determine the answer *in vivo* using ^{31}P-NMR spectroscopy, Russ et al. (2002) measured the metabolic cost and ATPase rates in human muscle (medial gastrocnemius) in response to various stimulation frequencies and durations. Their work confirmed the notion that in mammalian skeletal muscle, the metabolic cost of attaining isometric force is higher than maintaining that force output. ATPase rates during short contractions are higher than during long contractions, making the initial production of force more metabolically costly than maintaining it (Russ et al., 2002).

Contradictory to early studies in which energy output was thought to decrease during shortening to a level below isometric energy consumption, follow up work suggested that energy consumption increases when external work is performed (Reggiani et al., 1997). This phenomenon was dubbed the *Fenn Effect*, which dictates that when a muscle shortens and does mechanical work, additional energy is liberated above that appearing in the isometric contraction, the additional energy liberated is proportional to the work done (i.e. the distance shortened or the load) (Fenn, 1923; 1924). The energy liberated by contraction is not dependent solely upon the initial mechanical and physiological condition of the muscle, but can be modified by the nature of the load, which the muscle discovers during stimulation. The driving reactions are regulated by the force and or shortening occurring in contraction (Woledge, Curtin, & Homsher, 1985).

2.5.4.4. Activation Level

Level of activation, defined as the availability of crossbridge binding sites on the thin filament, is dependent upon $[Ca^{2+}]_i$ and thus the stimulation paradigm. Abbate, de Ruiter, Offringa, and Sargeant (2002) determined efficiency was lower when using maximal activation (150 Hz) compared to submaximal activation at two different frequencies (60 or 90 Hz) during in situ isovelocity shortening contractions of rat gastrocnemius. It is likely that maximal activation by high frequency stimulation leads to a decreased efficiency, as the result a larger efflux of Ca^{2+}, resulting in an increased energy expenditure by SERCA relative to total energy turnover. Another possible explanation is that the reduction in force at submaximal activation is accompanied by an alteration in the crossbridge efficiency.

Lewis & Barclay (2014) picked up where Abbate et al. (2002) and several other groups left off, as no clear consensus was reached as to the effect of activation level on efficiency. It was confirmed that less Ca^{2+} is released at submaximal than maximal stimulation frequencies, lending weight to the theory that increased SERCA activity reduces efficiency at during maximal activation (Abbate et al., 2002). However, it appears that skeletal muscles are actually less efficient during low levels of activation because a lower $[Ca^{2+}]_i$ leads to the performance of fewer crossbridge cycles, and more importantly, less work per crossbridge cycle (Lewis & Barclay, 2014).

Overall, it seems that the efficiency and economy of a working muscle is dependent on a number of factors, including the muscle fibre type, the force required to move a load, the distance of shortening, and the level of activation, whereas temperature and species do not play an important role.

2.5.5. Energy Producing Processes in Skeletal Muscle

Energy balance must be attained for proper functioning of skeletal muscle tissue, meaning that ATP utilization must be met with an equal ATP production. This is true even during times of intense exercise, when energy demands increase 100-fold almost instantaneously. The ATP concentrations in skeletal muscle tissue are low, ranging from 2 to 6 mmol of ATP per kilogram, which theoretically would only be sufficient to sustain up to two seconds of maximal work (Tiidus et al., 2012).

2.5.5.1. Adenylate Charge

Energy transduction and energy storage involving ATP, ADP, and AMP, collectively referred to as the *adenylates*, are at the core of skeletal muscle metabolism. These adenine nucleotides interact with every energy consuming and producing reaction within the muscle, and directly impact enzymatic reactions through mass action and end-product inhibition. Thus, uncontrolled changes in the relative concentrations of ATP, ADP and AMP would affect the rates of all metabolic reactions and be *highly* disruptive. Close control of the relative concentrations is essential to correlation of fluxes through metabolic pathways. Since ATP is consumed or regenerated in every metabolic sequence, the level of energy storage in the adenylate system can be controlled by governing the rates of all metabolic sequences, through sensing the energy level of the adenylate system and using this information as a basis of control (Atkinson, 1977).

A useful concept is the *Adenylate Energy Charge*, which allows the energetic state of a biological system to be expressed quantitatively. It is a measure of the phosphorylating power of an adenylate pool, equal to one half the average number of anhydride-bound phosphoric groups per adenosine moiety present in the pool (A. D. Smith, 2000). Defined in terms of the concentrations of AMP, ADP and ATP in the pool, and expressed by the quotient in Equation XIV.

$$\frac{([ATP] + 0.5[ADP])}{([ATP] + [ADP] + [AMP])}$$

Equation XIV. Adenylate energy charge.

The adenine nucleotides within the cell are often described using the analogy of chemicals in a battery (Atkinson, 1977; Hardie & Hawley, 2001): The battery of the skeletal muscle cell is charged up by converting ADP and P_i to ATP, while the battery is discharged by cellular processes coupled to ATP breakdown. Theoretically, a completely charged *battery* would be reflected by an adenylate energy charge of 1 (*all ATP*), while 0 (*all AMP*) would reflect a completely discharged battery. On average, the quantity of ATP used per second is equal to the steady-state amount of ATP in the cell, meaning that total ATP turnover time is typically of the order of 1 second or less (Atkinson, 1977). In

other words, the capacity of the adenylate battery is so small that it would be totally discharged in about a second if charging were to stop and energy use to continue at a normal rate.

2.5.5.2. Maintenance of the ATP:ADP Ratio

One of the most fundamental parameters that any healthy muscle cell must maintain is a high ratio of ATP to ADP, usually around 10:1. Healthy cells maintain the reactants and products of hydrolysis reactions many orders of magnitude away from their equilibrium ratios, ensuring that the energy from hydrolysis can be harnessed to perform useful work when coupled to processes requiring an input of energy (Hardie & Hawley, 2001). ATP is highly conserved by efficient buffering by the CK reaction, and any decrease in ATP is small. However since muscle content of ADP is 10-fold lower than ATP, even a small decrease in ATP can drastically increase ADP. Increases in [ADP] will reduce the free energy released during ATP hydrolysis (ΔG_{ATP}), and eventually impair all ATPase reactions, reducing the amount of useful work that can be performed. CKs important function is not only to defend ATP concentration but also prevent large increases in ADP. The concentration of ATP is maintained by three key energy systems, of which the two *anaerobic* systems will be discussed. The potential energy sources during muscular activity of short duration include partial depletion of the endogenous ATP store, breakdown of phosphocreatine (PCr), anaerobic glycolysis to lactate, and oxidative metabolism (Spriet, 1989).

The contribution of the endogenous ATP store is quantitatively insignificant in most contractile situations, as it is highly conserved, and oxidative metabolism contributes in only a minor way during intense exercise of short duration; thus, the major sources of ATP resynthesis during intense anaerobic muscular activity are PCr degradation, and glycolysis from glycogen (Spriet, 1989). The net production of ATP from these two anaerobic systems is known as *substrate-level phosphorylation*, and includes the following enzyme catalyzed reactions: the creatine kinase reaction, the adenylate kinase and AMP deaminase reactions, the glycolytic pathway reactions, and the lactate dehydrogenase reaction.

2.5.5.3. Creatine Kinase Reaction

A major problem facing skeletal muscle fibres is the large disparity between energy demand at rest, and the energy demands of contraction, as they differ by more than an order of magnitude (Sweeney, 1994). The creatine kinase (CK) reaction (Equation XV), also referred to as the *Lohmann reaction*, is very effective at maintaining the ATP concentration during muscular activity (Woledge et al., 1985). At the onset of contraction, the increased ATP demand is immediately met by a shift in the CK reaction that decreases [PCr] without a change in [ATP]. The reaction has an equilibrium constant of 100 at physiological pH and temperature; meaning that this near equilibrium dead-end reaction is pushed towards products, and the equilibrium shift keeps [ATP] relatively constant over a wide range of ATP fluxes in the cell (Woledge et al., 1985). Consequently, a reduction in the PCr:Cr ratio results in a much smaller reduction in the ATP:ADP ratio. PCr acts as an energy buffer by providing an additional pool of energy rich phosphate compounds (i.e. an energy reserve) to aid in maintaining cellular ATP levels. This reservoir of high-energy phosphates defends cellular ATP levels under anaerobic conditions, high rates of energy transfer, or rapid fluctuations in energy requirements (Sahlin & Harris, 2011).

$$PCr + ADP + H^{+} \xleftrightarrow{Creatine\ Kinase} ATP + Cr$$

Equation XV. Regeneration of ATP through the creatine kinase reaction.

To be considered a *biochemical capacitor*, the flux capacity of a buffer reaction must be greater than the flux of the reaction being buffered; indeed, the flux of CK is much higher than either maximal ATPase or ATP synthesis flux. PCr is a sensitive indicator of the energetic status of the cell because changes in ATP flux cause a shift in the CK equilibrium that is reflected in [PCr]. The CK reaction has well-established roles as a temporal and spatial buffer of ATP, a proton buffer, and a key controller of oxidative phosphorylation (Sahlin & Harris, 2011). Temporal buffering, or metabolic capacitance, allows for a lower mitochondrial density than would be necessary to support the peak energy demand during contraction. The metabolic capacitance offered by the CK reaction lowers the apparent peak demand and increases the period of elevated energy demand so

that much of the regeneration of ATP is distributed to the resting state. The CK reaction is a more *economical* energy delivery system used by cells that have a peak energy demand that is in excess of its average energy demand (Sweeney, 1994) such as fast twitch skeletal muscle. The CK reaction generates ADP, the key factor in regulating mitochondrial oxidative phosphorylation, and thus oxidative ATP supply. In essence, there is a double role of the shift in PCr, not only buffering short-term ATP demands, but also elevating the signal for longer-term oxidative ATP supply.

2.5.5.4. Adenylate Kinase and AMP Deaminase Reactions

During intense muscular activity, the rate of ATP hydrolysis increases instantaneously. Although ATP is being resynthesized from ADP and PCr through the CK reaction, there is an inevitable rise in [ADP]. Large increases in [ADP] activate the adenylate kinase (AK), or *myokinase* reaction (Equation XVI), which transfers the P_i from one ADP to another, regenerating one molecule of ATP while creating AMP, or adenosine monophosphate (Sahlin & Harris, 2011).

$$2\ ADP \xleftrightarrow{Adenylate\ Kinase} ATP + AMP$$

Equation XVI. Adenylate kinase reaction.

The rate constant of the AK reaction is unitary under normal resting conditions, implying that it does not play a major role in resynthesizing ATP, *except* during times of metabolic distress when accumulation of ADP pushes the near equilibrium reaction towards products in an attempt to restore the ATP:ADP ratio. Although the production of ATP is minimal, this reaction is another line of defense, preventing a drastic change in the all-important ATP:ADP ratio (Tiidus et al., 2012). The reaction proceeds at an substantial rate during exercise, and is rendered more effective by the subsequent removal AMP (Woledge et al., 1985). AMP deaminase (Equation XVII) irreversibly removes the amino group from the base adenine of AMP produced in the AK reaction, yielding ammonia (NH_3) and inosine monophosphate (IMP).

$$AMP \xleftrightarrow{AMP\ Deaminase} IMP + NH_3$$

Equation XVII. AMP deaminase reaction.

The irreversible deamination of AMP removes the product of the AK reaction, and drives the reaction forward through mass action to further diminish any increase in [ADP]. These two reactions work in concert during intense contractions, and are extremely important in maintaining optimal energy status in the muscle.

2.5.5.5. Glycolysis and Lactate Dehydrogenase Reactions

Much more complex than a single reaction, glycolysis (Equation XVIII) is the metabolic pathway for carbohydrate breakdown in all cells involving a sequence of enzyme-catalyzed reactions.

$$Glycogen_n + 3\ ADP + 3\ P_i + 2\ NAD^+ \rightarrow Glycogen_{n-1} + 2\ Pyruvate + 3\ ATP + 2\ NADH + 2\ H^+$$

Equation XVIII. Summary of the glycolysis pathway starting with glycogen.

Glycolysis is referred to as anaerobic if the energy production does not require oxygen, and only relies on substrate-level phosphorylation, such as pyruvate being reduced to lactate in the cytosol (Equation XIX) – this is a major energy source of ATP for skeletal muscle during intense exercise conditions.

$$Pyruvate + NADH + H^+ \xleftrightarrow{Lactate\ Dehydrogenase} Lactate + NAD^+$$

Equation XIX. Lactate dehydrogenase reaction.

Apparently, ATP consuming processes in skeletal muscle have preference as to their energy source. ATP for crossbridge cycling is supplied in equal proportion from glycolysis and the CK reaction (48 and 52%, respectively), while the ATP for E_A was preferentially derived from glycolysis versus CK (61 and 39%, respectively) as measured through ^{31}P-NMR (Baker et al., 1994).

2.5.6. Quantifying Anaerobic ATP Provision

Measurement of steady state oxygen consumption, along with a quick calculation are all that is required to determine the aerobic contribution to ATP production; however, the process of quantifying *anaerobic* ATP provision is more laborious. Since ATP hydrolysis is speedily reversed at the expense of PCr, and the net biochemical reaction is PCr hydrolysis (Barclay, 1996), measuring the change in [PCr] is indicative of ATP consumption.

$$Total\ ATP\ Provision = -\Delta[PCr] - 2\Delta[ATP] + 1.5\Delta[Lactate]$$

Equation XX. Calculating total ATP provision from substrate level phosphorylation.

In Equation XX, ΔPCr represents the ATP produced from the decline in muscle PCr content from rest. 1.5ΔLactate represents the ATP produced from the glycolytic production of lactate with a net gain of 1.5 ATP per lactate molecule generated, representing 3 ATP produced per glucose molecule derived from muscle glycogen. 2Δ[ATP] represents the total ATP utilization from the stored ATP pool in resting muscle. The change in ATP concentration is doubled because the reduction in muscle ATP with exercise is theoretically equivalent to the increase in IMP. In other words, 2 ATP must be hydrolyzed to produce a net change of 1 ATP, since IMP is produced from AMP in the AMP deaminase reaction, which was a product of the adenylate kinase reaction, requiring 2 ADP. Originally, those 2 ADP were produced from the hydrolysis of 2 ATP during ATPase reactions; however, the net decrease is only 1 ATP, as the adenylate kinase reaction was responsible for the production of 1 ATP (Tiidus et al., 2012). This equation is also referred to as *high-energy phosphate consumption* (HEPC), as discussed in previous sections.

2.6. Metabolic Consequences of Potentiation

Work published throughout the previous two decades has produced equivocal and contradictory results, leaving the question largely unanswered: Does a relationship exist between RLC phosphorylation-mediated potentiation and metabolism? *Equation 4* from the Brenner Two-State Model states that myosin ATPase rates are increased in proportion to the increased force produced by RLC phosphorylation; however, if potentiation augments the relationship between mechanical output of a muscle and the energetic input, it may have vast implications on the contractile economy of muscles in the working state. As the primary mechanism of RLC phosphorylation-mediated force potentiation is confined to fast twitch skeletal muscle, this section will not discuss slow twitch skeletal muscle. When considering all of the complexities inherent in the regulation of skeletal muscle contraction and chemical energy utilization, it seems helpful to approach this question by exploring the three plausible outcomes experimentation can lead to: (1) RLC phosphorylation has no effect on the economy of contraction (2) RLC phosphorylation increases the economy of contraction (3) RLC phosphorylation decreases the economy of contraction.

2.6.1. Evidence of No Consequence

If chemical energy consumption increases in proportion to the increase in work or force produced by fast twitch skeletal muscle in the potentiated state, there would be no demonstrable change in economy. Barsotti & Butler (1984) set out to determine whether RLC phosphorylation modulated the rate of chemical energy consumption using maximally stimulated rat EDL. Not surprisingly, they reported that elevated RLC phosphorylation had no effect on maximal twitch force or energy consumption (Barsotti & Butler, 1984). This result may be in part due to the stimulation paradigm that was selected. As discussed in previous sections, RLC phosphorylation increases twitch force, without an increase in tetanic force; thus, no increase in maximal force should have been expected. With muscle maximally activated, and no manifested force potentiation, the relationship between RLC phosphorylation and chemical energy usage cannot be accurately explored.

2.6.2. Evidence of Increased Economy

Increasing the force production of contraction to a greater extent than energy consumption during the potentiated state would suggest that RLC phosphorylation increases the economy of contraction. In this regard, Crow & Kushmerick (1982b) reported a correlation between a myosin RLC phosphorylation and reduced energy cost for isometric tetani in mouse fast twitch muscle. It was hypothesized that actin-myosin interaction can be down-regulated by reversible covalent modification of myosin light chains, as a form of thick filament regulation (Crow & Kushmerick, 1982c). If, indeed, RLC phosphorylation resulted in a decreased ATPase rate during isometric tetani, an increased economy would be extant. Downward regulation of actin-myosin turnover makes physiological sense during isometric contractions when their physiological utility is considered: While maintaining contraction of a mixed muscle type, the mechanical speed and power of fast fibers used for limb acceleration/rapid movements is no longer necessary or useful (Crow & Kushmerick, 1982b). Increased efficiency in the potentiated state seems possible, as RLC phosphorylation allows a specific level of force to be maintained at a lower [Ca^{2+}]. If a smaller ICT is required to produce the same amount of force as a muscle in an unpotentiated state, the working muscle will consume less energy clearing Ca^{2+} from the myoplasm (i.e. SERCA) during the contractile cycle (Sweeney et al., 1993). There is also some evidence to suggest that motor unit firing rate is down regulated while the muscle is in the potentiated state (Adam, 2005; Inglis, Howard, McIntosh, Gabriel, & Vandenboom, 2011). Decreasing the neural drive in vivo compensates for the short-lived potentiation of twitch force, another situation which would allow a given level of force output to be maintained with less frequent stimulation; theoretically, reducing the energetic overhead required for Ca^{2+} cycling.

2.6.3. Evidence of Decreased Economy

The most recent research conducted in this field claimed that post-tetanic potentiation in rat skeletal muscle increased the energetic cost to a larger extent than work; thus, reducing the economy of contraction (Abbate et al., 2001). There are several possible explanations as to why potentiation may lead to an increased energy cost. First and foremost, phosphorylation of the RLC still requires an initial investment of ATP, as

discussed in previous sections, the phosphorylation of upwards of 50% of RLCs in fast twitch muscle may be a costly endeavor, resulting in a large energetic overhead for the working muscle. Secondly, it is clear that complex interactions between RLC phosphorylation and muscle energetics exist. Any changes in the contractile function of the myofilament may be responsible for the reported increase in energy turnover, and it is suspected that there are metabolism-related alterations in crossbridge function during contraction (Stull et al., 2011). Although the fraction of cycling crossbridges transitioning to the force-generating state (f_{app}) increases with RLC phosphorylation, this may be accompanied by a reduced efficiency of the crossbridges. Ultimately, it is possible that there is a decreased mechanical output for each ATP hydrolyzed in the potentiated state, resulting in a reduced efficiency of the working muscle (Abbate et al., 2001).

Overall, evidence has been presented supporting each of the three possible relationships between RLC phosphorylation mediated force potentiation and energy consumption. Considering all lines of reasoning, it seems most plausible that RLC phosphorylation may increase the contractile economy of the working muscle *in vivo* due to a reduction in energetic overhead of Ca^{2+}-cycling (i.e. a reduced E_A) facilitated by increasing the Ca^{2+}-sensitivity of the contractile apparatus.

Statement of Problem

Conflicting evidence has been reported for the relationship between contractile economy and RLC phosphorylation. The biochemical processes responsible for the majority of skeletal muscle energy consumption (i.e. SERCA, myosin ATPase and Na^+-K^+ ATPase) have all been thoroughly described in past physiological research; however, little attention has been paid to the energetic cost of phosphorylating myosin RLCs and the cost of the accompanied force potentiation. The biochemical properties of the RLC phosphorylation system seem ideal for a modulatory mechanism, because the system should consume little energy; yet, phosphorylation of the RLCs still requires a continual investment of ATP increasing the energetic overhead, specifically the E_A, of the working muscle. Augmenting the relationship between mechanical output of a muscle and the metabolic input through RLC phosphorylation-mediated potentiation, would directly impact the economy of muscle contraction, and give insight into the physiological utility of this modulatory mechanism. Previous research produced equivocal, and occasionally contradictory results; thus, an investigation into this area is required to advance our knowledge of the bioenergetics of RLC phosphorylation-mediated force potentiation.

This gap in the literature can be attributed to the previous lack of an animal model that could serve as a negative control for RLC phosphorylation, since any stimulation and subsequent Ca^{2+} release will result in fractional activation of skMLCK. Recent advances in our field have led to the development of a skMLCK$^{-/-}$ mouse, which is currently exclusive to our laboratory in the Centre for Bone and Muscle Health at Brock University, allowing us to definitively parse out the effects of RLC phosphorylation.

3.1. Purpose

The primary purpose of this study is to determine the effect of RLC phosphorylation-mediated force potentiation on the economy of isometric contraction of fast twitch skeletal muscle. The secondary purpose of this study is to determine the quantity of energy consumed by skMLCK throughout the phosphorylation cycle of myosin RLCs during a low-frequency conditioning stimulus; thus, determining the contribution of RLC phosphorylation to the activation energy turnover (E_A) of fast twitch skeletal muscle.

3.2. Hypotheses

We hypothesized that Wildtype muscles, with an intact RLC phosphorylation mechanism, would be more economical than skMLCK$^{-/-}$ muscles. It was predicted that Wildtype muscles would consume more energy in the potentiated state than skMLCK$^{-/}$ muscles, but the force potentiation displayed by Wildtype muscles would be greater than the associated increase in energy consumption. Additionally, we hypothesized that the energetic overhead associated with RLC phosphorylation would be negligible (i.e. below level of detection) so that Wildtype and skMLCK$^{-/-}$ muscle E_A would not differ.

The following are observations expected during experimentation:

1. RLC phosphate content will be significantly higher in Wildtype muscles than skMLCK$^{-/-}$ muscles.
2. Wildtype muscles will display significantly higher twitch force potentiation than skMLCK$^{-/-}$ muscles
3. Wildtype muscles will perform more *isometric work,* as estimated by the force-time integral (FTI), than skMLCK$^{-/-}$ muscles.
4. Wildtype muscles will consume more energy during the contractile experiments than skMLCK$^{-/-}$ muscles.
5. E_A will not differ between Wildtype and skMLCK$^{-/-}$ muscles.

3.3. Rationale

A submaximal stimulation paradigm was chosen in an attempt to optimize fractional activation of skMLCK, while minimizing the negative effects of metabolic byproducts. Submaximal stimulation avoids super-physiological stimulation of the muscle, which is quite possible in an *in vitro* set up, and should prevent an unrealistic overconsumption of energy from SERCA, as well as preventing P_i accumulation that may ultimately inhibit Ca^{2+} release during times of metabolic stress (MacIntosh et al., 2012). A noticeable reduction in Ca^{2+} release does occur during repeated muscle activation, either through reduced availability after saturating myoplasmic Ca^{2+} buffers or by regulating processes of release (Allen, Lamb, & Westerblad, 2008). Fortunately, RLC phosphorylation-mediated potentiation allows for increased force production at any given submaximal [Ca^{2+}], permitting a decrease in Ca^{2+} release without sacrificing force production, with the advantage of a lower SERCA activity and a reduced ATP usage (MacIntosh et al., 2012). The same $Ca^{2+}{}_4$-CaM complex that activates skMLCK can also inhibits Ca^{2+} release; thus, muscle is actually capable of simultaneously decreasing Ca^{2+} release and preserving contractile function through increasing Ca^{2+} sensitivity (MacIntosh et al., 2012), which may lead to an increased economy of contraction in muscles with an intact myosin RLC phosphorylation mechanism.

Since both Wildtype and skMLCK$^{-/-}$ muscles are subjected to the same electrical stimulation, and thus may have an identical ICT, there should be no differences in energy consumption by SERCA or Na^+-K^+ ATPase between genotypes. Theoretically, RLC phosphorylation-induced loss of helical ordering of myosin heads will increase the number of crossbridges in the force producing state, and lead to an increased force production. Overall, considering an increased force output and a proportional increase in myosin ATPase energy consumption, accompanied by *no* alteration in E_A, the mechanical output should be increased to a greater extent than the total energetic input, ultimately improving contractile economy.

Methods

4.1. Animals

SkMLCK$^{-/-}$ mice (19.4 ± 0.7 g, 8-12 weeks old, n = 20) were obtained from our colony, established by breeder pairs graciously donated by Dr. James Stull at the University of Texas Southwestern Medical Center. These mice were originally generated from C57BL/6 mice by methods previously described by Zhi et al. (2005). Wildtype C57BL/6 mice (19.4 ± 0.3 g, 8-12 weeks old, n = 20) were purchased from Charles River Laboratories (Saint Constant, QC). All mice were housed for a minimum of 1 week at room temperature on a 12-hr:12-hr light:dark cycle in the Brock University Ventilated Housing Unit of the Comparative Bioscience Facility. Standard mouse chow (5015, LabDiet, Aberfoyle, ON) and water were ingested *ad libitum*. Mice from each genotype were randomly assigned to either the Control or BTS condition (Figure IX). This study was approved by the Brock University Animal Care Committee and conforms to the standards of the Canadian Council for Animal Care (Protocol # 14-09-01).

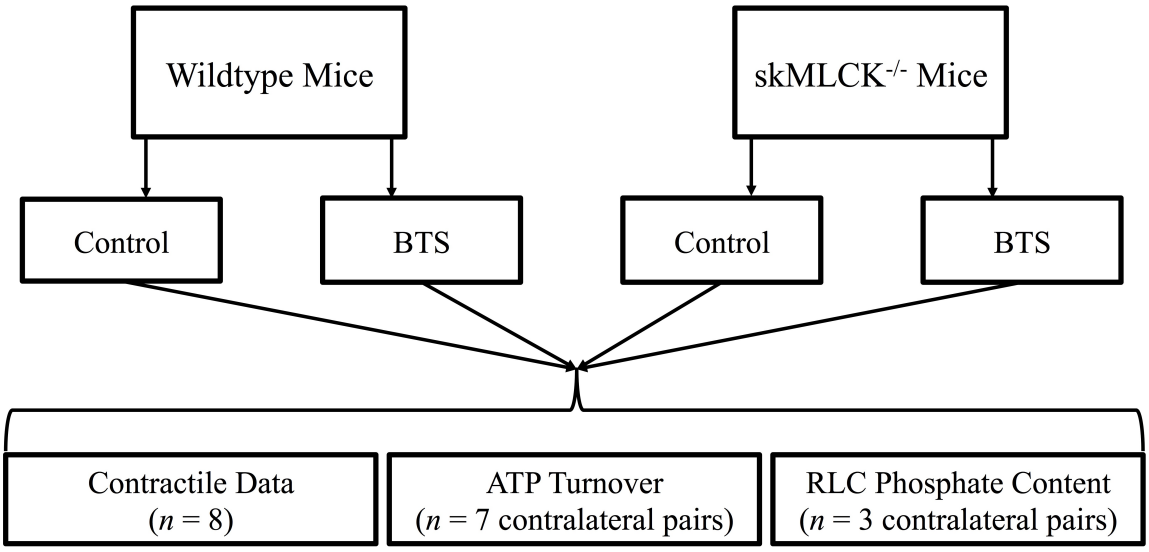

Figure IX. Allocation of isolated EDL muscles to experimental groups.

4.2. Materials

BTS, manufactured by Tocris Bioscience, was purchased from Cedarlane Labs (Burlington, ON), secondary antibody was purchased from Santa Cruz Biotechnology

(Dallas, TX), and all other reagents were purchased from Sigma-Aldrich (Oakville, ON) or BioRad Laboratories (Mississauga, ON). Myosin RLC antibody was a generous gift from Dr. James Stull.

4.3. Muscle Model and Experimental Apparatus

Contractile experiments were conducted using a 1200a *In Vitro* Muscle Testing System from Aurora Scientific Inc. (Aurora, Ontario), capable of accurately controlling muscle length, shortening speed, and temperature. The mouse extensor digitorum longus (EDL) muscle was chosen as a representative fast twitch muscle (Figure X), as it is comprised almost entirely of the fast myosin isoforms that display RLC phosphorylation and force potentiation (Vandenboom et al., 2013): 8.6% type IIA, 30.3% type IIX, and 59.7% type IIB (Gittings, Huang, Smith, Quadrilatero, & Vandenboom, 2011). Equally important in the decision to use the *in vitro* EDL muscle model was the viability of the tissue once it had been excised. The EDL is small enough in diameter to ensure that most fibres remain viable by receiving sufficient oxygenation and substrate delivery purely through diffusion (Barclay, 2005).

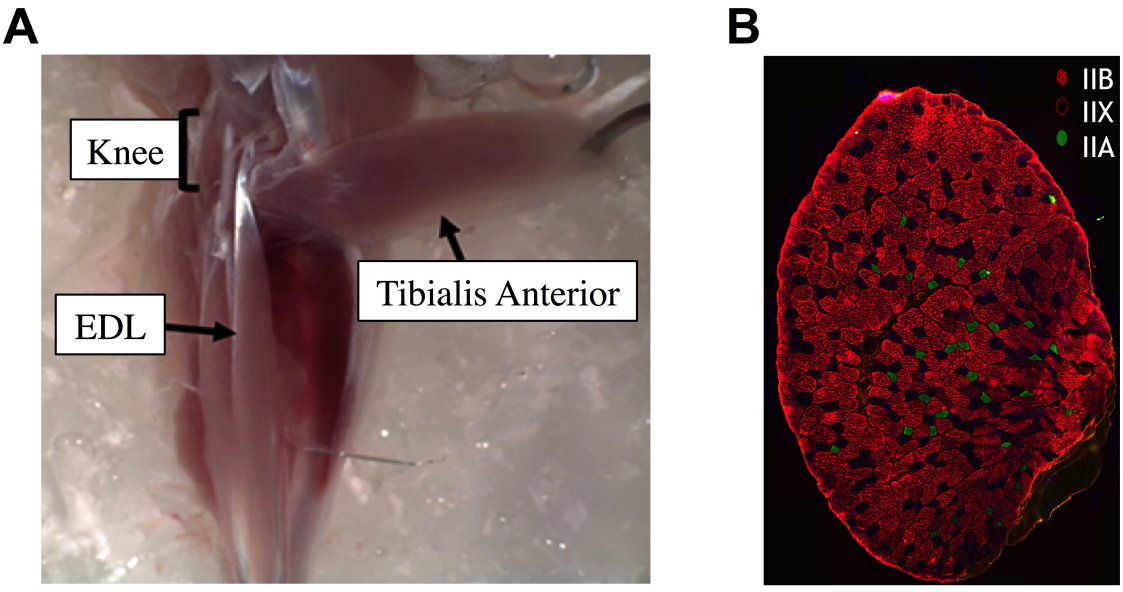

Figure X. The EDL of the mouse hind limb **(A)** is composed of predominately fast fibres **(B)**.

Excised muscles were suspended in a jacketed vertical organ bath (Radnoti LLC, Monrovia, CA) containing continuously oxygenated Tyrode's solution (molar composition described in *Section 4.4*) maintained at constant temperature using an Isotemp 4100 R20 circulator (Fisher Scientific Company, Ottawa, ON). Field stimulation was applied using flanking platinum electrodes driven by a Model 701B biphase stimulator (Aurora Scientific, Inc. [ASI]). Muscle length was measured using digital vernier calipers with LCD display. All contractile data were sampled and collected at 2000 Hz from a 305B servomotor acquired through a 604C analog-to-digital interface, and controlled by a dual-mode lever system (ASI). Data acquisition and basic analysis was performed using ASI 600a software (Version 1.60) and further examined using Excel (Microsoft Canada Co., Mississauga, ON).

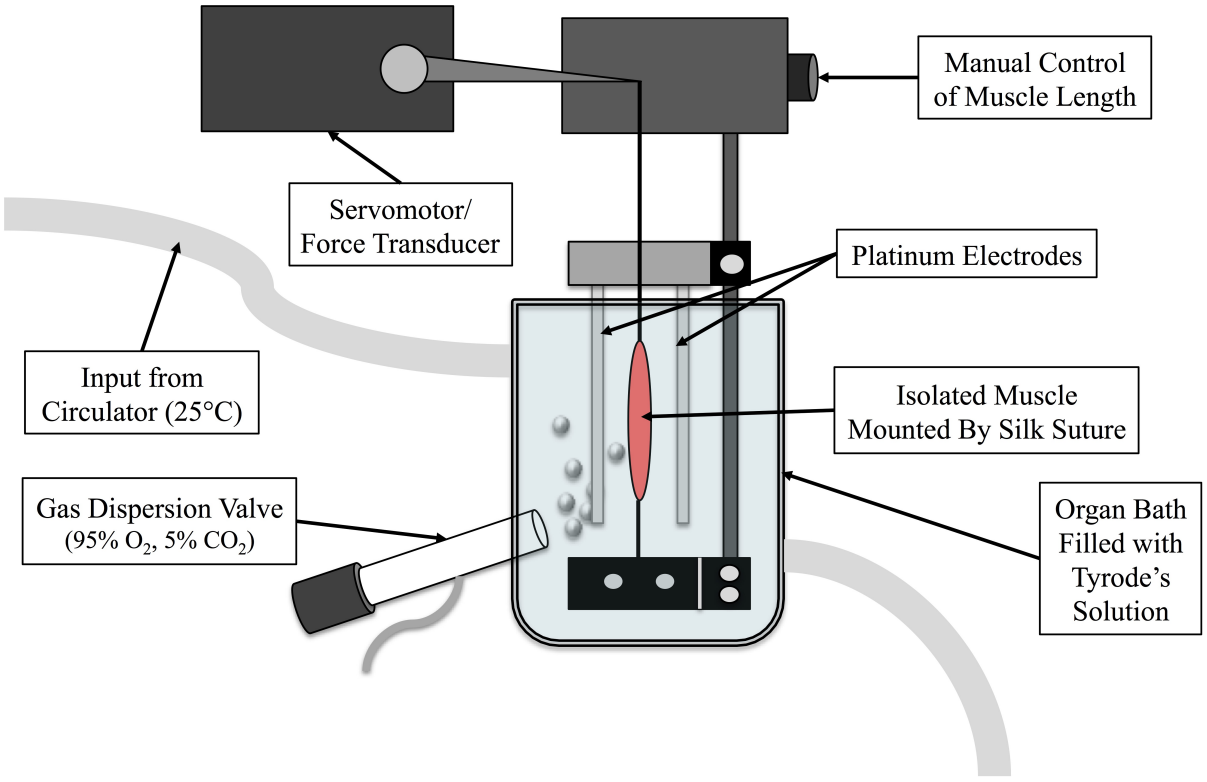

Figure XI. Schematic diagram of the *in vitro* muscle testing system used for contractile experiments.

4.4. Surgical Procedures and Preparation of Muscle Tissue

On the day of surgery, a stock solution of sodium pentobarbital (Euthanyl, 240 mg/mL: Bimedia, Cambridge, ON) was diluted 1:50 with sterile saline to obtain a working concentration of 4.8 mg/mL. Animals were weighed to the nearest 0.01 g, and then sedated with an intraperitoneal (IP) injection of sodium pentobarbital (*anesthetic dose*: 60 mg/kg body weight) using a 27.5 gauge needle. Surgery commenced only once an adequate depth of sedation was reached, as determined by the absence of the pedal withdraw reflex (i.e. toe-pinch). Bilateral EDL muscles were surgically isolated from each hind limb of Wildtype and skMLCK$^{-/-}$ mice after the tibialis anterior was removed, and a non-absorbable braided silk 4-0 suture (Surgical Specialties Corporation, Reading, PA) was tied to the proximal and distal tendons using a double square knot. From each animal, one EDL was mounted into the experimental apparatus immediately (<5 s) to maintain tissue viability, while the contralateral muscle was suspended in an adjacent bath to equilibrate and remain unstimulated, serving as a resting control. Following EDL dissection, the animals were euthanized humanely by an overdose of sodium pentobarbital delivered via intracardiac injection (*euthanasia dose*: 120 mg/kg body weight) and disposed of according to the established Brock University Comparative Bioscience Facility protocol.

Tyrode's solution, a physiological saline solution, was used in all contractile experiments to create a favorable environment for muscle contraction, by providing muscle tissue the essential substrates and ions present *in vivo*, as well as an isotonic environment in which to survive. Final ionic concentrations were (in mM): 121.0 NaCl, 5.0 KCl, 24.0 $NaHCO_3$, 0.4 NaH_2PO_4, 0.5 $MgCl_2$, 1.8 $CaCl_2$, 5.5 D-Glucose, and 0.1 EDTA. The solution was continuously gassed with 95% O_2 and 5% CO_2 using a scintillated glass dispersion valve (Radnoti LLC, Monrovia, CA), resulting in a pH of ~7.4. Temperature was maintained at 25.0 ± 0.1 ℃.

4.5. Contractile Experiment Protocol

The following experiments were conducted as a means of sequentially activating skMLCK, determining the relative RLC phosphorylation-mediated potentiation of twitch force in mammalian fast twitch skeletal muscle, as well as determining the Force Time Integral (FTI) to estimate isometric work.

4.5.1. Equilibration and Determination of Optimal Length

Initially, after the EDL muscle was set to a resting tension of ~3-5 mN, it was stimulated to produce three tetanic contractions (150 Hz for 300 ms, 60 s apart) forceful enough to remove any compliance within the muscle, and tighten suture knots to prevent slippage of the tendon-suture unions during future contractions. Subsequently, a single twitch was applied at 0.05 Hz while successively increasing current intensity (mA), to determine the current required to produce maximal twitch force. To guarantee maximal excitation of all muscle fibres, the stimulus intensity was then increased by ~25%, where it remained for the duration of each experiment. After establishing the preliminary settings, the muscle was subjected to standard 30-minute equilibration period designed to return the muscle to baseline conditions after the rigors of surgical stress. During this time, the EDL was stimulated to produce a single twitch, once every 3 min, over 30 min to monitor the recovery of twitch force. Equilibration was reached at the point where there were no further changes in the magnitude of twitch force.

Following the equilibration period, the optimal length (L_o), i.e. the length at which maximal twitch force is produced, was determined by stimulating the muscle at various lengths. The resting tension of the muscle was originally set to 0 mN (i.e. just taut length) and stimulated to produce a single twitch. Thereafter, twitches were elicited while resting tension was increased at 1.0 mN intervals up to 20 mN (~2.0 g of force). Force traces were analyzed and the resting tension at which active twitch force (i.e. total force minus passive force) reached a maximum (P_t), as well as 70% of maximal twitch force (i.e. 0.7 P_t) were determined. Muscle length was measured using digital vernier calipers with resting tension adjusted to P_t, and was documented as L_o . This length was used as the reference length for all subsequent steps. Resting tension was then adjusted to 0.7 P_t, and muscle length was measured. The muscle remained set to 0.7 P_t, corresponding to 0.9 L_o

on average, for the remainder of the contractile experiment. Following these standard preliminary procedures, the contractile experiment was conducted.

4.5.2. Contractile Experiment

Immediately following the equilibration period and determination of L_o, the muscle remained quiescent for a further 80 min period. The muscle was then subjected to the 10 Hz 15 s potentiating stimulation, producing a total of 150 individual twitches. Each experiment was officially terminated when the EDL was rapidly frozen (<2 s) using tongs pre-cooled in liquid nitrogen, and stored at -80°C for future biochemical analysis. Prior to the mounting of each EDL muscle, the Tyrode's solution was replaced with a fresh aliquot and given sufficient time to equilibrate (~15 min).

BTS, which inhibits P_i release from the actin-myosin-ADP-P_i complex and decreases myosin's affinity for actin (Shaw, Ostap, & Goldman, 2003), was used in a parallel set of experiments where crossbridge cycling was pharmacologically inhibited. This was done to partition energy consumption into contractile and non-contractile components. BTS was solubilized in dimethyl sulfoxide (DMSO) to create a 25 mM stock solution. A small volume of BTS stock solution was added to the organ bath following preliminary procedures (final concentration = 0.1% vol/vol), yielding a final concentration of 25 μM. Muscles were incubated in the presence of BTS for 80 minutes before the contractile experiment began; a time that pilot experiments revealed depressed ~95% of force production.

4.5.3. Quantifying Force Potentiation

Relative force potentiation was quantified as the ratio of final twitch force to initial twitch force, producing a value that reflects an increase or decrease in twitch force relative to baseline measures. During the potentiating stimulation, a rapid increase in force occurred in the initial 0.5 s due to partial fusion of contractile force; thus, twitch force was normalized to the twitch occurring at 0.5 s (i.e. the 6^{th} twitch) (Ryder, Lau, Kamm, & Stull, 2007).

4.5.4. Kinetic Analysis

Force traces were analyzed at predetermined time-points (initial twitch, 25th twitch, 50th twitch, and final twitch) to gain insight into how contractile kinetics changed throughout the 15 s potentiating stimulus. The following analyses were made: Time to peak tension (TPT), half-relaxation time ($RT_{1/2}$), average rate of force development (+ dP/dt), and average rate of relaxation (- dP/dt).

4.5.5. Quantifying Force-Time Integral (FTI)

Since the twitches were performed under isometric conditions, quantifying total work performed during the potentiating stimulus is impossible, as the force produced was not completed over a distance; thus, the force-time integral (FTI) was calculated to estimate *isometric work*. FTI is the area under the force-time curve, and was calculated using the trapezoidal method according to Equation XXI. Calculations were completed using Microsoft Excel.

$$\int_0^{15000} f(F)dF \approx \frac{\Delta t}{2}(F_0 + 2F_1 + 2F_2 + \cdots + 2F_{n-1} + F_n)$$

Equation XXI. Calculating the area under the force-time curve.

4.6. Biochemical Analysis of Skeletal Muscle Tissue

Each of the following biochemical analyses were completed using an entire EDL for sample preparation rather than sectioning muscles to obtain multiple samples from each, as whole muscle homogenate values reflect the spatially averaged change across all fibers present (Allen, 2008).

4.6.1. Quantifying Myosin RLC Phosphate Content

Myosin RLC phosphate content was quantified by Urea/Glycerol Polyacrylamide Gel Electrophoresis (-PAGE) followed by immunoblotting. Stimulated muscles and their contralateral controls were removed from -80°C storage for analysis and homogenized using 3.0 mL tissue grinders with glass pestles (Wheaton Industries Inc., Millville, NJ). Proteins were precipitated in 10% trichloroacetic acid (TCA), solubilized in a urea-based

sample buffer, and run through an ~8% polyacrylamide gel with glycerol added for density at 400 V for 85 min. Non-phosphorylated RLCs were separated from mono- and diphosphorylated RLCs based upon charge, with phosphorylated RLCs migrating further through the gel. Proteins were then transferred to nitrocellulose membranes (0.45 μm pore size; Bio-Rad Laboratories, Mississauga, ON) at 25 V for 1 hr, and probed with polyclonal primary antibodies raised in rabbits to purified skeletal RLCs. Goat anti-rabbit horseradish peroxidase (HRP)-conjugated secondary antibodies (sc-2004; Santa Cruz Biotechnology, Dallas, TX) were then used in conjunction with the Amersham ECL Western Blotting System (GE Life Sciences, Mississauga, ON). Blots were processed on a FluorChem 5500 Western Blot Imaging System (Alpha Innotech Corporation, San Leandro, CA) using AlphaEase software, and quantitative measurements (mol P/mol RLC) were made using Image Studio Lite software (LI-COR Biotechnology, Lincoln, NE).

4.6.2. Quantifying High Energy Phosphate Consumption

Muscles were removed from -80°C storage and lyophilized by a FreeZone 4.5 Liter Benchtop Freeze Dry System (Labconco, Kansas City, MO) for a minimum of 6 hrs to ensure removal of all water. After the silk sutures remaining from the contractile experiment were removed, the muscles were dissected free of connective tissue and blood, then powdered in a glass petri dish using stainless steel tweezers. Powder was aliquoted to 1.5 mL microcentrifuge tubes. Metabolites were extracted from aliquots of lyophilized tissue using 0.5 M perchloric acid ($HClO_4$), and neutralized with 2.3 M potassium carbonate ($KHCO_3$). The concentrations of metabolites were analyzed in triplicate in opaque black polypropylene 96-well microplates (Greiner Bio-One America Inc., Monroe, NC) using fluorometric techniques as previously described (Bergmeyer, Bergmeyer, & Grassl, 1983; Harris, Hultman, & Nordesjö, 1974).

Three specific assays were used to identify the concentration of the metabolites of interest, including ATP, phosphocreatine (PCr), creatine (Cr), and lactate. To adjust for variability in solid non-muscle constituents, all raw metabolite values were normalized to total Cr content (i.e. divided by the sum of the individual muscle's PCr + Cr, then multiplied by mean total Cr content for the all muscle samples) (Zhang et al., 2006). High-Energy Phosphate Consumption (HEPC), a measure of ATP turnover determined

through anaerobic ATP production, was calculated for each group from changes in concentrations metabolites using the following formula:

$$HEPC = -\Delta PCr - 2\Delta[ATP] + 1.5\Delta Lactate$$

Equation XXII. Calculating high-energy phosphate consumption.

The change (Δ) signifies the differences in metabolite concentrations between the experimental muscle and its contralateral resting control.

4.6.3. Quantifying Contractile Economy

Contractile economy was defined as the ratio of mechanical output to metabolic input, i.e. FTI to HEPC. The quantity is given in millinewton-seconds per micromole of high-energy phosphate (mNs/µmol ~P). (De Haan et al., 1986).

$$Economy\ (mNs \cdot \mu mol\ {\sim}P^{-1}) = \frac{FTI\ (mNs)}{HEPC\ (\mu mol\ {\sim}P^{-1})}$$

Equation XXIII. Calculating contractile economy of skeletal muscle.

4.7. Experimental Timeline

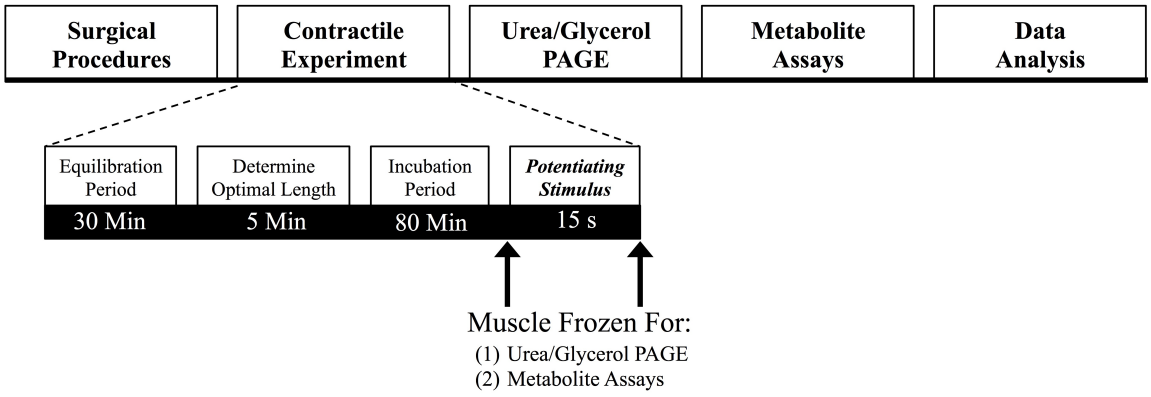

Figure XII. Overview of the timeline of experimental procedures.

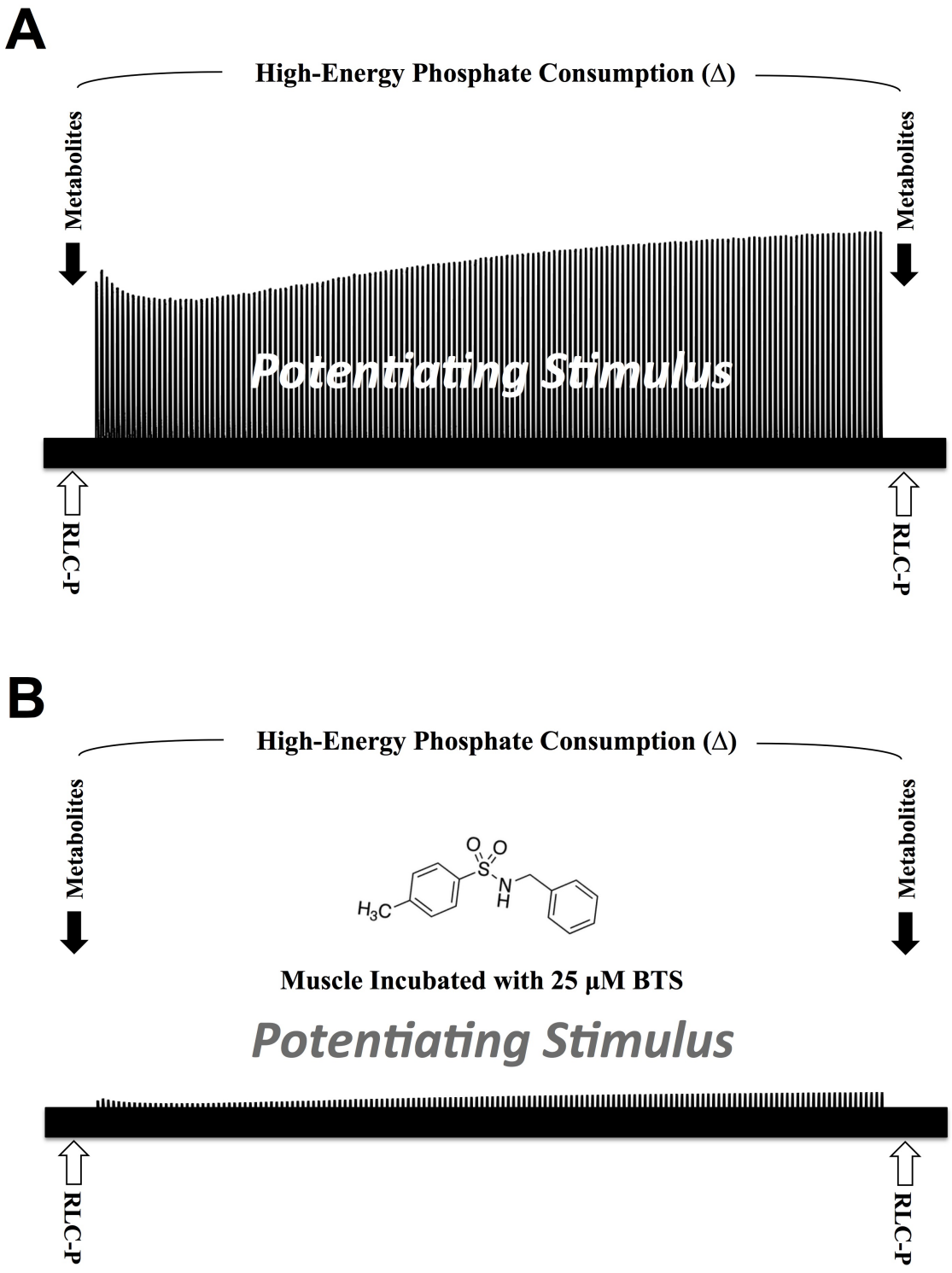

Figure XIII. Contractile experiment timelines for Control (**A**) and BTS (**B**) conditions. Arrows indicate freezing of muscle for biochemical analysis.

4.8. Data Presentation and Statistical Analyses

Data were initially screened for outliers, and the assumptions for parametric statistical tests were checked. The assumption of normal distribution was checked using Shapiro-Wilk Normality Tests, and F-tests were used to check the assumption of equality of variances. Following these preliminary steps, the appropriate analysis was selected for each set of data.

One-way ANOVAs were used to examine differences among conditions in all anthropometric measures, including age, body mass, muscle mass, muscle length, and physiological cross-sectional area. Post-hoc analyses were conducted using Tukey's HSD.

A two-way repeated measures ANOVA was conducted to evaluate the effect of skMLCK expression [Wildtype or skMLCK$^{-/-}$] and potentiating stimulation [Resting or Stimulated] on isometric twitch force in the control condition. Post-hoc analyses were conducted using Sidak's correction.

When checked for the assumptions of a *t*-test, it was determined that skMLCK$^{-/-}$ potentiation values were not normally distributed and the assumption of homogeneity of variances was violated. Thus, a non-parametric alternative, a one-tailed Mann-Whitney rank sum test, was conducted to determine the effect of skMLCK expression [Wildtype or skMLCK$^{-/-}$] on force potentiation (i.e. relative isometric force production).

Two-way repeated measures ANOVAs were conducted to examine differences among conditions in all kinetic measurements, including peak twitch force, time to peak tension, half-relaxation time, rate of force development, and rate of relaxation. Post-hoc analyses were conducted using Sidak's correction.

A one-tailed unpaired *t*-test was conducted to examine the effect of skMLCK expression [Wildtype or skMLCK$^{-/-}$] on total FTI, and another one-tailed unpaired *t*-test was conducted to examine the effect of skMLCK expression [Wildtype or skMLCK$^{-/-}$] on residual FTI during myosin II ATPase inhibition via BTS.

A two-way ANOVA was then conducted to compare the effect of skMLCK expression [Wildtype or skMLCK$^{-/-}$] and potentiating stimulation [Resting or Stimulated] on myosin RLC phosphate content. Post-hoc analyses were conducted using Tukey's HSD.

One-tailed unpaired *t*-tests were conducted to examine the effect of skMLCK expression [Wildtype or skMLCK$^{-/-}$] on total energy consumption (E_{Total}), activation energy turnover (E_A), and the crossbridge component of energy consumption (E_{XB}) during the 15 s potentiating stimulus.

Finally, a one-tailed unpaired t-test was conducted to determine the effect of skMLCK expression [Wildtype or skMLCK$^{-/-}$] on contractile economy. The assumption of homogeneity of variances was violated, thus Welch's correction was employed. All statistical analyses were conducted using GraphPad Prism 6 (La Jolla, CA), and the level of significance was set at $P < .05$. All values are presented as means ± standard error of the mean (SEM) unless otherwise stated.

Results

5.1. Animal Characteristics

Characteristics of the sampled animals are displayed in Table I. Results of the ANOVAs revealed significant differences between groups for age, [$F(3, 26) = 4.48$, $P = .012$, $\eta^2 = .3413$]. SkMLCK$^{-/-}$ BTS mice were significantly younger than Wildtype Control mice ($P = .012$), as well as Wildtype BTS mice ($P = .042$). Although these two differences in ages are statistically significant, the age of all mice within the present study only ranged a mere 10.6 days. Inclusion criteria dictated that all mice be sexually mature adults (Fox et al., 2006); thus, these differences are negligible and are presumed not to impact any findings.

Although there were no significant differences in body mass between groups, a significant difference between muscle masses was evident, [$F(3, 26) = 3.058$, $P = .046$, $\eta^2 = .261$]. It was determined that muscles in the skMLCK$^{-/-}$ Control condition were larger than those in the skMLCK$^{-/-}$ BTS condition ($P = .032$). While L_o did not differ between groups, a significant difference in PCSA was determined [$F(3, 26) = 3.37$, $P = .033$, $\eta^2 = .280$], as this value is calculated using the muscle masses already determined to be different. Once again, muscles in the skMLCK$^{-/-}$ Control group had a larger PSCA than muscles in the skMLCK$^{-/-}$ BTS conditions ($P = .024$).

Table I. *Anthropometric characterization of mice used for contractile experiments.*

	Age (days)	*n* (mice)	Body Mass (g)	Muscle Mass (mg)	L_o (mm)	PCSA (mm^2)
Wildtype						
Control	73.1 ± 1.6^{a}	8	19.9 ± 0.2	8.7 ± 0.6^{ab}	12.8 ± 0.1	1.62 ± 0.1^{ab}
BTS	71.7 ± 3.3^{a}	7	19.0 ± 0.6	9.2 ± 0.6^{ab}	12.8 ± 0.2	1.73 ± 0.1^{ab}
skMLCK$^{-/-}$						
Control	67.4 ± 2.0^{ab}	8	20.7 ± 1.6	10.0 ± 0.7^{a}	12.6 ± 0.2	1.92 ± 0.1^{a}
BTS	62.4 ± 1.9^{b}	7	18.0 ± 0.9	7.5 ± 0.5^{b}	12.4 ± 0.3	1.47 ± 0.1^{b}

Values are means ± SEM; BTS, *N*-benzyl-*p*-toluene sulfonamide; *n*, number of mice; L_o, optimal length; PSCA, physiological cross-sectional area; Means with different letters are significantly different from each other (Tukey's HSD, $P < .05$).

5.2. Contractile Data

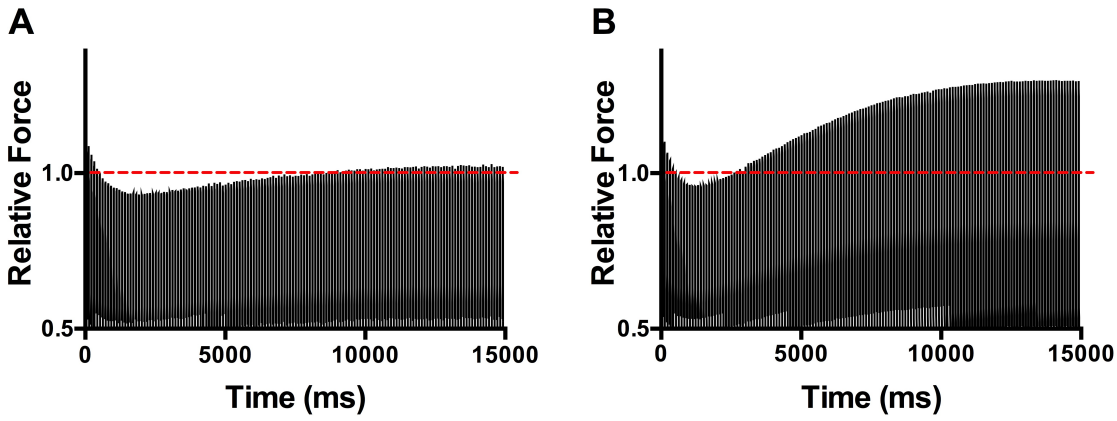

Figure XIV. Representative force traces of skMLCK$^{-/-}$ **(A)** and Wildtype **(B)** muscles during repetitive low-frequency potentiating stimulation.

5.2.1. Absolute Twitch Force

It was hypothesized that initial twitch force would not differ between Wildtype and skMLCK$^{-/-}$ muscles, and that 15 s of low-frequency stimulation would result in staircase potentiation of twitch force in both genotypes. Results of the two-way repeated measures ANOVA indicated a significant interaction between skMLCK expression and potentiating stimulation [$F(1,14) = 19.15$, $P = .0006$, $\eta^2 = .045$]. The potentiating stimulation combined with skMLCK expression significantly increased Wildtype twitch force ($P < .0001$), while potentiating stimulation in the absence of skMLCK did not impact twitch force of skMLCK$^{-/-}$ muscle ($P = .285$). There was no significant difference between initial twitch force of Wildtype and skMLCK$^{-/-}$ groups ($P = .340$); however, following the potentiating stimulation, Wildtype mean final twitch force was 33% greater than skMLCK$^{-/-}$ ($P = .004$). Means ± SEM are provided in **Table II**.

Table II. *The effect of a potentiating stimulus on isometric force production.*

	Initial (mN)	Final (mN)
Wildtype Control	45.8 ± 3.5^{a}	56.3 ± 2.4^{b}
skMLCK$^{-/-}$ Control	40.2 ± 2.8^{a}	42.2 ± 3.0^{a}

Values are means ± SEM, $n = 8$; Initial, twitch force determined from the twitch occurring at 0.5 s (i.e. the 6th twitch); Final, 150th twitch. Means with different letters are significantly different from each other (Sidak's correction, $P < .01$).

5.2.2. Relative Force Potentiation

It was hypothesized that Wildtype muscles would display greater isometric force potentiation (final twitch/initial twitch) than skMLCK$^{-/-}$ muscles. Results of the one-tailed Mann-Whitney rank sum test indicated that Wildtype force potentiation (*Mdn* = 1.22, *n* = 8) was greater than skMLCK$^{-/-}$ force potentiation (*Mdn* = 1.05, *n* = 8) forces; *U* = 6, Z = -2.741, *P* = .002, *r* = -.685.

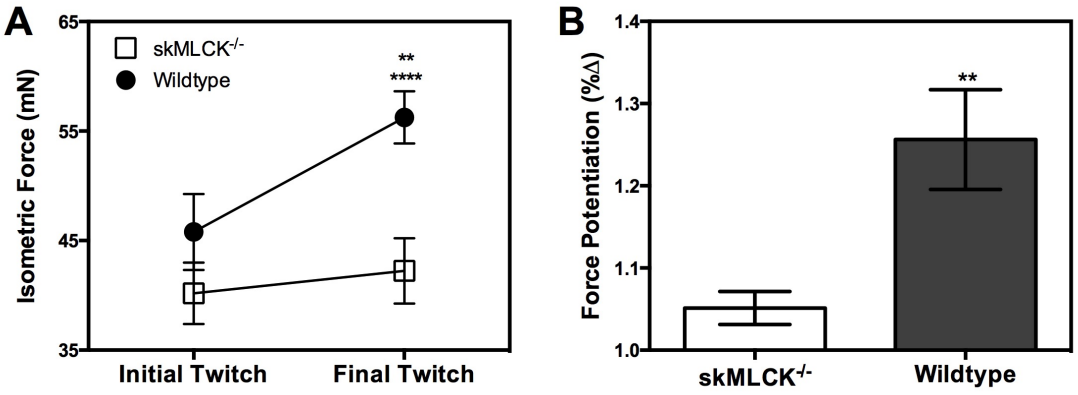

Figure XV. Presence of skMLCK potentiates twitch force during repetitive low-frequency stimulation. **(A)** The interaction between the effects of repetitive low-frequency stimulation and skMLCK content on absolute twitch force in skMLCK$^{-/-}$ and Wildtype muscle; ** indicates *P* = .004 vs. skMLCK$^{-/-}$ Final; **** indicates *P* < .0001 vs. Wildtype Initial. **(B)** Potentiation of relative twitch force (final twitch/initial twitch) resulting from repetitive low-frequency stimulation; ** indicates *P* = .002.

5.2.3. Twitch Kinetics

Various kinetic analyses were conducted at several time points throughout the potentiating stimulation: The initial twitch, 25th twitch, 50th twitch, and final twitch. Analyses included peak twitch force (P_t), time to peak tension (TPT), half-relaxation time ($RT_{1/2}$), rate of force development, and rate of relaxation. A repeated measures ANOVA was run for each genotype to compare the various time points, while unpaired *t*-tests compared the two genotypes at each individual time point. Means ± SEM, as well as the results of these tests are summarized in Table **III**.

Table III. *Kinetic characteristics of twitches sampled throughout the potentiating stimulus.*

	Initial Twitch	25th	50th	150th
Pt (mN)				
Wildtype	45.8 ± 3.5[a]	45.3 ± 3.2[a]	49.67 ± 3.0[b]	56.3 ± 2.4[c]
skMLCK$^{-/-}$	40.2 ± 2.8[ac]	37.5 ± 2.7[b]*	38.92 ± 2.8[ab]*	42.2 ± 3.0[c]*
TPT (ms)				
Wildtype	18.3 ± 0.3[a]	16.3 ± 0.3[b]	16.0 ± 0.3[c]	15.8 ± 0.3[c]
skMLCK$^{-/-}$	17.3 ± 0.4[a]*	15.6 ± 0.2[b]*	14.9 ± 0.3[c]*	14.4 ± 0.4[c]*
$RT_{1/2}$ (ms)				
Wildtype	12.1 ± 0.4[a]	8.1 ± 0.2[b]	7.6 ± 0.3[b]	9.6 ± 0.5[c]
skMLCK$^{-/-}$	10.9 ± 0.3[a]*	7.6 ± 0.3[b]	6.9 ± 0.2[b]	7.3 ± 0.2[b]*
+dP/dt (mN•ms^{-1})				
Wildtype	2.5 ± 0.2[a]	2.7 ± 0.2[b]	3.1 ± 0.2[c]	3.6 ± 0.2[d]
skMLCK$^{-/-}$	2.3 ± 0.1[a]	2.4 ± 0.2[a]	2.6 ± 0.2[b]*	2.9 ± 0.2[c]*
-dP/dt (mN•ms^{-1})				
Wildtype	1.9 ± 0.2[a]	2.8 ± 0.2[b]	3.3 ± 0.1[c]	3.0 ± 0.1[b]
skMLCK$^{-/-}$	1.9 ± 0.2[a]	2.5 ± 0.2[b]	2.9 ± 0.2[c]	2.8 ± 0.2[c]

Values are means ± SEM; n = 8; P_t, peak isometric twitch force; TPT, time to peak tension; $RT_{1/2}$, half-relaxation time; +dP/dt (mN•ms^{-1}), rate of force development; -dP/dt (mN•ms^{-1}), rate of relaxation. Means with different letters are significantly different within row (*within Genotype*; Sidak's correction, $P < .05$); * indicates that skMLCK$^{-/-}$ is significantly different than Wildtype at that time point (unpaired t-test, $P < .05$).

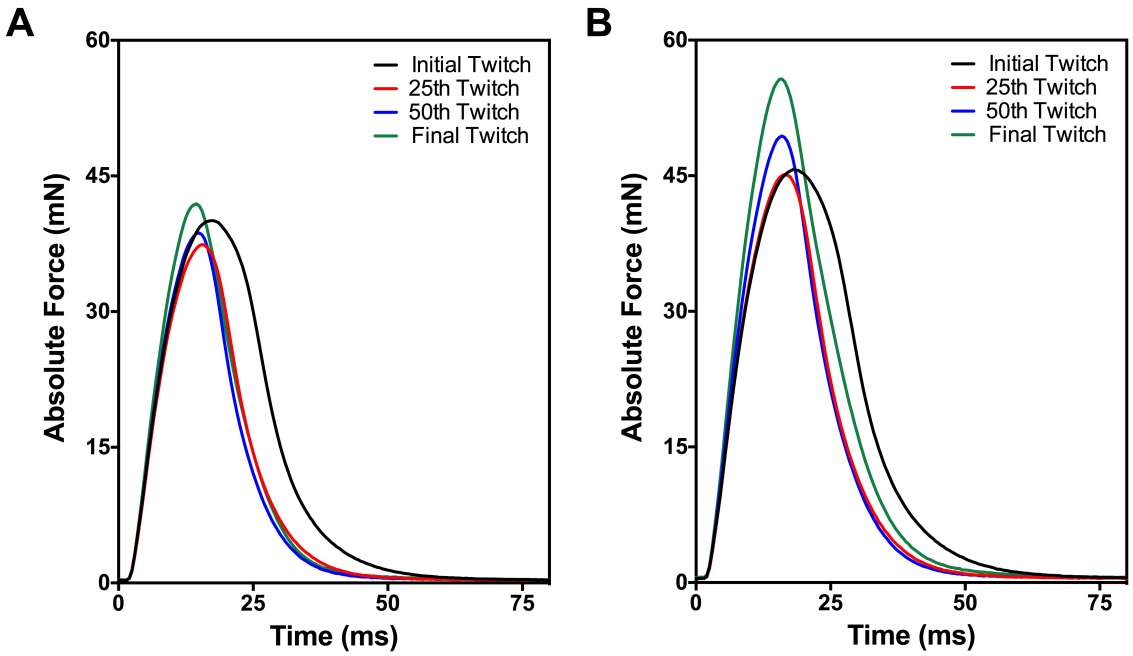

Figure XVI. Traces of isometric twitches evoked from skMLCK$^{-/-}$ **(A)** and Wildtype **(B)** muscles sampled throughout the 15 s of repetitive low-frequency stimulation.

5.2.4. Force-Time Integral

5.2.4.1. Control Groups

It was hypothesized that in the control groups, Wildtype muscles would perform more isometric work than skMLCK$^{-/-}$ muscles, as estimated by the total force-time integral (FTI). Results of the one-tailed unpaired *t*-test indicated that the mean Wildtype FTI (152.7 ± 11.6 mNs, n = 8) was larger than the mean skMLCK$^{-/-}$ FTI (105.8 ± 7.9 mNs, n = 8); [$t(14) = 3.40$, $P = .002$, $R^2 = .452$].

5.2.4.2. BTS Groups

It was hypothesized that in the BTS treated groups, Wildtype muscles would perform more isometric work as estimated by the force-time integral (FTI) than skMLCK$^{-/-}$ muscles. Results of the one-tailed unpaired *t*-test indicated that during myosin II ATPase inhibition via BTS the mean FTI of Wildtype muscles (17.01 ± 1.7 mNs, n = 7) was larger than the mean of skMLCK$^{-/-}$ muscles (10.21 ± 0.8 mNs, n = 7); [$t(12) = 3.63$, $P = .002$, $R^2 = .523$].

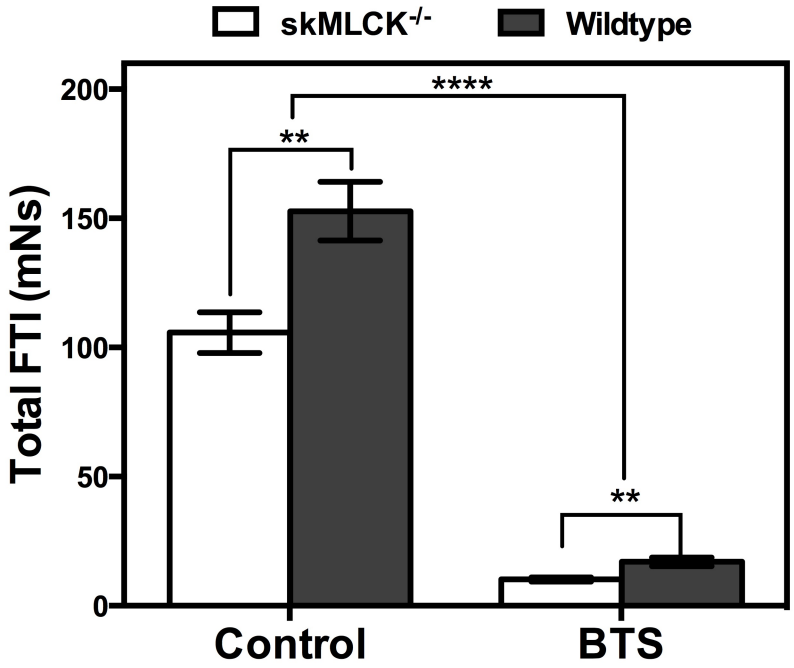

Figure XVII. Effects of skMLCK expression and BTS incubation on isometric work performed during repetitive low-frequency stimulation of isolated mouse EDL at 25 C. Open bars, *skMLCK$^{-/-}$*; Closed bars, *Wildtype*. Values are means ± SEM for each group (n = 7-8). ** indicates $P < .01$; **** indicates $P < .0001$ (Tukey's HSD).

5.2.5. Effects of BTS Incubation on Force Production

Following an 80 min incubation period, isometric twitch force of EDL muscles treated with BTS was abolished by 94.19 ± 1.14% and 94.73 ± 1.17% of the Wildtype and skMLCK$^{-/-}$ Control groups, respectively (n = 7). BTS treatment also inhibited the FTI by 88.2 ± 1.8% and 90.4 ± 0.8% of that in the Wildtype and skMLCK$^{-/-}$ Control groups, respectively (n = 7).

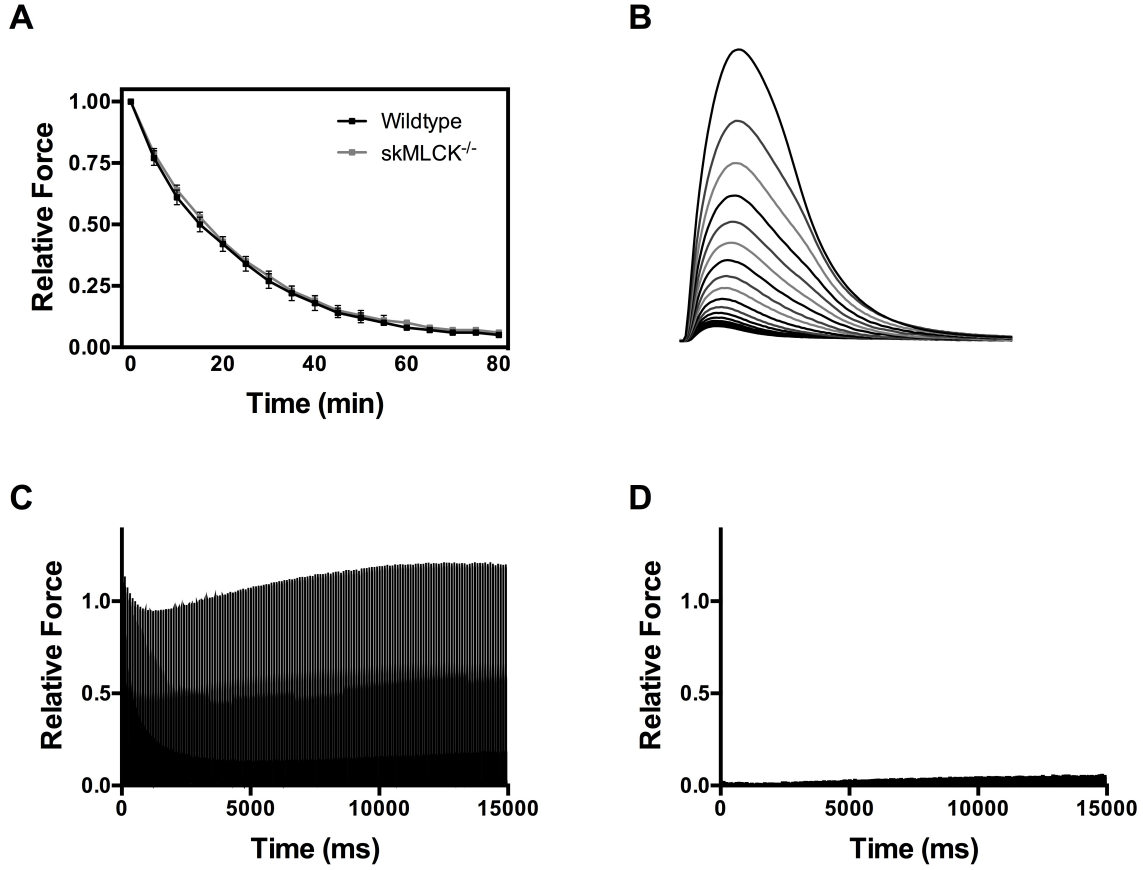

Figure XVIII. An 80 min incubation in 25 μM BTS abolishes ~94% of twitch force production of mouse EDL. **(A)** The time course of myosin II ATPase inhibition via BTS is the same for Wildtype and skMLCK$^{-/-}$ muscles. **(B)** Single twitches stimulated 5 min apart, depicting the depression of force during BTS incubation (*only Wildtype traces shown*). Representative traces of the low-frequency repetitive stimulation during control incubations **(C)** and BTS inhibition of myosin II ATPase **(D)** of a Wildtype muscle. BTS treated FTI is barely distinguishable from the X-axis.

5.3. Myosin RLC Phosphorylation

It was expected that 15 s of low-frequency stimulation would increase myosin RLC phosphate content of isolated EDL muscles from Wildtype, but not skMLCK$^{-/-}$ mice. Additionally, it was believed that due to its specificity as a myosin II ATPase

inhibitor, BTS treatment would not affect phosphorylation of the myosin RLC. An initial two-way ANOVA was conducted, followed by post-hoc analyses using Tukey's HSD, which revealed that no differences existed between any control condition and its matched BTS condition ($P > .900$). This evidence supported the hypothesis that myosin II ATPase inhibition via BTS has no effect on skMLCK-mediated phosphorylation of the myosin RLC; thus, Control and BTS groups were collapsed within Wildtype and skMLCK$^{-/-}$ genotypes to increase sample size.

A new two-way ANOVA was then conducted with Control and BTS groups collapsed to compare the effect of skMLCK expression [Wildtype or skMLCK$^{-/-}$], and potentiating stimulation [Resting or Stimulated] on myosin RLC phosphate content. Results of the ANOVA indicated a significant interaction between skMLCK expression and potentiating stimulation [$F(1,20) = 75.82$, $P < .0001$, $\eta^2 = .2236$]. Post-hoc analyses using Tukey's HSD revealed that in the absence of skMLCK, potentiating stimulation did not impact mean RLC phosphate content of skMLCK$^{-/-}$ muscle ($P = .997$). However, combining potentiating stimulation and skMLCK expression led to a 3-fold increase in RLC phosphate content in Wildtype muscle ($P < .0001$). Interestingly, resting Wildtype muscle had twice as much RLC phosphate content as skMLCK$^{-/-}$ muscle at rest ($P = .026$), and skMLCK$^{-/-}$ muscle after stimulation ($P = .016$). Means ± SEM are provided in **Table IV**, and example blots are depicted in **Figure XIX**.

Table IV. *RLC phosphate content of EDL muscles from Wildtype and skMLCK$^{-/-}$ mice collapsed across Control and BTS conditions*

	Resting	**Stimulated**
Wildtype	0.12 ± 0.01^{b}	0.35 ± 0.01^{c}
skMLCK$^{-/-}$	0.06 ± 0.01^{a}	0.05 ± 0.01^{a}

Values are means ± SEM, $n = 6$. Values given in mol P/mol RLC. Resting and stimulated muscles were frozen and RLC phosphate content was analyzed using urea/glycerol PAGE with immunoblotting. Means with different letters are significantly different from one another (Tukey's HSD, $P < .05$).

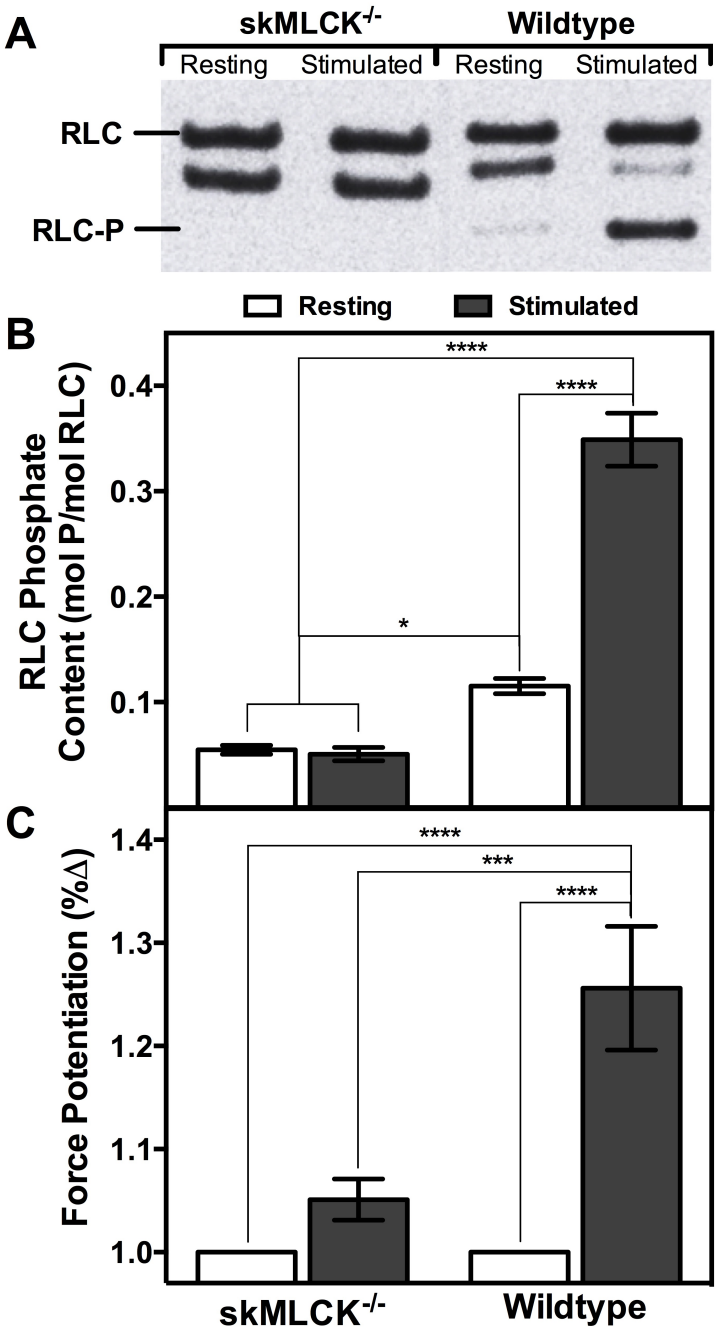

Figure XIX. Concomitant myosin RLC phosphorylation and isometric twitch force potentiation. **(A)** Representative urea/glycerol PAGE blot of non-phosphorylated and monophosphorylated myosin RLC of isolated EDL muscles from Wildtype and skMLCK$^{-/-}$ mice. One muscle was frozen after an 80 min equilibration period (*Resting*) while the contralateral muscle from the same animal was frozen after 15 s of potentiating stimulation that began immediately following the 80 min equilibration period (*Stimulated*) to determine the effects of skMLCK expression on myosin RLC phosphate content. (**B**) Two-way ANOVA of RLC phosphate content, values expressed as means ± SEM; n = 6. Open bars, *Resting*; Closed bars, *Stimulated*. (**C**) Two-way repeated measures ANOVA of relative isometric twitch force, values expressed as means ± SEM; n = 8. Open bars, *Initial Twitch*; Closed bars, *Final Twitch*. * indicates $P < .05$; *** indicates $P < .001$; **** indicates $P < .0001$.

5.4. Metabolite Concentrations

5.4.1. Resting Levels

Results of the two way ANOVAs revealed that no significant differences existed between genotypes or incubation conditions in resting concentrations of PCr ($P > .954$), Cr ($P > .954$), ATP ($P > .286$), or Lactate ($P > .934$). Means ± SEM are provided in Table V.

Table V. *Effect of BTS and skMLCK on metabolites in mouse EDL muscle in basal state.*

	PCr	Cr	ATP	Lactate
Wildtype				
Control	93.9 ± 1.1	17.8 ± 1.1	21.9 ± 0.6	2.84 ± 0.8
BTS	94.7 ± 1.0	17.0 ± 1.0	23.6 ± 0.8	2.49 ± 0.8
skMLCK$^{-/-}$				
Control	95.6 ± 3.0	16.1 ± 3.0	23.4 ± 0.6	3.08 ± 0.8
BTS	94.1 ± 3.4	17.6 ± 3.4	22.0 ± 0.6	2.49 ± 0.5

Values are means ± SEM, $n = 7$ muscles. Values are given in μmol/g dry wt. BTS, *N*-benzyl-*p*-toluene sulfonamide, skMLCK, skeletal myosin light chain kinase; EDL, extensor digitorum longus; PCr, phosphocreatine; Cr, creatine. Muscles were incubated for 80 min at 25°C in the absence (*Control*) or presence of 25 μM BTS. At 80 min, muscles were immediately snap-frozen and stored at -80°C until analyzed.

5.4.2. Stimulated Metabolite Levels

Results of the two way ANOVAs revealed that no significant differences existed between genotypes or incubation conditions in stimulated concentrations of PCr ($P > .063$), Cr ($P > .062$), or ATP ($P > .572$). There was a significant effect of treatment on lactate concentration [$F(1, 24) = 19.59$, $P = .002$, $\eta^2 = .4099$]. Wildtype Control muscles had significantly greater lactate concentrations after stimulation than Wildtype BTS ($P < .004$) and skMLCK$^{-/-}$ BTS muscles ($P < .001$). Means ± SEM are provided in Table VI.

Table VI. *Effect of BTS and skMLCK on metabolites in mouse EDL muscle after stimulation.*

	PCr	Cr	ATP	Lactate
Wildtype				
Control	59.6 ± 5.0	52.1 ± 5.0	23.2 ± 1.1	13.1 ± 0.8^{a}
BTS	71.1 ± 2.3	40.6 ± 2.3	22.1 ± 0.9	7.2 ± 1.1^{b}
skMLCK$^{-/-}$				
Control	62.9 ± 2.6	48.8 ± 2.3	21.0 ± 1.1	10.1 ± 1.2^{ab}
BTS	71.4 ± 1.8	40.3 ± 1.8	22.0 ± 1.6	6.5 ± 1.7^{b}

Values are means ± SEM, $n = 7$ muscles. Values are given in μmol/g dry wt. BTS, *N*-benzyl-*p*-toluene sulfonamide, skMLCK, skeletal myosin light chain kinase; EDL, extensor digitorum longus; PCr, phosphocreatine; Cr, creatine. Muscles were incubated for 80 min at 25°C in the absence (*Control*) or presence of 25 μM BTS. At 80 min, muscles were stimulated (10 Hz, 15 s), then immediately snap-frozen and stored at -80°C until analyzed. Means with different letters are significantly different (Tukey's HSD, $P < .05$).

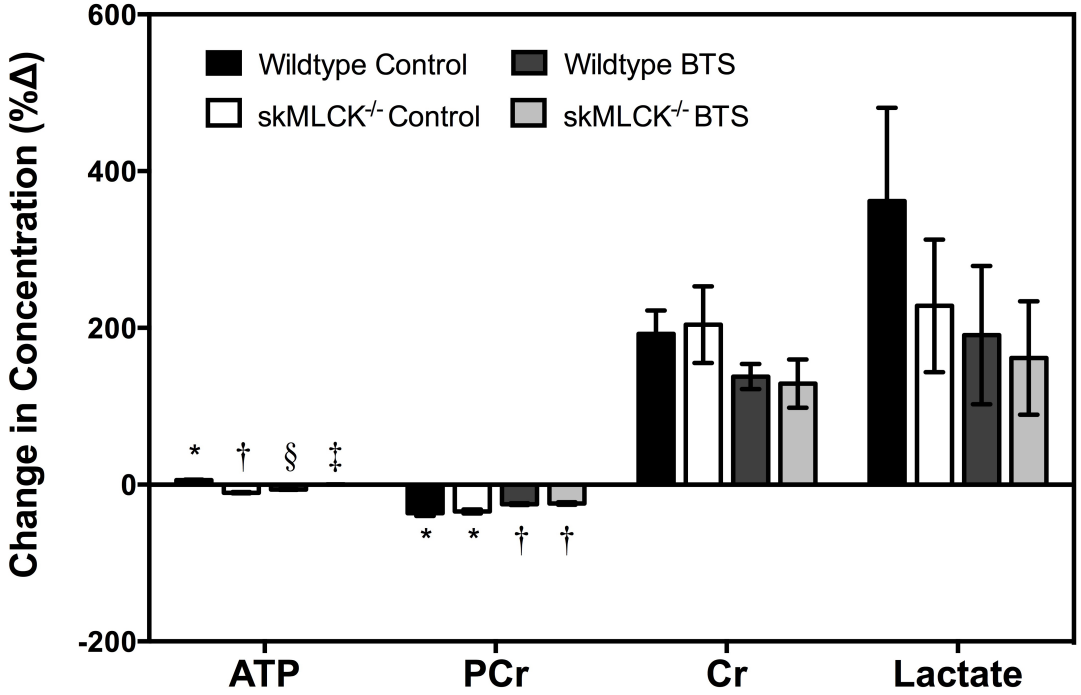

Figure XX. Change in metabolite concentration between contralateral pairings of resting and stimulated EDL from Wildtype and skMLCK$^{-/-}$ mice, incubated in the absence (*Control*) or presence (*BTS*) of 25 μM BTS. Values are means ± SEM, n = 7 contralateral pairs. For each metabolite, means with different symbols are significantly different from one another (Tukey's HSD, $P < .05$).

5.4.3. Energy Consumption

5.4.3.1. Total Energy Consumption (E_{Total})

It was hypothesized that Wildtype muscles would consume more high-energy phosphates than skMLCK$^{-/-}$ muscles during the 15 s low-frequency potentiating stimulation. However, results of the one-tailed unpaired *t*-test indicated that there was no significant difference in energy consumed during the potentiating stimulus between Wildtype muscles (47.1 ± 6.9 μmol~P, n = 7) and skMLCK$^{-/-}$ muscles (48.1 ± 3.1 μmol~P, n = 7); [$t(12) = 0.134$, $P = .448$, $R^2 = .001$]

5.4.3.2. Activation Energy Turnover (E_A)

It was hypothesized that Wildtype muscles would have a higher activation energy turnover than skMLCK$^{-/-}$ muscles. Results of the a one-tailed unpaired *t*-test revealed that there was no significant difference in activation energy turnover during the potentiating stimulus between Wildtype muscles (33.5 ± 3.6 μmol~P, n = 7) and skMLCK$^{-/-}$ muscles (28.6 ± 4.6 μmol~P, n = 7); [$t(12) = 0.8420$, $P = .208$, $R^2 = .056$].

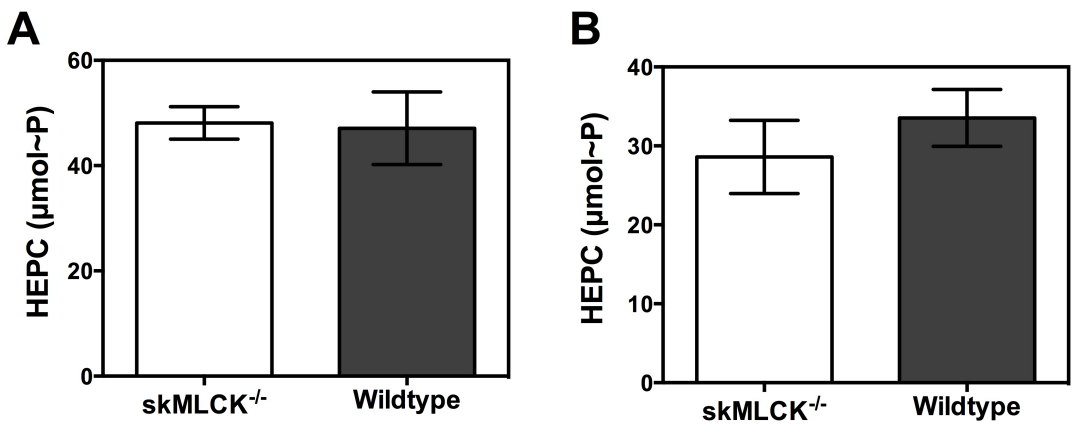

Figure XXI. SkMLCK expression does not augment total energy turnover (**A**, P = .448) or activation energy turnover (**B**, P = .208) during 15 s of repetitive low-frequency stimulation. Values are means ± SEM, n = 7 contralateral pairs.

5.4.3.3. Correction for Residual Force Production

To more accurately partition total energy consumption into contractile and activation energy components, the directly measured HEPC values were corrected for residual force production during the BTS incubation using the following formula (Zhang et al., 2006):

$$E_{XB\,Corrected} = \left(\frac{E_{Total} - E_A}{E_{Total}}\right)\left(\frac{100\%}{\%\,Force\ Inhibition}\right)(100\%)$$

Equation XXIV. Correcting for residual force production during myosin inhibition.

Once the percentages of contractile and activation components of energy consumption were obtained (Table VII), new corrected HEPC values for crossbridge and activation energy components were calculated and compared (Figure XXII).

Table VII. *Total energy consumption partitioned into Crossbridge and Activation components.*

	E_{Total} (µmol~P)	Raw E_A (µmol~P)	Inhibition (%)	E_{XB} (%)	E_A (%)
Wildtype	47.1 ± 6.9	33.5 ± 3.6	88.2 ± 1.8	32.7	67.3
skMLCK$^{-/-}$	48.1 ± 3.1	28.6 ± 4.6	90.4 ± 0.8	44.9	55.1

Values are means ± SEM, n = 7. E_{Total}, total energy consumption; E_A activation energy turnover; E_{XB}, crossbridge energy consumption.

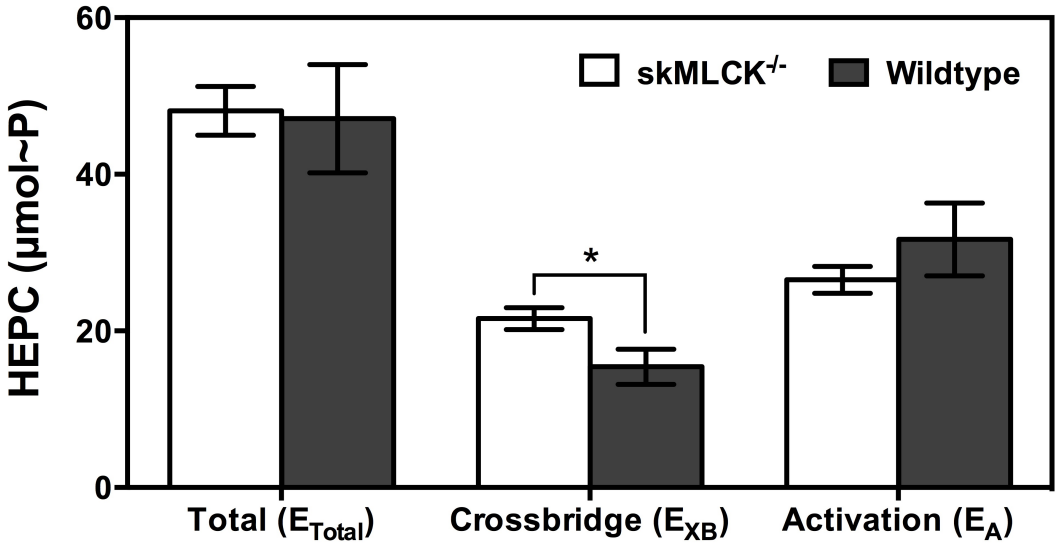

Figure XXII. Total high-energy phosphate consumption (E_{Total}), partitioned into crossbridge energy consumption (E_{XB}) and activation energy turnover (E_A). Values have been corrected for residual force production during myosin II ATPase inhibition via BTS. Open bars, *skMLCK*$^{-/-}$; Closed bars, *Wildtype*. Values expressed as means ± SEM, $n = 7$ contralateral pairs. * indicates $P < .05$ for one-tailed unpaired *t*-test.

Mean total high-energy phosphate consumption of skMLCK (48.10 ± 3.10 µmol~P) and Wildtype (47.10 ± 6.90 µmol~P) were similar [$t(12) = 0.132$, $P = .449$, $r^2 = .001$], and mean activation energy turnover between skMLCK (26.52 ± 1.71 µmol~P) and Wildtype (31.68 ± 4.64 µmol~P) were also similar [$t(12) = 1.04$, $P = .159$, $r^2 = .083$]. However, the contractile component of energy consumption was significantly larger for skMLCK$^{-/-}$ muscles (21.57 ± 1.39 µmol~P) than for Wildtype muscles (15.42 ± 2.26 µmol~P) [$t(12) = 2.32$, $P = .019$, $r^2 = .310$].

5.5. Contractile Economy

It was hypothesized that Wildtype muscles would be more economical than skMLCK$^{-/-}$ during the 15 s low-frequency potentiating stimulation. Results of the one-tailed unpaired *t*-test with Welch's correction indicated that Wildtype muscles (3.8 ± 0.8 mNs/mol~P, $n = 7$) had higher economy than skMLCK$^{-/-}$ muscles (2.2 ± 0.2 mNs/mol~P, $n = 7$); [$t(6.80) = 2.01$, $P = .043$, $r^2 = .372$].

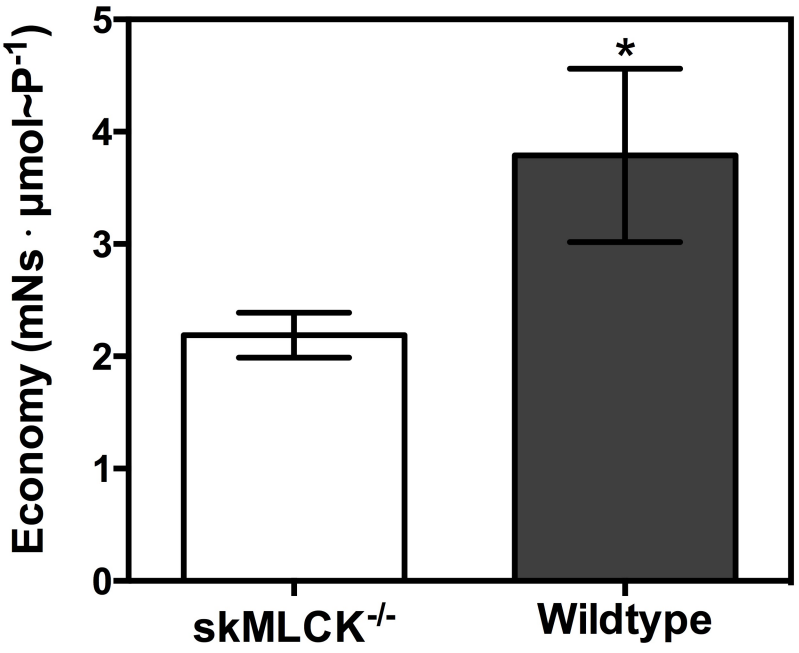

Figure XXIII. SkMLCK-mediated RLC phosphorylation increases contractile economy of isolated mouse EDL during repetitive isometric contraction at 25°C. Values expressed as means ± SEM. * indicates $P < .05$ for unpaired *t*-test with Welch's correction.

Discussion

6.1. General Summary

The present study investigated the effects of RLC phosphorylation-mediated force potentiation on the energetics of repetitive isometric activation of isolated fast twitch skeletal muscle. This study is the first to directly examine the effects of RLC phosphorylation on muscle energetics and contractile economy by using skMLCK$^{-/-}$ mice: a negative control generated through gene ablation. This study is also the first to use BTS to partition energy consumption into contractile and non-contractile components in this genetic model. Results indicated that (i) RLC phosphorylation did not impact total energy consumption or activation energy turnover, but decreased the crossbridge component of energy consumption (ii) RLC phosphorylation augmented peak twitch force and total isometric work production (iii) RLC phosphorylation significantly increased contractile economy.

6.2. Myosin RLC Phosphorylation

At rest, average fractional RLC phosphate content of Wildtype muscle was double that of skMLCK$^{-/-}$ muscle; values that are both in agreement with previously published resting values (e.g. Crow & Kushmerick, 1982b; Zhi et al., 2005). It is interesting to note that although skMLCK$^{-/-}$ muscles do not contain the enzymatic machinery responsible for RLC phosphorylation, a small fraction of RLCs appear to be phosphorylated. This phenomenon was originally noted by Zhi et al. (2005) when a monophosphorylated band of RLCs appeared after deliberately overexposing their skMLCK$^{-/-}$ blots. Presumably, this phosphorylation in the absence of skMLCK is due to a non-specific kinase, which, unlike skMLCK, is not stimulation-dependent. Indeed, the potentiating stimulation resulted in a 3-fold increase in RLC phosphate content in Wildtype muscle, while no change was evident in skMLCK$^{-/-}$ muscle. These data provide further evidence that whatever kinase is responsible for the phosphorylation noted in skMLCK$^{-/-}$ muscle, it is not activated by elevations of myoplasmic [Ca^{2+}].

Following the potentiating stimulus, Wildtype RLC phosphate content was 36%. While this number is lower than previous values reported from our lab and others (often >50%, see Vandenboom et al., 2013 for a review), this is most likely due to the particular

experimental design adopted for this study. Sequential activation of skMLCK during electrical stimulation leads to RLC phosphorylation, and even after the muscle has relaxed, the kinase remains active for a period of time (Stull et al., 2011). It had become commonplace to freeze muscles for analysis ~10-15 s after a potentiating stimulus, allowing skMLCK to continue its enzymatic activity, enabling researchers to catch the *peak* RLC phosphorylation (e.g. Caterini, Gittings, Huang, & Vandenboom, 2011; Gittings, Huang, & Vandenboom, 2012; Zhi et al., 2005). Since the present study ran parallel experiments to measure changes in metabolites, it was imperative that muscles be frozen *immediately* following the final pulse of the potentiating stimulus to prevent any further ATP breakdown or replenishment, negating the time required for peak phosphorylation to occur.

6.2.1. Comment on BTS Specificity

The original pharmacological inhibitor of fast muscle myosin, 2,3-butanedione monoxime (BDM), eventually experienced a loss of prominence due to its lack of specificity. It was discovered that BDM alters Ca^{2+} release, and, extremely relevant to the present study, significantly decreases myosin RLC phosphorylation (Siegman et al., 1994). BDM's successor, *N*-benzyl-*p*-toluene sulfonamide (BTS), is now the preferred pharmacological inhibitor of the myosin II ATPase used in energy partitioning experiments. Although several previous studies have investigated BTS specificity using purified enzymes, potential non-specific effects are always a cause for a concern when using intact muscle models. Work using single intact fibres, as well as intact fibre bundles, demonstrated that BTS does not affect intracellular calcium transients (Bruton, Pinniger, Lännergren, & Westerblad, 2006; Pinniger, Bruton, Westerblad, & Ranatunga, 2005), making it ideal for determining activation energy turnover. A novel finding of our study is that an 80 min incubation in 25 μm BTS did not impact skMLCK or its phosphorylation of the myosin RLC, providing further evidence of the highly specific nature of this small-molecule myosin II ATPase inhibitor.

6.3. Contractile Performance of Wildtype and skMLCK$^{-/-}$ Muscles

6.3.1. Staircase Potentiation of Force

Muscles from control Wildtype and skMLCK$^{-/-}$ mice were similar in mass, and PCSA, and unsurprisingly, their initial contractile characteristics were very similar. The higher resting RLC phosphate content of Wildtype muscle compared to skMLCK$^{-/-}$ muscle was not sufficient to augment Wildtype force output, as there were no differences in initial twitch force. The Ca^{2+} released during repetitive stimulation activated skMLCK, increasing fractional activation of skMLCK as stimulation continued due to the slow dissociation of $Ca^{2+}{}_4$-CaM from the enzyme complex (Stull et al., 2011). By the end of the 15 s potentiating stimulus, progressive RLC phosphorylation resulted in step-like increases in twitch force, culminating with a ~25% increase Wildtype muscle twitch force. Consistent with previous reports of divergent potentiation mechanisms (Gittings et al., 2011; Zhi et al., 2005), a ~5% increase in skMLCK$^{-/-}$ muscle twitch force was noted; however, as expected, the staircase potentiation of twitch force was significantly dampened in the skMLCK$^{-/-}$ muscles.

The phenomenon of RLC phosphorylation-independent force potentiation has been studied previously using lumbrical muscles (Smith et al., 2013). These unique fast twitch muscles have an unbalanced expression between skMLCK and skMLCP, thus displaying no detectable RLC phosphorylation at rest *or* after stimulation. The observed potentiation in the absence of RLC phosphorylation was attributed to an elevation in resting myoplasmic Ca^{2+} concentration ($[Ca^{2+}]_{resting}$) that resulted from tetanic stimulation (Smith et al., 2013), and more recent work has shown repetitive low-frequency stimulation produces an analogous effect (Smith, Vandenboom, & Tupling, 2014). This elevated $[Ca^{2+}]_{resting}$ effectively increases the Ca^{2+}-sensitivity of the contractile apparatus, either by increasing Ca^{2+} occupancy of TnC at rest, or by saturating Ca^{2+} buffering systems, thereby reducing the competition for Ca^{2+} occupancy of TnC (Smith et al., 2013). This effect occurs in both skMLCK$^{-/-}$ and Wildtype muscles; thus, the potentiating effect of skMLCK-mediated RLC phosphorylation can be parsed out by simply observing the disparities in force output between skMLCK$^{-/-}$ (i.e. increased $[Ca^{2+}]_{resting}$) and Wildtype muscles (i.e. increased $[Ca^{2+}]_{resting}$ in conjunction with RLC phosphorylation).

Although the 36% phosphorylation measured in the current study is on the lower end of previously reported values (see Vandenboom et al., 2013), contractile performance of Wildtype muscle was still augmented. The potentiating stimulation used allowed the Wildtype muscles to reach a near-optimal state of potentiation, where superior mechanical output is produced resulting from the counteracting effects of fatigue and potentiation. It has been documented that skMLCK gene ablation, and subsequent inhibition of RLC phosphorylation, exacerbates the reduction of low–frequency force seen in moderately fatigued skeletal muscle (Gittings et al., 2011). When examining the force traces in Figure XIV, an initial decrease in force production is apparent in skMLCK$^{-/-}$ muscles, while this effect is less severe in Wildtype muscles. Force production remains below baseline values in skMLCK$^{-/-}$ muscles for a period of time, yet force output from Wildtype muscles begins to steadily climb, in a classic demonstration of staircase potentiation.

The force response to repetitive low-frequency stimulation is essentially the result of the balance between mechanisms of force enhancement and force diminishment. As discussed in the literature review, the force of isometric contraction (Equation II) is primarily a function of the number of crossbridges that are engaged simultaneously in the strongly bound state. This is governed by Ca^{2+} occupancy of TnC, as well as the rate constants for the transition to the strongly bound state, and dissociation of crossbridge binding. Assuming that identical stimulation paradigms led to similar Ca^{2+} release between genotypes, there would be no differences in Ca^{2+} occupancy of TnC, nor the rate of crossbridge dissociation (which remains constant). Thus, RLC phosphorylation increases the rate constant for transition into strongly bound states in Wildtype muscle, increasing the rate of force development (Equation III) and peak force. During the repetitive stimulation, an elevation $[Ca^{2+}]_{resting}$ increases the Ca^{2+}-sensitivity of the contractile apparatus; an effect that is additive with RLC phosphorylation (Smith et al., 2013); however, Ca^{2+}-dependent inactivation of Ca^{2+} release from the SR has also been observed during closely spaced contractions (Barclay, 2012). In fact, the same $Ca^{2+}{}_4$-CaM complex that activates skMLCK is also able to induce inhibition of the RyR Ca^{2+} release channel, reducing the quanta of Ca^{2+} released during stimulation (Jones, Squier, Boschek, & Bigelow, 2007; Xiong, Zhang, He, & Hamilton, 2006). Wildtype muscle

simultaneously decreases the release of Ca^{2+} while preserving its contractile function through increasing Ca^{2+}-sensitivity. This effect is negated in skMLCK$^{-/-}$ muscle with depressed Ca^{2+} release and no compensatory mechanism. Even though Ca^{2+}-dependent inactivation of Ca^{2+} release occurs, recent work has shown a prolongation of the intracellular Ca^{2+} transient (ICT) during staircase potentiation in lumbrical muscle (Smith et al., 2014). Interestingly, the duration of the ICT appears to be more important than the amplitude for twitch force development. It was suggested that the lingering ICT could be due to accumulation of metabolic byproducts such as ADP and/or P_i that slow the Ca^{2+}-pumping activities of SERCA, and would accordingly be expected to prolong ICT decay times (Smith et al., 2014). Since equivalent quantities of high-energy phosphates were consumed by Wildtype and skMLCK$^{-/-}$ muscles, there would have been comparable accumulation of metabolic byproducts, and thus similar effects of fatigue; however, the effects of fatigue are masked by RLC phosphorylation in Wildtype muscle, and the improved contractile performance for which it is responsible. It is clear that the mechanisms of force enhancement outweigh those of force diminishment in Wildtype skeletal muscle, while the opposite is true in the absence of skMLCK.

6.3.2. Inhibition of Force Production

Previous energy partitioning studies employing BTS as a pharmacological inhibitor of myosin used incubation periods ranging from 30 min (Barclay, 2012) or 45 min (Barclay et al., 2008) for fibre bundles, to 60 min (Zhang et al., 2006) when using whole muscle preparations. Our study used a longer BTS incubation period, as pilot work revealed that 80 min was necessary for 25 μm BTS to inhibit nearly all (~94%) of twitch force production. Muscle viability during this incubation was not an issue, as the muscle was virtually quiescent, apart from a single twitch elicited at 5 min intervals to track inhibition of force. It is interesting to note, that while BTS was able to inhibit the vast majority of force production, there was still a significant potentiation of the remnant force during the potentiating stimulus (*data not shown*).

6.3.3. Potentiation of the Force-Time Integral

Expression of skMLCK, and the subsequent RLC phosphorylation for which it is responsible, resulted in an average total FTI (i.e. isometric work) that was 44% larger than the average FTI produced by muscles devoid of this enzyme. The ability of RLC phosphorylation to potentiate force and work is well documented (Caterini et al., 2011; Gittings et al., 2012; Gittings, Aggarwal, Stull, & Vandenboom, 2014). While muscles from both Wildtype and skMLCK$^{-/-}$ genotypes began the potentiating stimulus with similar peak twitch force, time to peak tension (TPT) was significantly longer in Wildtype muscles than skMLCK$^{-/-}$; a trend that continued throughout the duration of the stimulus. As the stimulation continued, $Ca^{2+}{}_4$-CaM activated skMLCK in Wildtype muscle, and Wildtype force was potentiated above skMLCK$^{-/-}$ levels. RLC phosphorylation was responsible for increased rate of force development (Equation III) during the stimulation, and increasing the number of cycling crossbridges in a force generating state (Brenner, 1988), allowing Wildtype muscle to produce higher peak forces. Furthermore, half-relaxation time ($RT_{1/2}$) was faster in skMLCK$^{-/-}$ muscles - an effect previously documented by Gittings et al. (2011). These changes in kinetics beneficially altered the summation of force during the repetitive stimulation: Wildtype muscles were unable to relax between successive stimuli as fully as skMLCK$^{-/-}$ muscles, ultimately enlarging the area under the force-time trace (FTI), significantly increasing the amount of isometric work performed during the 15 s protocol.

6.4. Skeletal Muscle Energetics

Neither myosin II ATPase inhibition or skMLCK expression impacted resting concentration of any metabolite that was measured. Following stimulation, Control Wildtype and skMLCK$^{-/-}$ groups had larger changes in metabolite concentrations, while and their respective BTS groups metabolized less PCr and produced less lactate, as would be expected with myosin II ATPase inhibition. At first glance, it appears that Wildtype muscles produced larger quantities of lactate, because stimulated Wildtype muscle had a significantly higher lactate concentration than the stimulated Wildtype or skMLCK$^{-/-}$ BTS groups; however, due to the large degree of variation apparent when change in lactate

concentrations were calculated, there were no significant differences in among groups for %Δ Lactate.

6.4.1. Total Energy Consumption (E_{Total})

It was assumed that the augmented contractile output of Wildtype muscles would be accompanied by an increase in energy consumption above that of skMLCK$^{-/-}$ muscles; however, only a 2% difference in E_{Total} between Wildtype and skMLCK$^{-/-}$ muscles was documented. Similar to Barsotti and Butler (1984) who reported no change in energy consumption upon RLC phosphorylation during isometric tetani, we found that an increased RLC phosphate content did not affect overall energy turnover during submaximal contraction. This apparent lack of effect of myosin phosphorylation upon the rate of chemical energy usage in mouse EDL also the corroborates findings of Morgan et al. (1976) who demonstrated RLC phosphorylation had little to no effect on the ATPase rates of isolated myosin.

6.4.2. Crossbridge Component of Energy Consumption (E_{XB})

It was somewhat unexpected that the crossbridge component of energy consumption (E_{XB}) was significantly larger for skMLCK$^{-/-}$ muscles than for Wildtype muscles. In fact, the opposite effect was theorized, since Equation IV dictates that myosin ATP consumption increases proportionally with RLC phosphorylation-mediated increases in the rate of crossbridge transition to force generating state (f_{app}), and no change in g_{app} (Brenner, 1988; Sweeney & Stull, 1990). This equation is built upon the assumption of *tight coupling*: one molecule of ATP is hydrolyzed per crossbridge cycle. If indeed one crossbridge cycle is completed per ATP molecule, then skMLCK$^{-/-}$ muscles may have performed *more* crossbridge cycles during the stimulus period than Wildtype muscles - a finding that is consistent with previous literature claiming that there is no change in ATPase rates, but a decreased crossbridge cycling rate, when the RLCs are phosphorylated (Barsotti & Butler, 1984). During an identical stimulation protocol, the myosin ATPases in skMLCK$^{-/-}$ muscle consumed more ATP, yet the Wildtype demonstrated clear force potentiation. If Wildtype muscles completed less crossbridge cycles, their improved performance must be explained by differences in *thermodynamic*

efficiency, that is the fraction of energy harnessed to perform mechanical work per ATP consumed by myosin ATPases.

Wildtype and skMLCK$^{-/-}$ thermodynamic efficiency (η) was calculated, assuming a ΔG_{ATP} of -60 kJ •mol^{-1} (or 100 zJ per molecule; z is *zepto*, the metric prefix describing 10^{-21}) in mammalian skeletal muscle (Barclay, Woledge, & Curtin, 2010a). Ultimately, an average Wildtype crossbridge cycle converted 19% of the free energy produced during the hydrolysis of ATP into mechanical work, while skMLCK$^{-/-}$ converted only 9%; thus, a ~2-fold increase in the maximum work completed per crossbridge cycle (W_{XB}) occurred concomitant with RLC phosphorylation.

Recall the thermodynamic efficiency equation (Equation XI):

$$\eta = \frac{W}{\Delta G_{ATP}}$$

Wildtype calculations:

$$\eta_{Wildtype} = \frac{FTI}{E_{XB} \cdot \Delta G_{ATP}} = \frac{152.7\ mNs}{13.6\ \mu mol{\sim}P \cdot 60\ mJ \cdot \mu mol^{-1}} = 0.19$$

$$W_{XB} = 100\ zJ\ molecule^{-1} \times 0.19 = 19\ zJ$$

skMLCK$^{-/-}$ calculations:

$$\eta_{skMLCK^{-/-}} = \frac{FTI}{E_{XB} \cdot \Delta G_{ATP}} = \frac{105.8\ mNs}{19.5\ \mu mol{\sim}P \cdot 60\ mJ \cdot \mu mol^{-1}} = 0.09$$

$$W_{XB} = 100\ zJ\ molecule^{-1} \times 0.09 = 9\ zJ$$

These data, and the estimates presented for discussion, indicate that RLC phosphorylation may have decreased the crossbridge cycling rate, and increased the average work per crossbridge cycle. Sweeney and Stull (1980) purported that RLC phosphorylation results in an increased rate at which crossbridges enter the force generating state, a finding that is in accordance with our results. However, Sweeney and Stull (1980) also believed it unlikely that RLC phosphorylation would affect average

force per crossbridge or the rate of detachment, which is a model that contradicts our data.

Results from *in vitro* motility assays have demonstrated that the covalent modification of the RLC causes an alteration to myosin's function as a molecular strain sensor, slowing the strain-dependent ADP release during crossbridge cycling – an effect that caused a decreased shortening velocity and an increased myosin duty cycle (Greenberg et al., 2009). This same work also suggested a phosphorylation-induced stiffening of the lever arm of myosin, capable of more efficiently transmitting conformational changes into force, and increasing unitary step-size (Greenberg et al., 2009). This mechanistic research supports Kerrick, Potter, and Hoar (1991), who suggested that the rate of dissociation of force generating crossbridges decreases with increased actin-myosin interaction. Increasing thin filament activation may increase the myosin duty cycle and the time required for ADP release from myosin's nucleotide pocket; thus, ATP turnover for each crossbridge may be reduced, as a new molecule of ATP cannot be hydrolyzed until ADP is released and myosin disassociates from actin. It is possible that in Wildtype muscle in our study, RLC phosphorylation was responsible for stiffening the lever arms, and altering the biochemistry of myosin. The accompanied increase in duty cycle reduced the crossbridge turnover, and the more efficient transmission of conformational changes into force increased work per crossbridge, resulting in a lower E_{XB} than skMLCK$^{-/-}$ muscle. These transient alterations to the contractile apparatus can be reconciled with the Brenner (1988) equations for the fraction of crossbridges in the force producing state (Equation I), isometric force (Equation II), and isometric ATPase rates (Equation IV) to explain the advantageous consequences of RLC phosphorylation.

During submaximal stimulation when [Ca^{2+}] is low, and the rate of crossbridge detachment (g_{app}) is far larger than the rate of crossbridges entering the force generating state (f_{app}), any increase in f_{app} causes large increases in the fraction of crossbridges in the force generating state (α_{Fs}) as determined by Equation I:

$$\boldsymbol{\alpha_{Fs} = f_{app}/(f_{app} + g_{app})}$$

$$\textbf{When } \boldsymbol{[Ca^{2+}]_i} \textbf{ is low } \boldsymbol{g_{app} \gg f_{app}}$$

$$\uparrow \boldsymbol{f_{app}/(\uparrow f_{app} + g_{app})} = \uparrow \boldsymbol{\alpha_{Fs}}$$

If indeed g_{app} decreases during RLC phosphorylation, as we have suggested, increases in α_{Fs} will be larger than if g_{app} had remained constant. Additionally, increasing f_{app} while simultaneously decreasing g_{app} may theoretically lower the isometric myosin ATP turnover as determined by Equation IV. Considering that the number of cycling crossbridges (n) and the number of half sarcomeres in the fibre (b) should remain constant, and ($f_{app} + g_{app}$) theoretically approaches g_{app} at low [Ca^{2+}], the largest and most determinate term in this equation is g_{app}.

If:

$$r_A = nbg_{app}\alpha_{Fs}$$

Then:

$$nb \downarrow \boldsymbol{g_{app}} \uparrow \alpha_{Fs} = \downarrow r_A$$

Reducing the rate at which crossbridges detach means increasing the time that myosin is bound to actin, i.e. increasing the myosin duty cycle, and according to Equation IV would cause a reduction in the associated ATP cost of force production, while

augmenting isometric force (F), as g_{app} is in the denominator of the term α_{Fs} in Equation II for isometric force ($F = n\bar{F}\alpha_{Fs}$).

It is commonly accepted that the myosin ATPase consumes the majority of energy during skeletal muscle contraction; however, our results indicate that during our 15 s stimulus, E_{XB} was a relatively small component (33-45%) of E_{Total}. EDL muscles from young mice generally display a twitch:tetanus ratio of 0.23 at the temperature used during our study (Brooks & Faulkner, 1988); additionally, peak twitch force has been said to represent ~5-20% of the maximum force a muscle can generate (MacIntosh et al., 2012). This means that during the 10 Hz stimulation frequency, the EDLs were producing only ~20% of maximal force. Experiments using chemically skinned frog fibres showed that the proportion of E_{XB} relative to total ATP consumption decreases as relative force decreases (Stienen, Zaremba, & Elzinga, 1995); thus, at the low activation frequency we employed, the E_{XB} is anticipated to be relatively small. A figure from Stienen et al. (1995) depicting the Ca^{2+}-dependence of both myosin ATPase and SERCA activity illustrates that during maximal force production, activation energy turnover (E_A) is ~25% while E_{XB} is ~75%. Conversely, during very low levels of activation, such as eliciting individual twitches, E_A actually accounts for ~55% of energy consumed, while E_{XB} is ~45%. It appears that E_A actually hits a peak and plateaus at ~20% of maximal activation, whereas the E_{XB} continually rises until maximal activation is achieved (Stienen et al., 1995).

The idea of a plateauing E_A is further supported by Tsianos, Rustin, and Loeb (2012), who demonstrated E_A was constant across a range of shortening speeds, while E_{Total} and E_{XB} were dynamic, both hitting their lowest point during isometric contraction. Finally, our study was conducted using a relatively short muscle length, ~0.90 L_o which is a length at which the muscle can only produce 70% of the maximal twitch force produced at L_o. Inevitably, having the muscle at a length below L_o reduces actin-myosin interaction and reduces the associated E_{XB} relative to E_{total}. Thus, it is not unreasonable to have a low percentage of E_{XB} given the experimental variables adopted by this study.

6.4.3. Activation Energy Turnover (E_A)

We expected that Wildtype muscles would have a higher activation energy turnover (E_A) than skMLCK$^{-/-}$, initially hypothesizing that the energetic overhead of myosin RLC phosphorylation may be inflating this non-contractile component of energy consumption. While Wildtype muscle did have a ~19% higher E_A, this difference failed to reach statistical significance, possibly due to the inherent variability involved in biochemical analysis of metabolites. Since BTS incubation did not affect the shape of the ICT, calcium handling, or its associated energy cost (Bruton et al., 2006; Pinniger et al., 2005), it is plausible that the larger E_A of Wildtype muscle is related to the cost of stimulation-induced elevations of RLC phosphorylation. The absolute difference in E_A between Wildtype and skMLCK$^{-/-}$ muscles was ~5 μmol~P, which equates to ~10% of the total energy consumed by Wildtype muscles. While Homsher (1987) claimed that the ATP consumed for RLC phosphorylation may be equivalent to 5% of the energy used during a 5 s tetanus (at 0°C), our study (at 25°C) did not employ tetanic stimulation, and thus the E_{Total} is much smaller, ultimately increasing the percentage of E_{Total} that can possibly be attributed to skMLCK-mediated RLC phosphorylation.

After correcting for residual force development during BTS incubation, E_A accounted for ~68% of E_{Total} for Wildtype, and ~55% for skMLCK$^{-/-}$. While these numbers fall on the higher end of the spectrum of previously reported values from isolated mouse EDL (Table VIII), they are not unreasonable. Many initial studies that reported ~33% E_A in various animal models have conducted experiments at much lower temperatures (see Barclay et al., 2007 for a review). Temperature-dependent increases in SERCA activity have been reported in chemically skinned amphibian muscle fibres, with SERCA ATP consumption jumping from ~28% of total ATP consumption at 5°C, to 48% of total ATP consumption at 20°C (Stienen et al., 1995). Additionally, an earlier study estimated that SERCA activity accounts for 56% of total energy liberation at 20°C (Rall, 1982). Thus, using a temperature of 25°C in the current study may explain the larger percentage of E_{Total} that is accounted for by only activation processes.

Interesting work conducted using human muscle revealed different ATPase activity in various fast muscle fibre types, leading to different energy consumptions for both contractile and non-contractile processes (Szentesi, Zaremba, Mechelen, & Stienen,

2001). In IIA/B and IIB fibres, SERCA activity is higher than myosin ATPase activity, and only in IIA fibres is the myosin ATPase activity higher than SERCA (Szentesi et al., 2001). As discussed previously, mouse EDL is mostly predominately IIX and IIB, with only a small percentage of IIA fibres; thus, it stands to reason that a muscle of this fibre composition would have a higher SERCA activity relative to myosin ATPase rates, leading to a larger E_A than reported in other models (amphibian, fish, mammalian soleus, etc.).

Table VIII. *Previously reported activation energy turnover of mouse EDL.*

Authors (Year)	E_A (%)	T (°C)	Stimulation Paradigm	Myosin Inhibition	Energy Measurement
Wendt & Barclay (1980)	33	27	100 Hz, 0.5 s	Pre-Stretch	Total heat production
Barsotti & Butler (1984)	37	23	66 Hz, 1 s	Pre-Stretch	Chemical analysis
	46	23	66 Hz, 7 s	Pre-Stretch	Chemical analysis
Siegman et al. (1994)	61	20	66 Hz, 7 s	BDM	Chemical analysis
Barclay (1996)	35	25	125 Hz, 0.2 s	Pre-Stretch	Initial heat production
Zhang et al. (2006)	47	15	50 Hz, 2 s	BTS	Chemical analysis
	76	30	50 Hz, 2 s	BTS	Chemical analysis
	81	30	50 Hz, 5 s	BTS	Chemical analysis
	82	30	50 Hz, 10 s	BTS	Chemical analysis
Barclay et al. (2008)	36	20	100 Hz, 1 s	Pre-Stretch	Total heat production
	31	30	140 Hz, 1 s	Pre-Stretch	Total heat production
	46	20	100 Hz, 1 s	BTS	Total heat production
	38	30	140 Hz, 1 s	BTS	Total heat production
	34	20	15 Hz, 1 s	BTS	Total heat production
	32	30	15 Hz, 1 s	BTS	Total heat production
Current Study	67	25	10 Hz, 15 s	BTS	Chemical analysis
	55	25	10 Hz, 15 s	BTS	Chemical analysis

E_A, activation energy turnover; T, temperature; Pre-stretch, crossbridge cycling inhibited progressively longer sarcomere lengths to decrease actin and myosin interaction creating a curve and extrapolating to zero; BDM, 2,3-butanedione monoxime; BTS, *N*-benzyl-*p*-toluene sulfonamide; Total heat production, heat arising in response to contraction (equivalent to O2 consumption), with energy turnover estimated via enthalpy (work + heat); Initial heat production, heat produced only with the time course of contraction, with energy turnover estimated via enthalpy (work + heat); Chemical analysis, energy turnover calculated using changes in metabolite concentrations measured by either spectrofluorimetry or HPLC.

Previous experiments (Table VIII), conducted at temperatures between 15-30°C, using various methods, measured E_A values that range between 31% and 82%; a range in which the results from the present study fall. Several studies conducted using pharmacological myosin II ATPase inhibition via BDM or BTS, and measuring energy turnover using chemical analysis (Siegman et al., 1994; S. J. Zhang et al., 2006), produced E_A values that most closely resemble the results of our study. While these values are in accordance with one another, they are higher than values produced from studies using pre-stretch methods and enthalpy measurements. This is very thought-provoking, since Barclay et al. (2008) found the pre-stretch method and pharmacological inhibition by BTS to produce equivalent results. Barclay and colleagues generally use EDL fibre bundles, whereas the studies producing higher E_A values, including the present one, used whole muscle preparations. It is possible that BTS is better able to diffuse into all muscle cells of the fibre bundle while failing to reach the deepest muscle cells in whole muscle preparations. This would lead to differences in myosin II ATPase inhibition, artificially inflating E_A in whole muscle studies. It is also worth noting that Barclay and colleagues estimate energy consumption by measuring heat production and work to calculate enthalpy, where as our study and others (e.g. Siegman et al., 1994; S. J. Zhang et al., 2006) snap-froze muscles before and after stimulation to quantify extracted metabolites. The inherent error propagation involved in calculating high-energy phosphate consumption from changes in metabolites may also play a role in large range of E_A values in the literature, and explain why values from different methods diverge.

Barclay and colleagues have also used brief stimulation durations (e.g. 0.2-1 s) while studies with results that more closely agree with our own have used relatively longer durations (e.g. 2-15 s). This may be an explanation for the different E_A values, as earlier studies have indicated that the percent contribution of E_{XB} to E_{Total} decreases as contraction duration is prolonged in mouse EDL (Crow & Kushmerick, 1982a), an effect that would cause a proportional increase in E_A. It is quite possible that the reported decrease in E_{XB} that manifested as stimulus duration increased was in part due to RLC phosphorylation. Barclay and colleagues' work, using brief stimulation, would not give sufficient time for RLC phosphorylation to occur; thus, the main phenomenon being investigated in our research would not be a factor capable of impacting their results.

Those who have measured the highest E_A of ~80% suggested that the submaximal activation utilized may have resulted in the large value (Zhang et al., 2006). This has become a point of contention (see Barclay et al., 2007), and previous work remains inconclusive as to the effect of activation level on E_A. Some researchers claim that lowering activation level increases E_A; and indeed, reducing activation from maximal to 1/3 resulted in a ~10% increase in E_A (Wendt & Barclay, 1980). Alternatively, others found that while myosin was inhibited via BDM, decreasing stimulation frequency either decreased or did not change E_A in Type II fibres, and it increased in Type I fibres (Buschman, Van der Laarse, Stienen, & Elzinga, 1996). It makes mathematical sense that E_A is increased in relation to E_{Total} when activation level decreases, since, as discussed in 6.4.2., E_A plateaus and remains constant across many activation frequencies and velocities, while E_{Total} and E_{XB} increase with increasing activation level and velocity. Overall, our results lend support to several previous findings that ion pumping accounts for a large majority of energy consumed during submaximal isometric contraction in mouse fast muscle.

6.5. Contractile Economy

Wildtype muscle with an intact RLC phosphorylation mechanism had a far higher contractile economy than muscle devoid of skMLCK. Since E_{Total} was very similar between genotypes, the increase in contractile performance and work per crossbridge cycle due to myosin RLC phosphorylation is responsible for boosting economy by 73% during 15 s of submaximal isometric activation. The efficiency (i.e. work/enthalpy) of fast twitch mouse EDL has been reported to fall between 0.29 – 0.33 (Barclay, 1996; Barclay et al., 1993), meaning that approximately 30% of the total energy consumed is converted to work. In the present study, Wildtype muscles and skMLCK$^{-/-}$ muscles had contractile economies (i.e. work/HEPC) of 0.38 and 0.22, respectively. Although efficiency and economy are measured differently, they attempt to answer a similar question, and our values seem comparable and acceptable. It is evident that skMLCK and RLC phosphorylation may play a major role in the ratio of force produced to energy consumed during contraction.

Initially, Barsotti & Butler (1984) reported that mouse EDL showed a reduction in average rate of energy consumption when myosin RLCs were phosphorylated; an effect

that was dependent upon both stimulation duration and history. After further experimentation, they were unable to find a consistent relationship between RLC phosphorylation and the energy consumption. Crow & Kushmerick (1982b) reported a correlation between a myosin RLC phosphorylation and reduced energy cost for isometric tetani in mouse fast twitch muscle. Although this current study did not use tetani, we saw that during low-frequency repetitive isometric activation, muscles capable of RLC phosphorylation showed a reduced energy cost for force production, supporting the relationship between RLC phosphorylation and a reduced cost of contraction. Considering that E_A was similar between genotypes, the economical difference is clearly a reflection of the average work performed during each crossbridge cycle.

Alternatively, our findings are in stark contrast to Abbate et al. (2001), who reported that RLC phosphorylation-mediated force potentiation increased the energetic cost of contraction to a higher extent than it increased work output. It was even suggested that, in the potentiated state, efficiency of the crossbridges may be compromised, reducing mechanical output for each ATP hydrolyzed and negatively impacting the economy of the working muscle. That idea opposes our findings, and seems counterintuitive. Brown and Loeb (1998) put forth the idea of potentiation being the normal operating state of muscle, and Tsianos and Loeb (2014) have described how muscles in the *unpotentiated* state exhibit "odd behavior" in their recent skeletal muscle modeling paper. For this reason, all of their modeling equations for fast twitch muscles capture their behavior in the fully potentiated state (Tsianos & Loeb, 2014). Moreover, skeletal muscles appear less economical during low levels of thin filament activation, possibly due to less work per crossbridge cycle (Lewis & Barclay, 2014); thus, heightening the Ca^{2+}-sensitivity of the contractile apparatus could have a beneficial effect on economy, analogous to, but in the absence of, further increases in $[Ca^{2+}]$ activation. Indeed, our findings indicated that the potentiated Wildtype muscle actually had a lower E_{XB}, and what appears to be an increased mechanical output for each ATP hydrolyzed. However, comparison directly to findings from Abbate et al. (2001) is problematic: the vastly different findings may be attributed to the dissimilar models used between studies, as they studied this phenomenon in rat EDL, *in situ*.

Conclusions & Significance

7.1. Major Findings

The present study provided evidence that RLC phosphorylation-mediated force potentiation improves the contractile economy of fast twitch mammalian muscle during repetitive isometric activation. SkMLCK-mediated phosphorylation of the myosin RLCs augmented the relationship between mechanical output and metabolic input by radically improving the contractile performance of muscle, without any associated increase in energetic cost. Our study demonstrates that during repetitive low-frequency activation, ion pumping and other non-contractile processes account for the majority of energy consumed. Additionally, it appears that the energetic overhead required to phosphorylate the myosin RLCs is insignificant compared to the overall energy cost of continued contraction.

7.2. Significance

Previous research investigating the effect of RLC phosphorylation on contractile economy has been unable to reach a definitive answer. The use of skMLCK$^{-/-}$ mice as a robust negative control was a novel aspect of this study, which allowed us to say with certainty that economy is improved in the presence of skMLCK. These findings provide further evidence of a teleological role of skMLCK *in vivo*, as a mechanism that can enhance contractile performance without further energetic cost. RLC phosphorylation by skMLCK appears to be a perfect modulatory mechanism, since it has a profound effect on performance, but itself does not consume a considerable amount of energy. While the activation cascade responsible for RLC phosphorylation and dephosphorylation are far too slow to be an obligatory mechanism for contraction, the continued expression of the components necessary for reversible myosin RLC phosphorylation seem to be ultimately related to enhanced contractile performance and thermodynamic efficiency at the level of the crossbridge.

7.3. Future Considerations

As with most *in vitro* experiments, these findings are undoubtedly paradigm-dependent; thus, future work must be aimed at determining the relationship between RLC phosphorylation, force potentiation, and the energetic cost of contraction in protocols that include concentric and eccentric contractions, as well as span a range of activation frequencies. While we were unable to conclusively quantify the energetic overhead of myosin RLC phosphorylation, there did appear to be a trend in increasing E_A for Wildtype muscle. Future work should be conducted using the skMLCK$^{-/-}$ model in laboratories equipped to perform higher resolution measurements such as HPLC, ^{31}P-NMR, or even enthalpy measurements. Perhaps a collaborative venture between labs is on the horizon.

The EDL muscle is an ideal model for studying RLC phosphorylation-mediated force potentiation due to composition of fast fibres that contain the necessary enzymatic machinery. However, this *in vitro* model is highly mechanistic, and future work investigating the effects of skMLCK on contractile economy should eventually be focused on whole body, *in vivo* studies. It would be interesting to compare whole body VO_2 of exercising Wildtype and skMLCK$^{-/-}$ mice, to determine whether the increased economy in solely fast twitch muscles carries over to a situation in which many muscles of mixed fibre types are concurrently activated.

7.4. Assumptions

In energy balance experiments measuring high-energy phosphate consumption (HEPC) during a brief bout of activity (<30 s), the contribution to overall ATP production by oxidative metabolism is no more than 9% (Westra, De Haan, Van Doorn, & De Haan, 1988). Even if oxygen delivery is interrupted, the muscle still has access to stores of oxygenated hemoglobin and myoglobin that can be used to oxidize pyruvate. To circumvent this issue, sodium cyanide (NaCN) is commonly introduced to the physiological solution in which the muscle preparation is bathed, as it is able to inhibit mitochondrial oxidative phosphorylation at mM concentrations (Barsotti & Butler, 1984). Many studies using NaCN elicit tetanic contractions, with no adverse affects on contractile activity reported; however, the addition of NaCN resulted in potentiation of

directly elicited *twitch* force, followed by a progressive depression of force (Adler, Lebeda, Kauffman, & Deshpande, 1999). Since our study elicited repetitive isometric *twitches*, and the force record is of utmost importance, NaCN was not used to abolish oxidative metabolism. This decision was made in an attempt to reduce confounding variables impacting the contractile data. Thus, for all metabolite calculations, it is assumed that the muscle preparation relies solely on anaerobic substrate-level phosphorylation during the brief contractile bout. In addition, HEPC is calculated using an equation with the following inherent assumptions: (i) glycogen is the sole source for lactate production during contraction, and (ii) any decrease in ATP within the muscle is associated with a stoichiometric increase in IMP (Zhang et al., 2006).

It is also assumed that using BTS selectively inhibits myosin II ATPase, in turn depressing force production, while not affecting any other energy consuming processes. It has previously been demonstrated that Ca^{2+} handling is unaffected by BTS in mammalian muscle (Pinniger et al., 2005) and pilot experiments revealed that myosin RLC phosphorylation is unaffected by BTS incubation.

7.5. Limitations

While the *in vitro* EDL model has become commonplace in this area of research, this model is only an approximation of what may be happening while the muscle is active *in vivo*. *In vitro*, the muscle is submerged in an oxygenated organ bath, recreating the osmolality and oxygen supply of *in vivo* conditions; however, this involves replacing circulating blood with Tyrode's solution, replacing neural control with electrical field stimulation, and bathing the muscle at sub-physiological temperatures to maintain viability. Obviously, temperature and other environmental variables greatly impact enzymatic function; thus, data from this study is strictly mechanistic in nature, and should eventually be replicated in an *in vivo* or *in situ* model.

One of the major limitations of rapid freezing followed by chemical analysis of extracts of the frozen muscle is the logistical dilemma that arises: each muscle preparation provides only a single measurement, at a single time point. Correspondingly, it is impossible to adopt a repeated measures design to minimize effects of inter-muscle variability, and both HEPC and phosphorylation data must be determined from multiple independent measurements.

Finally, this study is open to the inherent uncertainty in biochemical measurements, which is large compared to the magnitude of changes in concentration of the metabolites of interest, particularly when the extent of chemical breakdown is reduced due to inhibition of crossbridge cycling. Additionally, any errors in measurements are propagated through calculations of HEPC (Equation XXII). Protocols using long tetani or repeated brief contractions increase PCr breakdown and reduce relative uncertainty in its measurement, which is why a 15 s stimulation protocol was utilized in this project.

References

Abbate, F., de Ruiter, C. J., Offringa, C., & Sargeant, A. J. (2002). In situ rat fast skeletal muscle is more efficient at submaximal than at maximal activation levels. *Journal of Applied Physiology*, *90*(5), 2089–2096. http://doi.org/10.1152/japplphysiol.00498.2001

Abbate, F., Velden, J. V. D., Stienen, G. J. M., & De Haan, A. (2001). Post-tetanic potentiation increases energy cost to a higher extent than work in rat fast skeletal muscle. *Journal of Muscle Research and Cell Motility*, *22*(8), 703–710. http://doi.org/10.1023/A:1016383025358

Adam, A. (2005). Firing rates of motor units in human vastus lateralis muscle during fatiguing isometric contractions. *J Appl Physiol*, *99*(1), 268–280. http://doi.org/10.1152/japplphysiol.01344.2004

Adler, M., Lebeda, F. J., Kauffman, F. C., & Deshpande, S. S. (1999). Mechanism of action of sodium cyanide on rat diaphragm muscle. *Journal of Applied Toxicology*, *19*(6), 411–419. http://doi.org/10.1002/(SICI)1099-1263(199911/12)19:6<411::AID-JAT597>3.0.CO;2-1

Alamo, L., Wriggers, W., Pinto, A., Bártoli, F., Salazar, L., Zhao, F.-Q., et al. (2008). Three-dimensional reconstruction of tarantula myosin filaments suggests how phosphorylation may regulate myosin activity. *Journal of Molecular Biology*, *384*(4), 780–797. http://doi.org/10.1016/j.jmb.2008.10.013

Allen, D. G., Lamb, G. D., & Westerblad, H. (2008). Skeletal Muscle Fatigue: Cellular Mechanisms. *Physiological Reviews*, *88*(1), 287–332. http://doi.org/10.1152/physrev.00015.2007

Atkinson, D. E. (1977). Cellular Energy Metabolism and its Regulation. Toronto, ON: Elsevier. http://doi.org/10.1016/B978-0-12-066150-3.50001-6

Baker, A. J., Brandes, R., & Schendel, T. M. (1994). Energy use by contractile and noncontractile processes in skeletal muscle estimated by 31P-NMR. *American Journal of Physiology*, *266*(3), C825–C831. http://doi.org/10.1152/ajpcell.00279.2012

Barclay, C. J. (1996). Mechanical efficiency and fatigue of fast and slow muscles of the mouse. *The Journal of Physiology*, *497*(3), 781–794. http://doi.org/10.1113/jphysiol.1996.sp021809

Barclay, C. J. (2005). Modelling diffusive O_2 supply to isolated preparations of mammalian skeletal and cardiac muscle. *Journal of Muscle Research and Cell Motility*, *26*, 225–235. http://doi.org/10.1007/s10974-005-9013-x

Barclay, C. J. (2012). Quantifying Ca^{2+} release and inactivation of Ca^{2+} release in fast- and slow-twitch muscles. *The Journal of Physiology*, *590*(23), 6199–6212. http://doi.org/10.1113/jphysiol.2012.242073

Barclay, C. J., & Loiselle, D. S. (2007). Can activation account for 80% of skeletal muscle energy use during isometric contraction? *American Journal of Physiology. Cell Physiology*, *292*(1), C612. http://doi.org/10.1152/ajpcell.00122.2006

Barclay, C. J., Constable, J. K., & Gibbs, C. L. (1993). Energetics of fast- and slow-twitch muscles of the mouse. *The Journal of Physiology*, *472*(1), 61–80. http://doi.org/10.1113/jphysiol.1993.sp019937

Barclay, C. J., Lichtwark, G. A., & Curtin, N. A. (2008). The energetic cost of activation in mouse fast-twitch muscle is the same whether measured using reduced filament overlap or *N*-benzyl-*p*-toluenesulphonamide. *Acta Physiologica*, *193*(4), 381–391. http://doi.org/10.1111/j.1748-1716.2008.01855.x

Barclay, C. J., Woledge, R. C., & Curtin, N. A. (2007). Energy turnover for Ca^{2+} cycling in skeletal muscle. *Journal of Muscle Research and Cell Motility*, *28*, 259–274. http://doi.org/10.1007/s10974-007-9116-7

Barclay, C. J., Woledge, R. C., & Curtin, N. A. (2010a). Inferring crossbridge properties from skeletal muscle energetics. *Progress in Biophysics and Molecular Biology*, *102*(1), 53–71. http://doi.org/10.1016/j.pbiomolbio.2009.10.003

Barclay, C. J., Woledge, R. C., & Curtin, N. A. (2010b). Is the efficiency of mammalian (mouse) skeletal muscle temperature dependent? *The Journal of Physiology*, *588*(19), 3819–3831. http://doi.org/10.1113/jphysiol.2010.192799

Barsotti, R. J., & Butler, T. M. (1984). Chemical energy usage and myosin light chain phosphorylation in mammalian skeletal muscle. *Journal of Muscle Research and Cell Motility*, *5*(1), 45–64. http://doi.org/10.1007/bf00713151

Baylor, S. M., & Hollingworth, S. (2003). Sarcoplasmic reticulum calcium release compared in slow-twitch and fast-twitch fibres of mouse muscle. *The Journal of Physiology*, *551*(1), 125–138. http://doi.org/10.1111/j.1469-7793.2003.00125.x

Baylor, S. M., & Hollingworth, S. (2011). Calcium indicators and calcium signalling in skeletal muscle fibres during excitation–contraction coupling. *Progress in Biophysics and Molecular Biology*, *105*(3), 162–179. http://doi.org/10.1016/j.pbiomolbio.2010.06.001

Behrmann, E., Müller, M., Penczek, P. A., Mannherz, H. G., Manstein, D. J., & Raunser, S. (2012). Structure of the rigor actin-tropomyosin-myosin complex. *Cell*, *150*(2), 327–338. http://doi.org/10.1016/j.cell.2012.05.037

Bergmeyer, H. U., Bergmeyer, J., & Grassl, M. (1983). Methods of enzymatic analysis. Weinheim, Germany: Verlag Chemie.

Bergstrom, M., & Hultman, E. (1988). Energy cost and fatigue during intermittent electrical stimulation of human skeletal muscle. *J Appl Physiol*, *65*(4), 1500–1505.

Block, B. A., Imagawa, T., Campbell, K. P., & Franzini-Armstrong, C. (1988). Structural evidence for direct interaction between the molecular components of the transverse tubule/sarcoplasmic reticulum junction in skeletal muscle. *The Journal of Cell Biology*, *107*(6), 2587–2600. http://doi.org/10.1083/jcb.107.6.2587

Blumenthal, D. K., & Stull, J. T. (1980). Activation of skeletal muscle myosin light chain kinase by calcium(2+) and calmodulin. *Biochemistry*, *19*(24), 5608–5614. http://doi.org/10.1021/bi00565a023

Brenner, B. (1988). Effect of Ca^{2+} on cross-bridge turnover kinetics in skinned rabbit psoas fibers: Implications for regulation of muscle contraction. *Proceedings of the National Academy of Sciences*, *85*(9), 3265–3269.

Brooks, S. V., & Faulkner, J. A. (1988). Contractile properties of skeletal muscles from young, adult and aged mice. *The Journal of Physiology*, *404*(1), 71–82. http://doi.org/10.1113/jphysiol.1988.sp017279

Brown, I. E., & Loeb, G. E. (1998). Post-activation potentiation: A clue for simplifying models of muscle dynamics. *American Zoologist*, *38*(4), 743–754. http://doi.org/10.1093/icb/38.4.743

Bruton, J., Pinniger, G. J., Lännergren, J., & Westerblad, H. (2006). The effects of the myosin-II inhibitor *N*-benzyl-*p*-toluene sulphonamide on fatigue in mouse single intact toe muscle fibres. *Acta Physiologica*, *186*(1), 59–66. http://doi.org/10.1111/j.1748-1716.2005.01499.x

Buller, A. J., Kean, C. J. C., Ranatunga, K. W., & Smith, J. M. (1981). Post-tetanic depression of twitch tension in the cat soleus muscle. *Experimental Neurology*, *73*(1), 78–89. http://doi.org/10.1016/0014-4886(81)90046-7

Buschman, H. P., Van der Laarse, W. J., Stienen, G. J., & Elzinga, G. (1996). Force-dependent and force-independent heat production in single slow- and fast-twitch muscle fibres from Xenopus laevis. *The Journal of Physiology*, *496*(Pt 2), 503–89. http://doi.org/10.1016/0014-4886(81)90046-7

Calderón, J. C., Bolaños, P., & Caputo, C. (2014). The excitation–contraction coupling mechanism in skeletal muscle. *Biophysical Reviews*, *6*(1), 133–160. http://doi.org/10.1007/s12551-013-0135-x

Caterini, D., Gittings, W., Huang, J., & Vandenboom, R. (2011). The effect of work cycle frequency on the potentiation of dynamic force in mouse fast twitch skeletal muscle. *The Journal of Experimental Biology*, *214*(23), 3915–3923. http://doi.org/10.1242/jeb.061150

Chasiotis, D., Bergstrom, M., & Hultman, E. (1987). ATP utilization and force during intermittent and continuous muscle contractions. *J Appl Physiol*, *63*(1), 167–174.

Cheung, A., Dantzig, J. A., Hollingworth, S., Baylor, S. M., Goldman, Y. E., Mitchison, T. J., & Straight, A. F. (2001). A small-molecule inhibitor of skeletal muscle myosin II. *Nature Cell Biology*, *4*(1), 83–88. http://doi.org/10.1038/ncb734

Chin, E. R. (2010). Intracellular Ca^{2+} signaling in skeletal muscle: Decoding a complex message. *Exercise and Sport Sciences Reviews*, *38*(2), 76–85. http://doi.org/10.1097/JES.0b013e3181d495d2

Craig, R., & Padrón, R. (2004). Molecular structure of the sarcomere. In A. Engel, *Myology* (3rd ed., pp. 128–166). New York, NY: McGraw-Hill.

Craig, R., & Woodhead, J. L. (2006). Structure and function of myosin filaments. *Current Opinion in Structural Biology*, *16*(2), 204–212. http://doi.org/10.1016/j.sbi.2006.03.006

Crow, M. T., & Kushmerick, M. J. (1982a). Chemical energetics of slow- and fast-twitch muscles of the mouse. *The Journal of General Physiology*, *79*(1), 147–166. http://doi.org/10.1085/jgp.79.1.147

Crow, M. T., & Kushmerick, M. J. (1982b). Myosin light chain phosphorylation is associated with a decrease in the energy cost for contraction in fast twitch mouse muscle. *Journal of Biological Chemistry*, *257*(5), 2121–2124.

Crow, M., & Kushmerick, M. (1982c). Phosphorylation of myosin light chains in mouse fast-twitch muscle associated with reduced actomyosin turnover rate. *Science*, *217*(4562), 835–837. http://doi.org/10.1126/science.6285472

De Haan, A., De Jong, J., Van Doorn, J. E., Huijing, P. A., Woittiez, R. D., & Westra, H. G. (1986). Muscle economy of isometric contractions as a function of stimulation time and relative muscle length. *Pflügers Archiv - European Journal of Physiology*, *407*(4), 445–450. http://doi.org/10.1007/BF00652632

Ding, H-L., Ryder, J. W., Stull., J. T., & Kamm, K. E. (2009). Signaling processes for initiating smooth muscle contraction upon neural stimulation. *The Journal of Biological Chemistry, 284*(23), 15541-15548.

Dominguez, R. (2011). Tropomyosin: The gatekeeper's view of the actin filament revealed. *Biophysj*, *100*, 797–798. http://doi.org/10.1016/j.bpj.2011.01.018

Duggal, D., Nagwekar, J., Rich, R., Midde, K., Fudala, R., Gryczynski, I., & Borejdo, J. (2014). Phosphorylation of myosin regulatory light chain has minimal effect on kinetics and distribution of orientations of cross bridges of rabbit skeletal muscle. *American Journal of Physiology - Regulatory, Integrative and Comparative Physiology*, *306*(4), R222–R233. http://doi.org/10.1152/ajpregu.00382.2013

Dulhunty, A. F. (2006). Excitation–contraction coupling from the 1950s into the new millennium. *Clinical and Experimental Pharmacology and Physiology*, *33*(9), 763–772. http://doi.org/10.1111/j.1440-1681.2006.04441.x

Ebashi, S. (1991). Excitation-Contraction Coupling And The Mechanism Of Muscle Contraction. *Annual Review of Physiology*, *53*(1), 1–16. http://doi.org/10.1146/annurev.physiol.53.1.1

Fenn, W. O. (1923). A quantitative comparison between the energy liberated and the work performed by the isolated sartorius muscle of the frog. *The Journal of Physiology*, *58*(2-3), 175–203. http://doi.org/10.1113/jphysiol.1923.sp002115

Fenn, W. O. (1924). The relation between the work performed and the energy liberated in muscular contraction. *The Journal of Physiology*, *58*(6), 373–395. http://doi.org/10.1113/jphysiol.1924.sp002141

Fox, J. G., Barthold, S. W., Davisson, M. T., Newcomer, C. E., Quimby, F. W., & Smith, A. L. (Eds.). (2006). The Mouse in Biomedical Research (2nd ed.). Toronto, ON: Elsevier Science.

Franzini-Armstrong, C., & Porter, K. R. (1964). Sarcolemmal invaginations constituting the T system in fish muscle fibers. *The Journal of Cell Biology*, *22*(3), 675–696. http://doi.org/10.1083/jcb.22.3.675

Franzini-Armstrong, C., & Protasi, F. (1997). Ryanodine receptors of striated muscles: A complex channel capable of multiple interactions. *Physiological Reviews*.

Fujita, K., Fujita, K., Ye, L.-H., Sato, M., Okagaki, T., Nagamachi, Y., & Kohama, K. (1999). Myosin light chain kinase from skeletal muscle regulates an ATP-dependent interaction between actin and myosin by binding to actin. *Molecular and Cellular Biochemistry*, *190*(1-2), 85–90. http://doi.org/10.1023/A:1006925217536

Gillis, J. M. (1985). Relaxation of vertebrate skeletal muscle: A synthesis of the biochemical and physiological approaches. *Biochimica Et Biophysica Acta*, *811*(2), 97–145. http://doi.org/10.1016/0304-4173(85)90016-3

Gittings, W., Aggarwal, H., Stull, J. T., & Vandenboom, R. (2014). The force dependence of isometric and concentric potentiation in mouse muscle with and without skeletal myosin light chain kinase. *Canadian Journal of Physiology and Pharmacology*, *93*(1), 23–32. http://doi.org/10.1139/cjpp-2014-0118

Gittings, W., Huang, J., & Vandenboom, R. (2012). Tetanic force potentiation of mouse fast muscle is shortening speed dependent. *Journal of Muscle Research and Cell Motility*, *33*(5), 359–368. http://doi.org/10.1007/s10974-012-9325-6

Gittings, W., Huang, J., Smith, I. C., Quadrilatero, J., & Vandenboom, R. (2011). The effect of skeletal myosin light chain kinase gene ablation on the fatigability of mouse fast muscle. *Journal of Muscle Research and Cell Motility*, *31*(5-6), 337–348. http://doi.org/10.1007/s10974-011-9239-8

Goldspink, G. (1978). Energy turnover during contraction of different types of muscle. Biomechanics VI-A.

Gordon, A. M., Homsher, E., & Regnier, M. (2000). Regulation of Contraction in Striated Muscle. *Physiological Reviews*, *80*(2), 853–924. http://doi.org/10.1021/ja00218a034

Grange, R. W., Vandenboom, R., & Houston, M. E. (1993). Physiological Significance of Myosin Phosphorylation in Skeletal Muscle. *Canadian Journal of Applied Physiology*, *18*(3), 229–242. http://doi.org/10.1139/h93-020

Greenberg, M. J., Mealy, T. R., Watt, J. D., Jones, M., Szczesna-Cordary, D., & Moore, J. R. (2009). The molecular effects of skeletal muscle myosin regulatory light chain phosphorylation. *American Journal of Physiology - Regulatory, Integrative and Comparative Physiology*, *297*(2), R265–R274. http://doi.org/10.1152/ajpregu.00171.2009

Hardie, D. G., & Hawley, S. A. (2001). AMP-activated protein kinase: The energy charge hypothesis revisited. *BioEssays*, *23*(12), 1112–1119. http://doi.org/10.1002/bies.10009

Harris, R. C., Hultman, E., & Nordesjö, L. O. (1974). Glycogen, glycolytic intermediates and high-energy phosphates determined in biopsy samples of musculus quadriceps femoris of man at rest: Methods and variance of values. *Scandinavian Journal of Clinical and Laboratory Investigation*, *33*(2), 109–120. http://doi.org/10.3109/00365517409082477

Hogan, M. C., Ingham, E., & Kurdak, S. S. (1998). Contraction Duration Affects Metabolic Energy Cost and Fatigue in Skeletal Muscle. *American Journal of Physiology - Endocrinology and Metabolism*, *274*, E397–E402.

Homsher, E. (1987). Muscle enthalpy production and its relationship to actomyosin ATPase. *Annual Review of Physiology*, *49*(1), 673–690. http://doi.org/10.1146/annurev.ph.49.030187.003325

Homsher, E., Mommaerts, W. F. H. M., Ricchiuti, N. V., & Wallner, A. (1972). Activation heat, activation metabolism and tension-related heat in frog semitendinosus muscles. *The Journal of Physiology*, *220*(3), 601–625. http://doi.org/10.1113/jphysiol.1972.sp009725

Huxley, A. F. (1957). Muscle structure and theories of contraction. *Progress in Biophyics and Biophysical Chemistry*, *7*, 255–318.

Huxley, H. E. (1969). The mechanism of muscular contraction. *Science, 164,* 1356-1366.

Huxley, H., & Hanson, J. (1954). Changes in the cross-striations of muscle during contraction and stretch and their structural interpretation. *Nature*, *173*, 973–976.

Imagawa, T., Smith, J. S., Coronado, R., & Campbell, K. P. (1987). Purified ryanodine receptor from skeletal muscle sarcoplasmic reticulum is the Ca^{2+}-permeable pore of the calcium release channel. *Journal of Biological Chemistry*, *262*(34), 16636–16643.

Inglis, J. G., Howard, J., McIntosh, K., Gabriel, D. A., & Vandenboom, R. (2011). Decreased motor unit discharge rate in the potentiated human tibialis anterior muscle. *Acta Physiologica*, *201*(4), 483–492. http://doi.org/10.1111/j.1748-1716.2010.02233.x

Jones, T. E., Squier, T. C., Boschek, C. B., & Bigelow, D. J. (2007). Calcium occupancy of N-terminal sites within calmodulin induces inhibition of the ryanodine receptor calcium release channel. *Biochemistry*, *46*(37), 10621–10628. http://doi.org/10.1021/bi700655h

Kerrick, W. G. L., Potter, J. D., & Hoar, P. E. (1991). The apparent rate constant for the dissociation of force generating myosin crossbridges from actin decreases during Ca2+ activation of skinned muscle fibres. *Journal of Muscle Research and Cell Motility*, *12*(1), 53–60. http://doi.org/10.1007/BF01781174

Klug, G. A., Botterman, B. R., & Stull, J. T. (1982). The effect of low frequency stimulation on myosin light chain phosphorylation in skeletal muscle. *Journal of Biological Chemistry*, *288*(19), 13446–13454. http://doi.org/10.1074/jbc.M113.455444

Koubassova, N. A., & Tsaturyan, A. K. (2011). Molecular mechanism of actin-myosin motor in muscle. *Biochemistry (Moscow)*, *76*(13), 1484–1506. http://doi.org/10.1134/S0006297911130086

Krans, J. L. (2010). The sliding filament theory of muscle contraction. *Nature Education*, *3*(9), 66. http://doi.org/10.1371/journal.pone.0064404.g005

Krendel, M., & Mooseker, M. S. (2005). Myosins: Tails (and heads) of functional diversity. *Physiology*, *20*, 239–251. http://doi.org/10.1152/physiol.00014.2005

Leong, P., & MacLennan, D. H. (1998). Complex interactions between skeletal muscle ryanodine receptor and dihydropyridine receptor proteins. *Biochemistry and Cell Biology*, *76*(5), 681–694. http://doi.org/10.1139/o98-079

Lewis, D. B., & Barclay, C. J. (2014). Efficiency and cross-bridge work output of skeletal muscle is decreased at low levels of activation. *Pflügers Archiv - European Journal of Physiology*, *466*(3), 599–609. http://doi.org/10.1007/s00424-013-1344-7

Lou, F., Curtin, N., & Woledge, R. (1997). The energetic cost of activation of white muscle fibres from the dogfish Scyliorhinus canicula. *The Journal of Experimental Biology*, *200*(3), 495–501.

Lymn, R. W., & Taylor, E. W. (1971). Mechanism of adenosine triphosphate hydrolysis by actomyosin. *Biochemistry*, *10*(25), 4617–4624. http://doi.org/10.1021/bi00801a004

MacIntosh, B. R., Gardiner, P. F., & McComas, A. J. (2006). Skeletal Muscle: Form and Function (2nd ed.). New York, NY: Human Kinetics.

MacIntosh, B. R., Holash, R. J., & Renaud, J. M. (2012). Skeletal muscle fatigue: Regulation of excitation-contraction coupling to avoid metabolic catastrophe. *Journal of Cell Science*, *125*(9), 2105–2114. http://doi.org/10.1242/jcs.093674

Manning, D. R., & Stull, J. T. (1982). Myosin light chain phosphorylation-dephosphorylation in mammalian skeletal muscle. *American Journal of Physiology*, *242*, C234–C241.

Manuel, M., & Heckman, C. J. (2011). Adult mouse motor units develop almost all of their force in the subprimary range: A new all-or-none strategy for force recruitment? *The Journal of Neuroscience*, *31*(42), 15188–15194. http://doi.org/10.1523/JNEUROSCI.2893-11.2011

Matsumura, F., & Hartshorne, D. J. (2008). Myosin phosphatase target subunit: Many roles in cell function. *Biochemical and Biophysical Research Communications*, *369*(1), 149–156. http://doi.org/10.1016/j.bbrc.2007.12.090

Morgan, M., Perry, S. V., & Ottaway, J. (1976). Myosin light-chain phosphatase. *Biochemical Journal*, *157*, 687–697.

Perrie, W. T., Smillie, L. B., & Perry, S. V. (1973). A phosphorylated light-chain component of myosin from skeletal muscle. *Biochemical Journal*.

Pessah, I. N., Waterhouse, A. L., & Casida, J. E. (1985). The calcium-ryanodine receptor complex of skeletal and cardiac muscle. *Biochemical and Biophysical Research Communications*, *128*(1), 449–456. http://doi.org/10.1016/0006-291X(85)91699-7

Pinniger, G. J., Bruton, J. D., Westerblad, H., & Ranatunga, K. W. (2005). Effects of a myosin-II inhibitor (*N*-benzyl-*p*-toluene sulphonamide, BTS) on contractile characteristics of intact fast-twitch mammalian muscle fibres. *Journal of Muscle Research and Cell Motility*, *26*(2-3), 135–141. http://doi.org/10.1007/s10974-005-2679-2

Pires, E., Perry, S. V., & Thomas, M. (1974). Myosin light-chain kinase, a new enzyme from striated muscle. *FEBS Letters*, *41*(2), 292–296.

Porter, K. R., & Palade, G. E. (1957). Studies on the endoplasmic reticulum III. Its form and distribution in striated muscle cells. *The Journal of Cell Biology*, *3*(2), 269–300. http://doi.org/10.1083/jcb.3.2.269

Potma, E. J., Stienen, G. J., & Barends, J. P. (1994). Myofibrillar ATPase activity and mechanical performance of skinned fibres from rabbit psoas muscle. *The Journal of Physiology*, *474*(2), 303–317. http://doi.org/10.1113/jphysiol.1994.sp020023

Preller, M., & Holmes, K. C. (2013). The myosin start-of-power stroke state and how actin binding drives the power stroke. *Cytoskeleton*, *70*(10), 651–660. http://doi.org/10.1002/cm.21125

Rall, J. A. (1982). Energetics of Ca^{2+} cycling during skeletal muscle contraction. *Federation Proceedings*, *41*(2), 155–160.

Rayment, I., & Holden, H. M. (1994). The three-dimensional structure of a molecular motor. *Trends in Biochemical Sciences*, *19*(3), 129–134. http://doi.org/10.1016/0968-0004(94)90206-2

Rayment, I., Holden, H. M., Whittaker, M., Yohn, C. B., Lorenz, M., Holmes, K. C., & Milligan, R. A. (1993a). Structure of the actin-myosin complex and its implications for muscle contraction. *Science*, *261*(5117), 58–65. http://doi.org/10.1126/science.8316858

Rayment, I., Rypniewski, W. R., Schmidt-Base, K., Smith, R., Tomchick, D. R., Benning, M. M., et al. (1993b). Three-dimensional structure of myosin subfragment-1: A molecular motor. *Science*, *261*(5117), 50–58. http://doi.org/10.1126/science.8316857

Rebbeck, R. T., Karunasekara, Y., & Board, P. G. (2014). Skeletal muscle excitation–contraction coupling: Who are the dancing partners? *The International Journal of Biochemistry and Cell Biology*, *48*, 28–38. http://doi.org/10.1016/j.biocel.2013.12.001

Reggiani, C., Potma, E. J., Bottinelli, R., Canepari, M., Pellegrino, M. A., & Stienen, G. J. M. (1997). Chemo-mechanical energy transduction in relation to myosin isoform composition in skeletal muscle fibres of the rat. *The Journal of Physiology*, *502*(2), 449–460. http://doi.org/10.1111/j.1469-7793.1997.449bk.x

Rolfe, D. F., & Brown, G. C. (1997). Cellular energy utilization and molecular origin of standard metabolic rate in mammals. *Physiological Reviews*, *77*(3), 731–758.

Russ, D. W., Elliott, M. A., Vandenborne, K., Walter, G. A., & Binder-Macleod, S. A. (2002). Metabolic costs of isometric force generation and maintenance of human skeletal muscle. *American Journal of Physiology - Endocrinology and Metabolism*, *282*(2), E448–E457. http://doi.org/10.1152/ajpendo.00285.2001

Ryder, J. W., Lau, K. S., Kamm, K. E., & Stull, J. T. (2007). Enhanced skeletal muscle contraction with myosin light chain phosphorylation by a calmodulin-sensing kinase. *Journal of Biological Chemistry*, *282*(28), 20447–20454. http://doi.org/10.1074/jbc.M702927200

Sahlin, K., & Harris, R. C. (2011). The creatine kinase reaction: A simple reaction with functional complexity. *Amino Acids*, *40*(5), 1363–1367. http://doi.org/10.1007/s00726-011-0856-8

Sandow, A. (1952). Excitation-contraction coupling in muscular response. *The Yale Journal of Biology and Medicine*, *25*(3), 176–201.

Shaw, M. A., Ostap, E. M., & Goldman, Y. E. (2003). Mechanism of Inhibition of Skeletal Muscle Actomyosin by N-Benzyl- p-toluenesulfonamide †. *Biochemistry*, *42*(20), 6128–6135. http://doi.org/10.1021/bi026964f

Siegman, M. J., Mooers, S. U., Warren, T. B., Warshaw, D. M., Ikebe, M., & Butler, T. M. (1994). Comparison of the effects of 2,3-butanedione monoxime on force production, myosin light chain phosphorylation and chemical energy usage in intact and permeabilized smooth and skeletal muscles. *Journal of Muscle Research and Cell Motility*, *15*(4), 457–472. http://doi.org/10.1007/BF00122119

Smith, A. D. (2000). Oxford Dictionary of Biochemistry and Molecular Biology. Oxford University Press, USA.

Smith, I. C., Gittings, W., Huang, J., McMillan, E. M., Quadrilatero, J., Tupling, A. R., & Vandenboom, R. (2013). Potentiation in mouse lumbrical muscle without myosin light chain phosphorylation: Is resting calcium responsible? *The Journal of General Physiology*, *141*(3), 297–308. http://doi.org/10.1085/jgp.201210918

Smith, I. C., Vandenboom, R., & Tupling, A. R. (2014). Juxtaposition of the changes in intracellular calcium and force during staircase potentiation at 30 and 37°C. *The Journal of General Physiology*, *144*(6), 561–570. http://doi.org/10.1085/jgp.201411257

Smith, N. P., Barclay, C. J., & Loiselle, D. S. (2005). The efficiency of muscle contraction. *Progress in Biophysics and Molecular Biology*, *88*(1), 1–58. http://doi.org/10.1016/j.pbiomolbio.2003.11.014

Spriet, L. L. (1989). ATP utilization and provision in fast-twitch skeletal muscle during tetanic contractions. *American Journal of Physiology - Endocrinology and Metabolism*, *257*(4), E595–E605.

Stienen, G. J., Zaremba, R., & Elzinga, G. (1995). ATP utilization for calcium uptake and force production in skinned muscle fibres of Xenopus laevis. *The Journal of Physiology*, *482*(Pt 1), 109. http://doi.org/10.1111/(ISSN)1469-7793

Stull, J. T., Kamm, K. E., & Vandenboom, R. (2011). Myosin light chain kinase and the role of myosin light chain phosphorylation in skeletal muscle. *Archives of Biochemistry and Biophysics*, *510*(2), 120–128. http://doi.org/10.1016/j.abb.2011.01.017

Sweeney, H. L. (1994). The importance of the creatine kinase reaction: The concept of metabolic capacitance. *Medicine and Science in Sports and Exercise*, *26*(1), 30–36.

Sweeney, H. L., & Houdusse, A. (2010). Structural and functional insights into the myosin motor mechanism. *Annual Review of Biophysics*, *39*(1), 539–557. http://doi.org/10.1146/annurev.biophys.050708.133751

Sweeney, H. L., & Stull, J. T. (1990). Alteration of cross-bridge kinetics by myosin light chain phosphorylation in rabbit skeletal muscle: Implications for regulation of actin-myosin interaction. *Proceedings of the National Academy of Sciences*, *87*(1), 414–418. http://doi.org/10.1073/pnas.87.1.414

Sweeney, H. L., Bowman, B. F., & Stull, J. T. (1993). Myosin light chain phosphorylation in vertebrate striated muscle: Regulation and function. *American Journal of Physiology. Cell Physiology*, *264*(5), C1085–C1095.

Szentesi, P., Zaremba, R., Mechelen, W. V., & Stienen, G. J. M. (2001). ATP utilization for calcium uptake and force production in different types of human skeletal muscle fibres. *The Journal of Physiology*, *531*(2), 393–403. http://doi.org/10.1111/j.1469-7793.2001.0393i.x

Tiidus, P., Tupling, A. R., & Houston, M. (2012). Biochemistry Primer for Exercise Science (4 ed.). Windsor, ON: Human Kinetics.

Tsianos, G. A., & Loeb, G. E. (2014). Physiology and computational principles of muscle force generation. In *Encyclopedia of Computational Neuroscience*. New York, NY. http://doi.org/10.1007/978-1-4614-7320-6_246-2.pdf

Tsianos, G. A., Rustin, C., & Loeb, G. E. (2012). Mammalian muscle model for predicting force and energetics during physiological behaviors. *Neural Systems and Rehabilitation Engineering, IEEE Transactions on*, *20*(2), 117–133. http://doi.org/10.1109/TNSRE.2011.2162851

Tupling, A. R. (2009). Excitation-Contraction Coupling. *Encyclopedia of Neuroscience*. http://doi.org/10.1007/978-3-540-29678-2_3191.pdf

Vandenboom, R., & Houston, M. E. (1996). Phosphorylation of myosin and twitch potentiation in fatigued skeletal muscle. *Canadian Journal of Physiology and Pharmacology*, *74*(12), 1315–1321. http://doi.org/10.1139/cjpp-74-12-1315

Vandenboom, R., Gittings, W., Smith, I. C., Grange, R. W., & Stull, J. T. (2013). Myosin phosphorylation and force potentiation in skeletal muscle: Evidence from animal models. *Journal of Muscle Research and Cell Motility*, *34*, 317–332. http://doi.org/10.1007/s10974-013-9363-8

Wendt, I. R., & Barclay, J. K. (1980). Effects of dantrolene on the energetics of fast- and slow-twitch muscles of the mouse. *American Journal of Physiology. Cell Physiology*, *238*(1), C56–C61.

Westra, H. G., De Haan, A., Van Doorn, J. E., & De Haan, E. J. (1988). Anaerobic chemical changes and mechanical output during isometric tetani of rat skeletal muscle in situ. *Pflügers Archiv - European Journal of Physiology*, *412*(1-2), 121–127. http://doi.org/10.1007/BF00583740

Winkelmann, D. A., Baker, T. S., & Rayment, I. (1991). Three-dimensional structure of myosin subfragment-1 from electron microscopy of sectioned crystals. *The Journal of Cell Biology*, *114*(4), 701–713. http://doi.org/10.1083/jcb.114.4.701

Woledge, R. C., Curtin, N. A., & Homsher, E. (1985). Energetic aspects of muscle contraction. London, England: Academic Press.

Xiong, L., Zhang, J.-Z., He, R., & Hamilton, S. L. (2006). A Ca^{2+}-Binding Domain in RyR1 that Interacts with the Calmodulin Binding Site and Modulates Channel Activity. *Biophysj*, *90*(1), 173–182. http://doi.org/10.1529/biophysj.105.066092

Yang, Z., Stull, J. T., Levine, R. J. C. & Sweeney, H. L. (1998). Changes in interfilament spacing mimic the effects of myosin regulatory light chain phosphorylation in rabbit psoas fibers. *Journal of Structural Biology*, *122*, 139-148.

Zhang, S. J., Andersson, D. C., Sandstrom, M. E., Westerblad, H., & Katz, A. (2006). Cross bridges account for only 20% of total ATP consumption during submaximal isometric contraction in mouse fast-twitch skeletal muscle. *American Journal of Physiology: Cell Physiology*, *291*(1), C147–C154. http://doi.org/10.1152/ajpcell.00578.2005

Zhi, G., Ryder, J. W., Huang, J., Ding, P., Chen, Y., Zhao, Y., et al. (2005). Myosin light chain kinase and myosin phosphorylation effect frequency-dependent potentiation of skeletal muscle contraction. *Proceedings of the National Academy of Sciences*, *102*(48), 17519–17524. http://doi.org/10.1073/pnas.0506846102

Appendix I:
Preliminary Procedures for Contractile Experiments

Setting Up the In Vitro Apparatus

1. After turning on the computer, open the single channel data collection program (Linux systems only require a single click, as opposed to the Windows or Mac OS X double-click)
2. Open 'Set Up', 'Protocol' and 'Scope' windows
3. Switch ASI stimulator and servomotor/force transducer control units ON
4. Zero the force in signal by clicking 'Record F_{in}' in 'Set Up' window periodically until the value stabilizes around a given number (usually 27-32 mV) - servomotor arm needs voltage to stabilize in resting position
5. Turn Circulator ON – compressor should stay ON, set to LOW
6. Pack ice around auxiliary organ bath if necessary
7. Insert closed needle valve into vertical jacketed organ bath
8. Pour fresh Tyrode's solution into both baths
9. Open master value on mixed gas cylinder, followed by secondary black valve located on the regulator
10. Open cut off valves on tubing that feed the organ baths required for the experiment
11. Fine tune the oxygen flow to each bath with fine black adjustment knobs on the gas dispersal units to obtain a steady stream of bubbles
12. Turn tank off until experiment begins to conserve oxygen

Surgical Procedures

1. Dilute stock sodium pentobarbital to working concentration
2. Weigh mouse and calculate anesthetic dose required
3. Administer the IP injection
4. Begin procedures once the pedal reflex is absent
5. Remove skin to expose hind limb musculature
6. Pin foot down
7. Remove fascia from TA and relieve tendons held under the tensor ligament
8. Isolate TA tendon, and remove TA
9. Stop bleeding associated with rupture of TA blood supply using Tyrode's soaked gauze
10. Tie non-absorbable silk sutures to the proximal and distal tendons of the EDL
11. Cut tendons and mount muscle

Mounting Isolated Muscles

1. Zero F_{in}
2. Open bottom clamp
3. Loop top suture onto servomotor lever arm
4. Straighten bottom suture and insert into bottom clamp

5. Tighten bottom clamp
6. Adjust muscle length with coarse adjustment knob until just taut length is reached
7. Tighten white screw behind apparatus to lock in place
8. Use fine adjustment knob to obtain 3-5 mN resting tension.
9. Measure muscle length using digital vernier calipers
10. Input value as 'Reference Length' in Set Up window, hit Enter, then record L_{in}
11. Check boxes for $L_o=L_{ref}$ and $L_f=L_o$
12. Click 'Verify Sequence', and 'Save'
13. Flip stimulator to Gated Trigger Mode (from Follow)
14. Leave voltage knob as maximal, and adjust the current to achieve maximal twitch force through manual triggering (usually around 7-8 mA)

Equilibration and Determining L_o

1. Load equilibration sequence in Sequencer view of Protocol window
2. Enable Slip Tetanus and Equilibration protocols
3. Manually stimulate muscle at various lengths to determine L_o - from 0 mN to 20 mN resting tension is a good range
4. Allow muscle to rest ~30 s between twitches
5. Determine the resting tension at which the largest active force is produced (i.e. total tension – passive tension)
6. Set muscle length to resting tension that best represents L_o, and if there are 2 similar results then pick the lower value
7. Use digital vernier calipers to measure the new length, input as Reference Length and record L_{in}

Appendix II:
Measurement of Myosin Regulatory Light Chain Phosphorylation by Urea/Glycerol-PAGE with Immunoblotting

Myosin regulatory light chains (RLCs) are small ($18 - 20\ kDa$) acidic (pI about 4.8 with net charge of -18) proteins that migrate easily in polyacrylamide gels containing glycerol for density. RLCs are denatured with trichloroacetic acid (TCA) and solubilized in urea to dissociate the RLCs from the myosin heavy chains. The addition of a single phosphate introduces two additional negative charges at pH 8.6 (the pH of the running buffer) so the phosphorylated protein migrates faster than the non-phosphorylated RLC. Thus, the phosphorylation measurements are quantitative (mol per mol), not relative (degree of change) after measurements of the protein band density by immunoblotting.

Sample Preparation

Prepare Stock Solutions

Acetone-Based Protein Precipitation Solution (5 mL)

10% Trichloroacetic acid (TCA), 10 mM DTT in ice-cold acetone (-20 C)

TCA *(T8657)*	0.5 g
DTT *(D0632)*	7.71 mg
Acetone	2.5 mL
Dissolve	
Acetone	Q.S. to 5 mL

N.B. Make fresh on day of sample preparation, and store in -20 C until use.

Water-Based Protein Precipitation Solution (5 mL)

10% Trichloroacetic acid (TCA), 10 mM DTT in

TCA *(T8657)*	0.5 g
DTT *(D0632)*	7.71 mg
dH_2O	2.5 mL
Dissolve	
dH_2O	Q.S. to 5 mL

N.B. Make fresh on day of sample preparation, and store in -20 C until use.

Prepare Buffers

Gel Buffer (500 mL)

Trizma base	13.7 g
Glycine	10.0 g
dH_2O	250 mL
Dissolve	
dH_2O	Q.S. to 500 mL

N.B. Store at 2-8 C.

Sample Buffer

8 M Urea	1.83 mL
Urea Gel Buffer	167.0 uL
0.5 M DTT	40.0 uL
Saturated Sucrose	100 uL
0.2% Bromophenol Blue	40.00 uL
0.4 M EDTA	1.00 uL

N.B. Make fresh on day of sample prep.

Sample Denaturation

1. Pipet 0.5 mL Acetone-Based Protein Precipitation Solution into as many microcentrifuge tubes as you have muscle samples (pre-labeled), and freeze in liquid N_2
2. Measure frozen weight of muscle sample (~10 mg for EDLs) and record
3. Remove microcentrifuge tube from N_2, open lid and place on ice
4. Introduce muscle preparation (with sutures removed) to the microcentrifuge tube of frozen Acetone-Based Protein Precipitation Solution slurry, as it forms a slurry when warming up to about -35°C on ice
5. Remove the tubes from ice and allow them to come to room temperature

Sample Homogenization

1. Transfer each denatured muscle sample (tissue only, no liquid) to a ground glass homogenizing tube, and pipet in 0.5 mL Water-Based Protein Precipitation Solution
2. Homogenize muscle sample thoroughly
3. Transfer the homogenate to a microcentrifuge tube by pouring – samples may sit on ice for 10 mins or more
4. Centrifuge at 2000 RPM for 3 minutes at room temperature – do not over pack the protein pellet or resuspension will be difficult
5. Discard the supernatant by pouring off into a waste beaker
6. Wash pellet with 0.5 mL of ether, 3 times for 5 minutes each to remove TCA
7. Let residual ether evaporate from the tube for 5 minutes in the hood or blow gently into the tube if you are impatient
8. DO NOT let the pellet go totally dry or resuspension will be difficult

Resuspension

1. Add 30 µL of urea sample buffer per mg frozen tissue weight
2. Vortex and manually disperse the pellet if necessary
3. pH should be around 9, check by confirming blue colour of the sample – if yellow/green at 2 M Tris base (pH 11) 1 µL at a time until colour becomes uniform between samples
4. Add ~__mg of urea to microcentrifuge tube that contains 300 µL of sample buffer
5. Shake samples for 15 minutes at RT, adding more urea if the others have dissolved
6. Repeat until same is saturated by urea – do NOT oversaturate or the sample will become solid and unusable
7. Store at -80°C if you do not use immediately.
8. Thaw samples on day of use in an ice bath, and mix after 1 hr of thawing
9. Do not heat urea samples on thawing – this can lead to breakdown of urea at high pH to cyanide with carbamylation of protein, which changes charge.

Hand Casting of Polyacrylamide Gels

10% (w/v) APS

Ammonium persulfate *(A3574)*	0.10 g
dH_2O	1.0 mL

N.B. Make fresh when casting gels.

Urea/Glycerol Polyacrylamide Gels (2)

dH_2O	4.2 mL
Glycerol *(G5516)*	9.0 mL
30% Acrylamide/Bis 29:1	7.5 mL
Urea Gel Buffer	1.9 mL
Stir 10 mins under vacuum to degas	
10% APS	100 uL
TEMED	10 uL
Mix By Swirling	
Quickly pour into minigel apparatus & insert combs	

N.B. Make just prior to pouring. Gel starts polymerizing immediately after APS and TEMED are introduced to the solution – have everything ready to cast before adding these and move quickly.

1. Place magnetic stir bar in small vacuum flask
2. Mix dH_2O, glycerol, acrylamide, and urea gel buffer in flask
3. Close flask and turn on vacuum
4. Stir for 10-15 minutes under vacuum to degas the solution
5. Prepare plates/combs for casting
6. Pour degassed solution into 50 mL falcon tube
7. Draw 100 uL of 10% APS and 10 µL TEMED in pipettes
8. Quickly add the APS and TEMED, mix by swirling – do NOT shake or you will regass the solution you just spent 15 minutes degassing

9. Cast gels using a disposable transfer pipet, pouring only into the centre of the plates – the solution will naturally spread and you do not need to move the pipet, as you may risk formation of bubbles
10. Insert newly cleaned combs, and wipe up any spillage before polymerization - this protocol does not use a stacking gel
11. Mix upper and lower buffers while gels polymerize (~45 mins)

Lower Buffer (1 L)

Urea Gel Buffer	83.0 mL
dH_2O	Q.S. to 1000 mL

N.B. this buffer is poured into the electrophoresis tank.

Upper Buffer (200 mL)

DTT	73.3 mg
Thioglycolate	53.3 mg
Lower Buffer	200 mL

N.B. this buffer is poured into the electrode assembly.

Electrophoretic Separation of Proteins

Pre-Electrophoresis

1. Carefully remove combs from polymerized gel – it must be removed while remaining parallel to the gel to prevent damage to any wells
2. Rinse wells with dH_2O to remove any debris
3. Rinse wells with Upper Buffer immediately before pre-electrophoresis
4. Place gels into electrode assembly after wetting the gasket, ensuring that the plates are fully inserted into the brackets
5. Check seal for leak using dH_2O
6. Pre-electrophorese at 400 V for 1 hour to force thioglycolate into the gel – this reduces any residual APS that was used to initiate polymerization, preventing protein oxidation which will effect protein migration

Electrophoretic Separation of Proteins

1. Load 5-20 µL of each sample – this gel system does not have a stacking gel so the tip of the pipet should be close to the gel in the well with slow addition of the sample. Urea and sucrose were added for increased density so the sample should layer in the well as a sharp band
2. Amount to load depends on tissue source so optimal amount needs to be determined - Load at lease 5 µL to get good bands – if protein is too concentrated, sample can be diluted with urea sample buffer
3. Do NOT use the end wells, as samples in the end wells tend to distort
4. Electrophorese at 400 V for 85 minutes - Dye will run off gel but you can look at it during electrophoresis to make sure migration is normal
5. Prepare 1X Transfer Buffer from 10X Transfer Buffer stock during electrophoresis – 1 L is enough for 1-2 gels

10X Transfer Buffer (1 L)

1.9 M Glycine, 250 mM Tris, 0.5% (w/v) SDS

Glycine	144.12 g
Tris	30.29 g
SDS	5.0 g
dH_2O	500 mL
Dissolve	
dH_2O	Q.S. to 1 L

N.B. Store at 2-8 C.

Transfer Buffer (1 L)

192 mM Glycine, 25 mM Tris, 0.05% (w/v) SDS

10X Transfer Buffer	100 mL
100% Methanol	200 mL
dH_2O	700 mL

N.B. Make from concentrated stock on the day of transfer.

Transferring Protein From Polyacrylamide Gel to the Nitrocellulose Membrane

1. Cut ~8.5 x 7.0 cm pieces of nitrocellulose paper (0.45 mm pore size)
2. Pour 1x Transfer Buffer into trays in preparation for blotting sandwich
3. Disassemble electrode assembly, and remove gel cassettes
4. Separate plates using green plastic wedge
5. Cut off approximately one quarter of the upper part of gel
6. Notch the upper left corner of the gel to aid in discerning orientation later
7. Rinse gels gently in transfer buffer for 5 minutes to equilibrate
8. Place a magnetic stirbar into the transfer tank, half fill with cooled 1X Transfer Buffer and position on stirrer
9. Immerse nitrocellulose membrane in transfer buffer for 1 minute to wet it – it should be pre-notched in the upper left corner of the membrane to match the orientation of the gel
10. With the black (cathode) side of the gel holder cassette submerged in Transfer Buffer, assemble the blotting sandwich in the following order, wetting each layer before its addition: sponge, blotting paper, gel, nitrocellulose membrane, blotting paper and sponge
11. Roll after adding each layer to remove any air bubbles – having enough Transfer Buffer in the tray to cover all layers will help when removing bubbles
12. Close the cassette, slide white latch to lock, and place into blotting module with the latch side up, and the black side of the cassette facing the black side of the blotting module
13. Repeat for any additional blots, then place the blotting module with the gel holder cassettes into the tank
14. Insert icepack into tank, add transfer buffer to the tank until the fill line is reach, and begin stirring

15. Place lid on top of the cell, connect cables to power supply, turn on power supply and transfer membrane at 25 V for 1 hour by selecting the pre-set method entitled "Transfer"

Immunobloting

Blocking of Non-Specific Sites

1. Remove the nitrocellulose membrane from the blotting sandwich, and transfer to a square petri dish, ensuring that only the corner of the membrane is touched by tweezers and that the membrane remains protein-side up
2. Wash the membrane in TBST three times for 10 minutes each
3. Incubate with Blocking Buffer for 1 hour at room temperature to prevent non-specific binding in a clean tray

Primary Antibody Incubation

1. Wash membrane in TBST twice, 5-10 min per wash
2. Add 1:7,500 skMLCK polyclonal primary antibodies to fresh blocking buffer (i.e. 1.5 μL in 10 mL) in a clean tray and incubate with rocking overnight at 4°C

Secondary Antibody Incubation

1. Remove primary antibody and wash the membrane with TBST, six times for 10 minutes in a clean tray
2. Incubate with secondary antibody, 1:10,000 dilution of Goat Anti-Rabbit IgG-HRP in TBST (i.e 1 μL in 10 mL) for 1 hour in a clean tray

Detection of Target Proteins

1. Wash the membrane in TBST six times for 10 minutes
2. Transfer membrane to a clean tray after rinsing with dH_2O, and drip drying onto Kim Wipe
3. Make detection buffer using equal volumes of ECL Prime luminol and oxidizing reagents
4. Incubate the membrane in detection buffer for 2 minutes, constantly pipetting to cover entire membrane
5. Decant the ECL Prime, lift membrane with tweezers and blot all excess reagent from the corner of the membrane using a Kim Wipe
6. Cover membrane with sheet protector, and roll to remove air bubbles and/or excess liquid
7. Turn on the CCD imaging machine – flip the power switches at the back of the unit (bottom right) and on the shelf
8. Open the FluorChem application
9. Place blot on imager platform and center on the screen, zoom if necessary
10. Imager should be on setting 1 for chemiluminescence
11. Select "Chemidisplay", "Normal Sensitivity/Resolution", and check "UV" for "Transluminator" and "Reflective" settings
12. Select exposure time of 30-60 seconds, and select 'Acquire Image'
13. Save image to appropriate folder

Appendix III:

Lyophilization of Muscle Tissue

1. Turn lyophilizer on by switch on both the condenser and vacuum unit
2. Press 'Refridgeration – Auto' and 'Vacuum' buttons
3. Close all valves on the tree
4. Ensure digital temperature and pressure gauges begin to drop
5. Pour liquid N_2 into thermoflask from storage dewar
6. Remove samples from -80°C freezer and place in N_2
7. Transfer samples into ventilated microcentrifuge tubes (if not in one already) ensuring they stay frozen
8. Precool LABCONCO 600 mL evacuation vessel with liquid N_2 in a metal bowl
9. Place samples in vessel, submerging the bottom of the flask in N_2
10. Close vessel with rubber top
11. With the vessel still sitting in liquid N_2, attach the metal tube to the vacuum tree
12. When a good seal has been made, open valve and the vessel should evacuate (very obvious to both see and hear)
13. Let machine run for minimum of 6 hours or over night (if you trust leaving it alone)
14. Check occasionally to ensure it is running properly
15. Shut machine down when finished
16. Store the lyophilized samples in -80°C in a box with desiccant if not extracting immediately
17. Open the circular lid of the condenser and allow it to return to room temperature
18. Wipe up condensation from the inside of the condenser after room temperature has been reached
19. Sign the log including name, date, usage etc.

Appendix IV:

Metabolite Extraction

Often the preparation of the tissue is the most critical. In the case of metabolite assays, the most hazardous period is usually the period between the experimental stimulus and the moment the enzyme activity is finally stopped. Rapid freezing is essential; therefore, most metabolite analysis is performed on extracts prepared from frozen tissue. Most metabolites are assayed in protein-free extracts prepared with perchloric acid ($HClO_4$). $HClO_4$ is preferred because most of it can be easily removed by precipitation as a potassium salt. All of the following analyses are performed on freeze-dried tissue. Not only does it circumvent the problem of changing water contents in tissue, but also because the tissue is much easier to work with. Enzymes are rendered inactive in a water-free environment, and will remain so until water is re-added. Therefore, the weighing of the samples can be performed at room temperature and the tissue can be dissected free of connective tissues and blood.

Required Solutions

0.5 M PCA (500 mL)

70% w/v Perchloric acid	21.55 mL
dH_2O	125 mL
Mix	
dH_2O	Q.S. to 500 mL

N.B. Store at 0-4 ℃ for up to 1 month; 70% PCA stored under fume hood.

1. In fume hood, pour PCA into small (>50 mL) beaker
2. Measure 21.6 mL of PCA in 25 mL graduated cylinder
3. Add 21.6 mL PCA to 125 mL dH_2O in 500 mL graduated cylinder
4. Rinse 25 mL graduated cylinder with dH2O into 500 mL graduated cylinder
5. Bring to 500 mL with dH_20
6. Store in fridge (0-4ºC) for up to 1 month

2.3 M $KHCO_3$

Potassium bicarbonate (237205)	2.3 g
dH2O	5 mL
Dissolve	
dH2O	Q.S. to 10 mL

N.B. Make fresh on day of extraction.

1. Weigh out 2.3 g $KHCO_3$
2. Measure ~5mL dH2O in small graduated cylinder
3. Add to small amount of distilled H_2O
4. Bring to 10.0 mL
5. Make fresh on day of extraction

Confirm Neutral pH

1. Calibrate the pH meter
2. Combine 4 mL PCA and 1 mL $KHCO_3$
3. Measure and record pH - values between 6.5 and 7.5 are acceptable

Perchloric Acid Metabolite Extraction Procedure

1. Freeze dry tissue (overnight to ensure all water is removed)
2. Store with dry rite in freezer until powdering
3. Tease out connective tissue and powder
4. Place in pre-weighed 12x75 glass centrifuge tube and weigh ($\sim 2.5\ mg$)
5. Place tubes in an ice bucket (make sure tubes remain cold)
6. Add 300 µL of pre-cooled 0.5 M PCA
7. Extract for 15 minutes, vortexing several times and ensure all tissue is in contact with PCA
8. Centrifuge for 10 minutes at 15000 G and 4°C– the glass tubes are compatible with the S4180 rotor (spinning helps remove some of the enzymes that can influence concentration)
9. Remove 270 µL, aliquot to micocentrifuge tube and place in freezer (-20ºC) for 10 min
10. To the frozen supernatant add 67.5 µL of 2.3 M $KHCO_3$ and vortex until liquid (addition of $KHCO_3$ to a frozen supernatant prevents foaming over)
11. Centrifuge for 10 min 0ºC at 15 000 G – the microcentrifuge tubes are compatible with the F2402H rotor - Potassium salt will precipitate.
12. Remove supernatant, aliquot to new pre-labeled microcentrifuge tubes – this is the extraction that will be assayed for metabolites.

Using the Centrifuge

1. Power on the unit by flicking the black switch on the back of the unit
2. When centrifuging, ensure that it is completely balanced and samples of the same volume are placed "across the street" from one another
3. Different rotors are used for different sized tubes and are stored in the drawer directly underneath the unit
4. To change rotor, remove central bolt and remove the current rotor, replace with the required rotor and replace and tighten the central bolt – this bolt does not need to be tightened with a ton of force, snug is fine. Program the correct rotor.
5. Press "Enter" after making any changes to the settings
6. Always turn unit off when you are finished and leave lid open
7. Record use of the unit on the tracking sheet attached to the side

Appendix V:

Fluorometric Assays

Pyridine nucleotides are natural oxidizing and reducing agents in a wide variety of enzyme systems. In the reduced form the nucleotide NADH/NADPH is fluorescent while in its oxidized form (NAD/NADP) it is not. The reduced form is also capable of fluorescent emission at 460nm when excited at 340nm. Due to these two physical properties, reactions can be quantified based directly on the change in the oxidative state of these coenzymes. Therefore the limiting factor, in the conversion of any of the metabolites, and production of the fluorescent material, NADH/NADPH, will be the amount of metabolite in the muscle because all other substrates/cofactors/enzymes in the assay are in excess. The presence of certain compounds in the assay, removes certain substrates, essentially forcing all reactions to occur one direction. Therefore the amount of fluorescence determined using the fluorometer is directly proportional to the amount of the metabolite in the muscle.

Muscle Adenosine Triphosphate (ATP) and Phosphocreatine (PCr) Assay

$$\text{P-Creatine + ADP} \xrightarrow{\textit{Creatine Kinase}} \text{Creatine + ATP}$$

$$\text{ATP + Glucose} \xrightarrow{\textit{Hexokinase}} \text{ADP + Glucose-6-P}$$

$$\text{Glucose-6-P + NADP}^{+} \xrightarrow{\textit{Glucose-6- Dehydrogenase}} \text{6-P-Glucanolactone + NADPH}$$

Reagent	Storage	Stock Conc.	Final Conc.	Volume in 25 mL	Volume in 50mL	Volume in 100mL
1. **Tris Buffer** *Trizma Base* (T1503)	Room Temp (Shelf)	1.00 M	50.0 mM	1.25 mL	2.50 mL	5.00 mL
2. **$MgCl_2$** *Magnesium Chloride* (M8266)	Room Temp (Shelf)	1.00 M	1.00 mM	25.00 µL	50.00 µL	100.00 µL
3. **DTT** *Dithiothreitol* (D0632)	2 − 8 ℃ (Fridge)	0.50 M	0.5 mM	25.00 µL	50.00 µL	100.00 µL
4. **Glucose** (G8270)	Room Temp (Shelf)	100.00 mM	100.00 µM	25.00 µL	50.00 µL	100.00 µL
5. **NADP** (N5755)	−20 ℃ (Freezer)	50.0 mM	50.0 µM	25.00 µL	50.00 µL	100.00 µL
6. **G-6-P-DH** (G5760)	2 − 8 ℃ (Fridge)	4920 U /ml	0.03 U /mL	1.00 µL	2.00 µL	4.00 µL
7. **ADP** (A2754)	−20 ℃ (Freezer)	Solid	−	−	−	−
8. **Creatine Kinase** (C3755)	−20 ℃ (Freezer)	324 U/mg	−	−	−	−
9. **Hexokinase** (H4502)	−20 ℃ (Freezer)	130 U/mg	−	−	−	−
Note: Mix reagents 1-5 together. Bring to volume with dH_2O and adjust to pH 8.1. Then add reagent 6. Mix by inversion with enzymes.						

Preparation of Dilute Enzyme

For *PART 2*: Mix 2.5 µL of Hexokinase with 1.0 ml of buffer (for each plate). Mix by inversion. CAREFUL NOT TO FOAM

For *PART 3*. Mix ~1.5 mg of phosphocreatine kinase and 5 mg of ADP into 5 ml of buffer. Mix by inversion.

Procedure for Assay (Note: Run everything in triplicate)

Ensure you vortex each sample before pipetting

Part 1.

1. Fill first three wells – A1, A2 and A3 - with $10.00\ \mu L$ of dH_2O per well
2. **F**ill the next five rows of wells with $10.00\mu L$ of varying concentrations of ATP Standard
   B1, B2 and B3 0.05 mM
   C1, C2 and C3 0.1 mM
   D1, D2 and D3 0.2 mM
   E1, E2 and E3 0.3 mM
   F1, F2 and F3 0.4 mM
3. Fill the next five rows of wells with $10.00\ \mu L$ of varying concentrations of the PCr standard.
   (0.08 mM, 0.16 mM, 0.32 mM, 0.64 mM, 0.96 mM)
4. Add $10.00\ \mu L$ of sample to the appropriate wells
5. Add $185\ \mu L$ of buffer to each well
7. Incubate the plate for 25 minutes (if time permits - probably not necessary)
6. Read the plate at sensitivity of 80 (Ex/Em 340nm/460nm) (base line reading = R1)

Part 2.

1. Add $6\ \mu L$ of dilute Hexokinase to all of the wells
2. Incubate in the dark drawer for ~80 minutes (can also track by multiple measures)
3. Read the plate (Ex/Em 340nm/460nm)
($R2 - R1 =\ reflects\ ATP\ in\ extract$)

Part 3.

1. Add $6\ \mu L$ of dilute Creatine Kinase to all of the wells
2. Incubate in the dark drawer for ~120 minutes
3. Read the plate (excitation setting 340, emission setting 460)

($R3 - R2 =\ reflects\ PCr\ in\ extract$)

ATP (A7699) Standard Curve

To make fresh 2.0 mM solution: 5.69 mg ATP into 5 mL dH_2O

Concentration (mM)	Stock Volume (µL)	dH_2O Volume (µL)	Dilution Factor
0.05	25	975	40.0
0.1	50	950	20.0
0.2	100	900	10.0
0.3	150	850	6.67
0.4	200	800	5.00

Phosphocreatine (P7936) Standard Curve

Stored in 8.0 mM aliquots in the -80ºC

To make 8.0 mM stock: 21.85 mg phosphocreatine into 10 mL dH_2O

Concentration (mM)	Stock Volume (µL)	dH_2O Volume (µL)	Dilution
0.08	10	990	100.0
0.16	20	980	50.0
0.32	40	960	25.0
0.64	80	920	12.5
0.96	120	880	8.3

Muscle Creatine (Cr) Assay

$$\text{Creatine} + \text{ATP} \xrightarrow{\textit{Creatine Kinase}} \text{P-Creatine} + \text{ADP}$$

$$\text{ADP} + \text{Phophopyruvate} \xrightarrow{\textit{Pyruvate Kinase}} \text{ATP} + \text{Pyruvate}$$

$$\text{Pyruvate} + \text{NADH} \xrightarrow{\textit{Lactate Dehydrogenase (LDH)}} \text{Lactate} + \text{NAD}$$

Reagent	Storage	Stock Conc.	Final Conc.	Volume 250 mL	Volume 50mL	Volume 100mL
1. Imidazole (I0250)	Room Temp	1.00 M	50 mM	1.25 mL	2.50 mL	5.00 mL
2. $MgCl_2$ *Magnesium Chloride* (M8266)	Room Temp	1.00 M	5.0 mM	125.00 µL	250.00 µL	500.00 µL
3. KCl *Potassium Chloride* (P9541)	Room Temp	1.00 M	30.00 mM	0.75 mL	1.5 mL	3.00 mL
4. PEP *Phosphoenolpyruvate* (P7002)	−20 ℃ (Freezer)	10.0 mM	25.0 µM	60.0 µL	120.00 µL	240.00 µL
5. ATP (A2383)	−20 ℃ (Freezer)	SOLID	200.0 µM	3.27 mg	6.54 mg	13.08 mg
6. NADH (N8129)	−20 ℃ (Freezer)	15.0 mM	45 µM	75.00 µL	150.00 µL	300.00 µL
7. LDH (L2500)	2 − 8 ℃ (Fridge)	5264 U /mL	0.24 U /mL	1.10 µL	2.3 µL	4.6 µL
8. Pyruvate Kinase (P1506)	2 − 8 ℃ (Fridge)	1252 U /mL	0.75 U /mL	15.00 µL	30.00 µL	60.00 µL
9. Creatine Kinase (C3755)	−20 ℃ (Freezer)	324 U /mg	3.6 U/mL	–	–	–
Note: Mix reagents 1-6 together. Bring to volume with distilled water and adjust to pH 7.5. Then add reagents 7 & 8. Mix by inversion when enzymes added.						

Preparation of Dilute Enzyme

For step 2. Mix 1.0 mg of Creatine Kinase with 2.6 ml of buffer. Mix by inversion.

Before beginning to pipette the samples you must test the fluorescence of the buffer (might have to change gain)

Procedure for Assay

Part 1.

1. Fill three wells with a blank (10.00 µL dH_2O per well)
2. a. Vortex each concentration mixture before pipetting
   b. Fill the next five wells with 10.00µL of varying concentrations of Cr standard (0.1mM, 0.2 mM, 0.4 mM, 0.8 mM, 1.2 mM)
3. a. Vortex each sample before pipetting
   b. Add 10.00 µL of sample to the appropriate wells
4. Add 185 µL of buffer to each well
5. Incubate for 30 minutes
6. Read the plate at a sensitivity of 100 (excitation setting 340, emission setting 460) (base line reading)

Part 2.

1. Add 6 µL of dilute Creatine Kinase to all of the wells
2. Place in the dark for 55 minutes
3. Read the plate (excitation setting 340, emission setting 460)

Note: Everything analyzed in triplicate

Creatine (Sigma C0780-50g) Standard Curve
Stored in 10 mM aliquots in the -80ºC
To make 10 mM stock: 131.1 mg into 100 ml dH_2O

Concentration (mM)	Stock Volume (µL)	dH_2O Volume (µL)	Dilution Factor
0.1	10	990	100
0.2	20	980	50
0.4	40	960	25
0.8	80	920	12.5
1.2	120	880	8.33

Muscle Lactate Assay

$$\text{Lactate} + \text{NAD}^+ \xrightarrow{Lactate\ Dehydrogenase} \text{pyruvate} + \text{NADH} + \text{H}^+$$

$$\text{Pyruvate} + \text{Hydrazine} \longrightarrow \text{Pyruvate Hydrazone}$$

Reagent	Stock Conc.	Final Conc.	Volume 250 mL	Volume 50mL	Volume 100mL
1. Hydrazine	1.00 M	100.0 mM	2.50 mL	5.00 mL	10.00 mL
2. Glycine	1.00 M	100.0 mM	2.50 mL	5.00 mL	10.00 μL
3. NAD^+	100.0 mM	0.5 mM	125 μL	250 μL	500.00 μL
4. LDH	5264 U $/mL$	8.00 U $/mL$	–	–	–
Note: Mix reagents 1-3 together. Bring to volume with dH_2O and adjust to pH 10.					

Preparation of Dilute Enzyme

Add 17.25 µL of LDH (L2500) to 1.0 mL of reagent.

Procedure for Assay

Part 1.

1. Fill three wells with a blank (10.00 µL dH_2O per well)
2. a. Vortex each concentration mixture before pipetting
   b. Fill the next five wells with 10.00µL of varying concentrations of lactate standard (0.025 mM, 0.05 mM, 0.1 mM, 0.2 mM, 0.8 mM)
3. a. Vortex each sample before pipetting
   b. Add 10.00 µL of sample to the appropriately wells
4. Add 185 µL of buffer to each well
5. Incubate for 15 minutes
6. Read the plate at a sensitivity of 120 (Ex/Em 340nm/460nm) (base line reading)

Part 2.

1. Add 10 µL of dilute LDH to all of the wells
2. Place in the dark for 120 minutes
3. Read the plate (excitation setting 340, emission setting 460)

Note: Run everything in triplicate

Lactate Standard Curve

Pre-made lactate standard (4.44 mM)

Conc (mM)	Stock (µL)	dH_2O (µL)
0.1	23	977
0.2	45	955
0.4	90	910
0.8	180	820
1.2	270	730

Conc (mM)	Stock (µL)	dH_2O (µL)
0.025	5.6	994
0.05	11.25	988
0.1	22.5	978
0.2	45	955
0.8	180	820

$$Dilution\ Factor\ (DF) = \frac{total\ volume}{sample\ volume}$$

$$DF_{total} = DF_a \cdot DF_b$$

$$DF_a = \frac{Total\ Volume}{Sample\ Volume} = \frac{volume\ of\ PCA\ (\mu L) + muscle\ mass\ (\mu L)}{muscle\ mass\ (\mu L)}$$

$$DF_b = = \frac{volume\ of\ Supernatant\ (\mu L) + volume\ of\ KHCO_3 (\mu L)}{volume\ of\ Supernatant\ (\mu L)}$$